12-2024

Designing a Robust Lab Scale Electrocoagulation Reactor For Removal of Micro- and Nanoplastics from Drinking Water

Emmanuel Louis Aduhene
Utah State University

DESIGNING A ROBUST LAB SCALE ELECTROCOAGULATION REACTOR FOR REMOVAL OF MICRO- and NANOPLASTICS FROM DRINKING WATER.

by

Emmanuel Louis Aduhene

A project report submitted in partial fulfilment
of the requirements for the degree

of

MASTER OF SCIENCE

In

Civil and Environmental Engineering

Approved:

_____	_____
Joan E. McLean MS	Yiming Su PhD
Major Professor	Committee Member

_____
David W. Britt PhD
Committee Member

UTAH STATE UNIVERSITY
Logan, Utah

2024

Abstract

The widespread occurrence of micro and nanoplastics in drinking water sources could cause serious public health issues. These plastics particles, products of industrial operations and weathering of larger plastics, can interact with other contaminants in the environment, leading to more severe environmental pollution. Present drinking water treatment technologies were designed to remove suspended colloids. However, due to the distinct chemical and physical properties of micro and nanoplastics from conventional colloids, it is challenging for traditional chemical coagulation/flocculation/sedimentation process to achieve satisfying removal performance. This report investigates a design of a lab-scale electrocoagulation reactor for the removal of nanoplastics from drinking water sources. Synthesized polystyrene nanoplastics (246.50 ± 16.12 nm, spheres) were added to a 200 ml solution of 5 mM sodium chloride to a concentration of 1.585 mg/l. Electrode holders, printed in 3D using acrylonitrile butadiene styrene (ABS) filament (1.75 mm), were specifically designed, and made with an adjustable bar to hold the electrodes in precise, measurable vertical positions. A DC power supply and multimeter were used for precise voltage and current control during electrocoagulation. Two aluminum plates with an active surface area of 1.0 x 10^{-3} m^2 were used as the electrodes. The design was tested under a constant voltage (5 V) but varying currents (10 mA, 25 mA, and 50 mA). After 2 hr electrocoagulation and 2 hr settling, the concentration of nanoplastics in the water column was determined using a turbidity meter. Electrocoagulation reduced the nanoplastics concentration by 83.6 %, 90.8 % and 93.9 % (n=3 x 3 trials for each current) with a current of 10 mA, 25 mA, and 50 mA, respectively, without the addition of a flocculant or coagulant. The impact of current was statistically significant. It was also observed that the pH increased in the solution from 5.5 to a stable pH of 8.3, which facilitates aluminum hydroxide

formation for removal of the nanoplastics through hetero aggregation. The distribution of nanoplastics in the produced foam and the settled phase were also determined, and mass balance analysis on total nanoplastics were performed. While the volume of foam produced correlated with the current intensity, nanoplastic content in foam increased first then appeared to reach a peak. The mass balance performed across the systems with different currents recorded an average percentage recovery of 114 ± 2.2 (std error).

These findings demonstrate that electrocoagulation can be employed for removing nanoplastics from drinking water sources. This study lays the groundwork for the systematic evaluation of the impact of different water chemistries (different ionic strengths, concentration and types of dissolved organic matter, pH buffering capacity) and different plastic type (size, shape, and surface morphology) on the effectiveness of electrocoagulation. Future studies will aid in process scale up and further improving drinking water safety addressing this crucial environmental and public health problem.

Acknowledgement

First and foremost, I would like to thank God Almighty for granting me the strength, knowledge, and perseverance to successfully complete this research report. This research would not also have been feasible without the financial support from the Mineral Lease Funds through the Utah Water Research Laboratory, for which I am incredibly appreciative. My profound gratitude to my advisor and professor Joan E. McLean and my committee members Dr. Yiming Su, and Dr. David Britt for their counsel, support and encouragement during this project. I also would like to thank Dr. Abdulazeem Eltaweil and Junjie Tang for their essential contribution in synthesizing the polystyrene nanoparticles used in this study. To Benji Merrell at IDEA Factory, Utah State University, Logan and Jedd Castleton Powell, Hach Regional Sales Manager for Utah & Idaho, for their invaluable assistance with 3-D designing and printing, and generously sponsoring the 2100N turbidimeter calibration solutions, which were crucial for this work respectively.

Lastly, I want to express my heartfelt appreciation to my family, friends, and colleagues for their support and encouragement throughout this journey.

Table of Contents

Table of Figures

Table of Tables

1 Introduction

The pollution of water sources by micro (MPs) and nanoplastics (NPs) have emerged as a serious environmental and public health problem. MPs and NPs are plastics measuring between 1 micron (1 μm) and 5 millimeters (5 mm) and less than 100 nanometers (nm), respectively. These plastics originating from cosmetic products, industrial abrasives and can also be formed from weathered plastics and mechanical abrasions of larger plastic products. MPs and NPs pose a significant threat to aquatic ecosystems and human health due to their widespread distribution and persistence in the environment. The nature of plastics enhances their mobility and bioavailability in aquatic environments, influencing their distribution and uptake by organisms (Baldwin et al., 2020; Chowdhury et al., 2023). Studies have shown the widespread distribution of MPs and NPs in both natural water bodies and treated drinking water (Baldwin et al., 2020; Chowdhury et al., 2023; Mason et al., 2016, 2018, 2020; Sana et al., 2020). MPs and NPs exhibit distinct characteristics that differentiate them in terms of physicochemical properties, environmental fate, interactions with pollutants, and ecological impacts. NPs possess a higher specific surface area and exhibit Brownian motion, leading to stronger interactions with surrounding pollutants compared to MPs (Chen et al., 2023). Present drinking water treatment technologies were designed to remove suspended solids and colloidal material from water however the distinct properties of these plastics, especially NPs, may limit the effectiveness of these conventional treatment processes. Lapointe et al. (2020) demonstrated the removal of MPs from a drinking water source using chemical coagulation whereas others research reported limited efficiencies for removal of MP and NPs due to their physiochemical properties (Wang et al., 2020; Zhang et

al., 2020). These findings underscore the urgent need to develop an advanced treatment method capable of effectively removing these plastics to ensure safe drinking water.

Electrocoagulation (EC) presents an innovative approach by using electrical current and sacrificial electrode at the anode to achieve higher contaminant removal (Akarsu et al., 2021; Akarsu & Deniz, 2021) compared to traditional chemical coagulation. The process generates coagulants in situ by dissolving metal ions from aluminum or iron electrodes directly into the water that hydrolyze to form metal hydroxides (Akarsu & Deniz, 2021; Holt, 2002; Tsai et al., 2023). These hydroxides act as coagulant, destabilizing and aggregating the suspended particles including MPs and NPs which can then be removed by sedimentation or floatation. This method not only reduces the need for chemical additives but also offers significant advantages in terms of operational simplicity, cost-effectiveness, and environmental impact (Akarsu & Deniz, 2021; Hakizimana et al., 2017; Holt, 2002). Electrocoagulation has been noted for its ability to effectively remove a wide range of contaminants, including heavy metals, MPs, NPs and organic compounds from wastewater making it highly applicable for drinking water treatment for the removal of MPs and NPs.

Despite much information on EC's effectiveness in MPs and NPs removal from wastewater (Akarsu et al., 2021; Akarsu & Deniz, 2021; Pawak et al., 2023; Shen et al., 2022) not much is known about its application for the removal of NPs in drinking water treatment. The design of a laboratory-scale EC reactor offers a promising approach for experimentation for optimizing NPs removal from drinking water sources. By considering key electrochemical design parameters such as electrode material, current, voltage, NP properties, and water quality parameters such, as pH and electrolyte concentration, and understanding the mechanisms of NP removal reactor performance can be optimized for efficient and

sustainable removal of NPs from drinking water. However, further research is needed to address the optimization of the electrocoagulation process, environmental and health implications and scaling up from lab and pilot studies to full operating drinking water treatment facilities before EC technology is considered for widespread application in drinking water treatment systems.

2 Research Questions

1. How effective is EC in removing NPs from drinking water at the lab scale? This question will be explored through:
    a. A review of the literature.
    b. Designing and building a lab scale reactor for optimizing electrocoagulation under differing water quality and NP properties.
    c. Evaluating the new reactor design for consistency of results and effectiveness of EC for removal of polystyrene (PS) -NPs under operating conditions of 5V and 10mA, 25mA, and 50 mA. Data will be compared to results from previous studies.

3 Hypothesis and Objectives

1. Hypothesis:
    a. Electrocoagulation will effectively remove NPs from water in a lab-scale reactor through the formation of aluminum hydroxide ($Al(OH_3)$) which facilitates hetero-aggregation between NPs and the $Al(OH_3)$ flocs.
2. Objectives:
    a. Literature review to evaluate effectiveness of EC under various electrochemical, water quality conditions and NP properties.

b. Construct a lab-scale electrocoagulation reactor with adjustable parameters for voltage, current density, and electrode configuration.
c. Investigate the NPs removal efficiency of the electrocoagulation reactor under a specific operating condition of 5 V with 10mA, 25 mA or 50 mA.

4 Literature Review

4.1 Problems with MPs and NPs

4.1.1 Sources of MPs and NPs and their Pathways

Baldwin et al. (2020), Chowdhury et al. (2023), Lin et al. (2024), and Mason et al. (2016, 2020) have reported the presence MPs and NPs in the aquatic environment which includes rivers, lakes, seas, and oceans. As MPs and NPs have been identified as an environmental problem, it has become an area of research to ascertain how best they can be handled to safeguard all environments. Kiran et al. (2022) from their review article developed a graphical display of the amount of research done on MPs and NPs (Figure 1) from 2010 to 2021. From the graph, the urgency for research on MPs and NPs are on the increase due to improper handling and environmental exposure.

MPs and NPs can be classified into primary and secondary sources (Cole et al., 2011; Pruter A. T., 1987). The primary sources of MPs and NPs are manufactured at the microscale and nanoscale for specific uses such as microbeads in cosmetics, industrial abrasives, and preproduction plastic pellets. Various industrial activities also generate NPs as a by-product. In contrast, secondary MPs are produced when larger plastic objects such as bottles and packaging materials, are broken apart and degraded by weathering, UV radiation, mechanical abrasion, and other environmental factors. The further breakdown of MPs leads

to the formation of NPs that enter the ecosystem via runoff, wind dispersal and direct disposal. Both sources contribute a significant amount of MPs and NPs pollution into the ecosystem. However, Chen et al. (2023) underscores the distinct characteristics and sources of NPs, suggesting that they pose unique challenges compared to MPs.

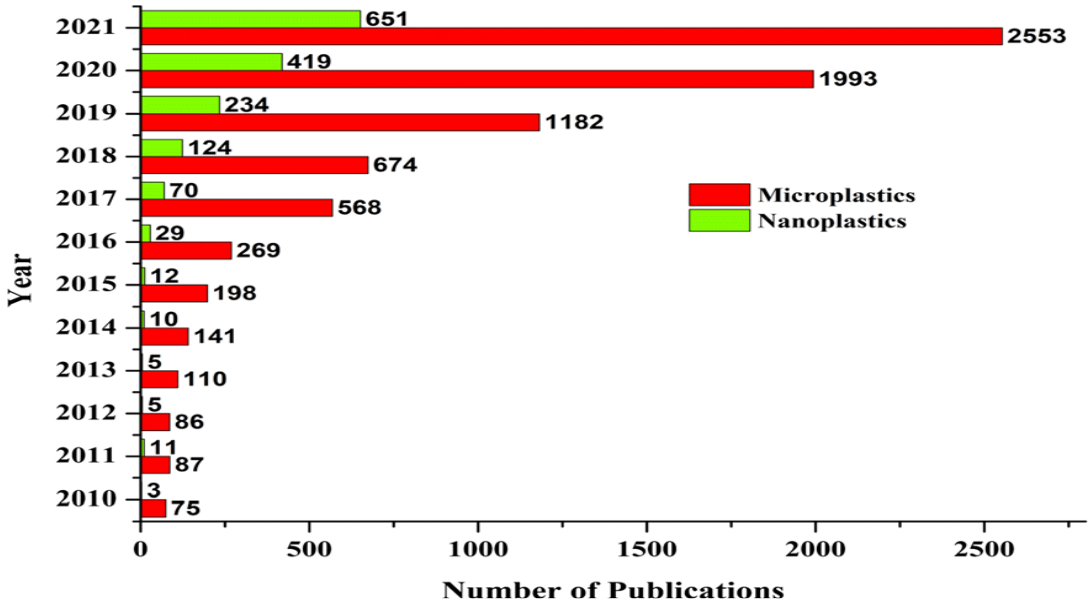

Figure 1 The aggregate sum of yearly scholarly articles issued concerning MPs and NPs (Kiran et al., 2022)

4.1.2 MPs and NPs Environmental Impact

4.1.2.1 Physical Impact on Aquatic Life and Drinking Water Quality

The ingestion of MPs by aquatic organisms, such as fish, zooplankton and other marine life which are a part of the food chain, has been extensively studied. Bank et al. (2022) and Cole et al. (2011) in their reviews on impact of MPs in the marine environment observed that these plastic particles can cause physical harm, including internal abrasions and blockage in the digestive tract which can lead to false satiation, resulting in reduced feeding and stunted growth. Furthermore, when smaller organisms ingest MPs, these plastic particles can move up the food chain, ultimately affecting larger predators and humans who consume them as

food. These findings highlight the widespread distribution of these plastics in various aquatic environments and the significant risk posed to aquatic life and human health due to their ingestion and subsequent food chain transfer.

4.1.2.2 Chemical Impact and Contaminant Vectoring

An additional environmental concern with MP and NPs is that these particles can adsorb pollutants in water including metals (Gao et al., 2021), persistent organic pollutants (Browne et al., 2013) and pathogens (Nath et al., 2023). These plastics can be easily ingested by organisms which will further have a toxicological impact. Studies by Shen et al., (2019) buttress the point that the presence of MPs in the environment is worsened since they can also act as a vector for various pollutants and pathogens.

4.1.2.3 MP and NP in Drinking Water

MPs and NPs are distributed into the aquatic environment by runoff, wind dispersion or direct disposal. The extent of contamination in the various water bodies is influenced by population density, industrial activities, and solid and liquid waste treatment efficiencies. It can be inferred that most of these plastic particles in the marine environment were conveyed by rivers and streams that were polluted by human activities.

Thomas et al. (2024) recorded a range of MP concentrations from 0.83 to 1.4 particles/L in western Lake Superior. Harbor areas in the lake had concentrations from 0.62-3.32 particles/L due to proximity to urban areas and river outlets. Mason et al. (2020) reported 230,000 plastic particles/km^2 and 45,000 plastic particles/km^2 for Lakes Ontario and Erie, respectively. Baldwin et al. (2020) observed a MP concentration of 0.44 to 9.7 particles /m^3 in Lakes Mead and Lake Mohave. In a review on MP pollution, Lin et al. (2024) summarized the results from 228 publications on the concentration of MPs in surface waters in Asia

reporting that eleven of the rivers exceeded 100,000 MP particles/m^3 in areas known for high pollution of plastic waste. Yang et al. (2024) summarized the world-wide distribution of MPs in drinking water sources.

4.1.2.4 Health Implications

Kiran et al. (2022) highlighted the necessity for comprehensive risk assessment to evaluate the exposure pathways and potential health effects related to the ingestion of MPs through food and water sources. Additionally, Allen et al. (2022) stressed the importance of understanding the long-term effects of NPs exposure on human health, calling for more research to fill this knowledge gap. Research consistently emphasizes (Chae & An, 2017; Nath et al., 2023; Yee et al., 2021) that these plastic particles are of environmental concern and their impacts need to be mitigated to save aquatic and terrestrial life.

4.1.3 Type and Properties of Plastic

MPs and NPs are composed of various polymer types that exhibit distinct physical, chemical and ecological properties that influence their impact and behaviour in various environments. Some of the known plastic types found in the environment and are researched are Polyethylene Terephthalate (PET or PETE), Polyvinyl Chloride (PVC), Polyethylene (PE), Polypropylene (PP), and Polystyrene (PS).

4.1.3.1 Polyethylene Terephthalate (PET or PETE)

With a density of 1.38 g/cm^3, PET, a material used in beverage bottles and synthetic fibers, sinks in water. It is frequently discovered in aquatic systems impacted by wastewater discharge as fibers from synthetic apparel (Browne et al., 2011). It is also resistant to environmental deterioration and is reasonably stable.

4.1.3.2 Polyvinyl Chloride (PVC)

PVC is denser than most other plastics (1.3-1.45 g/cm³), which causes it to be submerged in water bodies and adsorb to sediments as reported by Kudzin et al. (2024). Cole et al. (2011) in their review observed that PVC particles can settle in benthic zones, posing risks to bottom-dwelling organisms. It is commonly found as MPs from construction debris and medical waste. PVC contains a high chlorine content, making it more resistant to oxidation and weathering.

4.1.3.3 Polyethylene (PE)

PE is the most produce and used plastic globally and is the most found plastic pollutant in various environments. It has a density of (0.91-0.96 g/cm³) which makes it float on the water surface. Fragments of PE are mostly irregularly shaped. The relatively hydrophobic nature of PE enhances its ability to adsorb hydrophobic contaminants in water as reviewed by Cole et al. (2011).

4.1.3.4 Polypropylene (PP)

PP is frequently used in textiles, automobile components, and packaging. It is slightly higher in density (0.85-0.92 g/cm³) than PE. In addition, it is resistant to a wide range of bases, acids, and solvents. The fact that it has slightly higher hydrophilicity than PE, and like all other plastics, its surface can adsorb pollutants, although less effectively (Koelmans et al., 2017). When marine species consume PP particles, the effects on their bodies and environments are comparable to those of PE.

4.1.3.5 Polystyrene (PS)

PS is mostly used in disposable food container packages, insulation materials, construction, and other goods packaging. It is lightweight and brittle, leading to the formation of small,

easily dispersed fragments. PS is hydrophobic and can adsorb pollutants such as polycyclic aromatic hydrocarbons (PAHs) as reviewed by Wright et al. (2013). It also contains residual styrene monomers, that are present as a result of the manufacturing process rather than being formed through aging which are potential human carcinogens. PS particles are found in both marine and freshwater environments, often ingested by marine organisms.

4.1.4 Size and Shape of MPs and NPs

As the study of MPs and NPs is increasingly gaining attention due to their adverse impact on the environment, an aspect of understanding their behaviour, impact and mitigation is their shape and size. As the sizes of MPs and NPs are defined, the shape of MPs is defined as fragments, pellets or granules, film, foam, and fibres (NOAA Marine Debris Program, 2015). The size and shape of the MPs and NPs are key factors that influences their environmental behaviour, impact, and removal efficiency in water treatment. NPs with their high specific surface area and strong environmental interactions pose greater ecological risks as compared to MPs. The size and shape of MP and NP will influence removal efficiency in water treatment, highlighting the need of strategies to address the various forms of plastic pollutions.

4.1.5 Surface Properties of MPs and NPs

The surface properties of MPs and NPs are key influencers in their behavior and interactions with the environment. These properties include surface area, surface charge and surface morphology. The following is a general discussion of how these properties influence environmental behaviour; how these properties influence the effectiveness of removal of MPs and NPs from water is discussed in detail in sections 4.1.8.1.1.2.

4.1.5.1 Surface Area

An important characteristic of MPs and NPs that influences their interaction with the environment is their surface area. Chen et al. (2023) summarized in a review article that NPs possess a higher specific surface area than MP increasing the reactivity of the NPs and enhancing its adsorption properties to heavy metals and organic pollutants. NPs high surface area influences and also exhibits Brownian motion that leads to an enhanced interaction with its surrounding environment and can lead to increased aggregation compared to MPs. The study also observed that NPs which have a robust interaction with their environment has more detrimental impacts on the ecosystem.

4.1.5.2 Surface Charge

Another key characteristic that affects how MPs and NPs behave in the environment is their surface charge. MPs and NPs surfaces can be positive, negative, or neutral. The charge will influence the extent of surface interactions with other pollutants, aggregation, and bioavailability. Aging of MPs and NPs and surface coating alter surface properties.

4.1.5.3 Surface Morphology

The porosity and surface roughness of MPs and NPs plays a significant role in how they interact with the environment. A higher surface roughness on MPs and NPs can increase their ability to adsorb substances like heavy metals and other organic substances. Scanning Electron Microscopy (SEM) and Atomic Force Microscopy (AFM) have been extensively used to characterize these features of MPs and NPs.

4.1.6 Properties and Water Treatment Considerations

MP and NP have unique properties differentiating them from natural suspended and colloidal particles in water. The removal of MPs and NPs from water systems poses

significant challenges due to their sizes and surface properties. The traditional treatment technologies, including coagulation, flocculation, settling, and filtration, were designed for removing various suspended solids and colloidal material rather than MPs and NPs from drinking water and wastewater. Natural solids, such as clay minerals, Fe and Mn oxides, carbonate minerals and organic matter are typically negatively charged under environmental conditions which readily coagulate when a coagulant is applied. MPs and NPs may however have surface properties that significantly impact their removal efficiency from a water treatment facility. These properties include surfaces that are hydrophobic or are positively charged limiting removal with traditional coagulants. As certain MPs and NPs have very low densities, thereby causing it to float on water, their buoyant nature complicates their removal from water during the treatment processes such as settling or sedimentation. These unique physical and chemical plastic characteristics can influence the overall removal efficiency from water treatment systems necessitating specialized approaches to effectively address the diverse behaviors of MPs and NPs in drinking water sources.

4.1.7 Challenges in Detection and Quantification

Understanding the distribution, behavior and effects of MPs and NPs in environmental samples requires their detection and quantitation which has been challenging due to the size of these particles, different chemistries, and the complexity of environmental samples. A variety of sophisticated analytical techniques for identifying and describing MPs and NPs are included in Kundu et al. (2021) review. The Matrix-Assisted Laser Desorption/Ionization Time-of-Flights Mass Spectrometry (MALDI-TOF MS) enables a rapid identification of MPs based on their mass spectra. Raman spectroscopy provides insight into the chemical composition and structure of the plastic particles. The utilization of Inductively Coupled

Plasma Mass Spectrometry (ICP-MS), specifically single-particle ICP-MS, yields significant insights to the chemical composition, size distribution and particle mass concentration. Furthermore, the Field Flow Fractionation (FFF), contributes to a thorough assessment of plastic contamination in aquatic habitat by sorting and sizing environmental particles which includes MPs and NPs.

Mason et al. (2020) used Scanning Electron Microscopy with Energy-dispersive X-ray Spectroscopy (SEM/EDS) providing detailed images and elementary data differentiating between plastics and non-plastic materials. Fourier Transform Infrared Spectroscopy (FTIR) was used to determine the polymer makeup of the larger MP particles by comparing their spectrum to records of known polymer spectra. The integrations of FTIR and SEM/EDS analysis highlights the value of using a variety of analytical methods in studying MP pollution in the aquatic environment. Advanced and multiple analytical techniques are essential for precise identification and quantification of MPs and NPs to assess their environmental distribution and behavior in the environment.

4.1.8 Current Removal Method for Various Pollutant from Water

The development and implementation of an effective removal strategy for MPs and NPs is crucial to ensuring safe drinking water. There are existing technologies in wastewater and drinking water treatment for removal of suspended solids and colloidal material, but these technologies may not be adequate for removal of MPs and NPs.

4.1.8.1 Chemical Coagulation (CC)

Chemical coagulation (CC), also known as traditional or conventional coagulation, is the fundamental process of treating water for removing suspended particles and other

impurities. Various coagulants such as alum (aluminum sulfate), ferric chloride, and polymers are used to destabilize and aggregate particles in the water.

4.1.8.1.1 Fundamental Of Coagulation and flocculation Process

4.1.8.1.1.1 Chemical Coagulation and flocculation (CCF)

CCF is a critical step for removing suspended particles from water being it drinking water or wastewater. It involves the addition of chemical coagulants such as aluminum sulfate, ferric chloride and polymers such as polyaluminum chloride (PAC). CCF is also able to remove organic matters, metals, and emerging contaminants to some degree. It is a crucial step in ensuring the quality and safety of the treated water. However, the effectiveness of CCF at removing MPs and NPs remains largely unknow. CCF adheres to three primary steps or principles:

1. Coagulant administration: After the chemical coagulant is applied to the water, the coagulant spreads out quickly.
2. Destabilization of particles: Particles come together due to the repulsive forces being suppressed by neutralizing the charges on them.
3. Formation of floc: Larger flocs formed by destabilized particles are further removed by sedimentation and filtering.

4.1.8.1.1.2 Coagulation Mechanism

In CCF, it is essential to understand how coagulants interact with the particles in the water and how this interaction results in the production of bigger flocs that are easily separated from the water treated. In the treatment of water using CCF, several processes come together to destabilize particles and facilitate particle aggregation making it easier to be removed from the water. Removal of MPs and NPs, being emerging pollutants, were not

considered during the develpoment of CCF. Crittenden et al. (2012) reports on the various mechanisms that takes place during chemical coagulation of naturally occurring pollutant such as organic matter, metals, pathogens, etc. These mechanisms are compression of the electrical double layer (section 4.1.8.1.1.1.1.1), adsorption and charge neutralization (section 4.1.8.1.1.1.1.2), aggregation and interparticle bridging (section 4.1.8.1.1.1.1.3) and enmeshment in a precipitate (sweep floc) (section 4.1.8.1.1.1.1.4).

4.1.8.1.1.2.1.1 Compression of the Electrical Double Layer

Compression of the electrical double layer (EDL) that envelops the charged particle in water is one of the CCF removal processes. The EDL is formed when negatively charged colloidal or particles attract a layer of positive counter ions from the surrounding water. This results in the formation of two regions, the first being the Helmholtz layer also known as the fixed charge (Stern) layer. The Stern layer is the region near the surface of a charged particle where the counter ions are directly and tightly adsorbed or bound on the particle surface forming a stable layer which is approximately 5 Å thick (Figure 2). Beyond this layer is an electric field that attracts excess cations and repelling anions. This is known as the diffuse ion layer. This layer extends from the Stern layer to the bulk solution where electroneutrality is accomplished. This layer can measure up to 300 Å depending on the characteristics of the water. The diffuse and Stern layer are termed the electrical double layer.

The stability of colloids in water as explained by the Derjaguin, Landau, Vervey, and Overbeek (DLVO) theory (Equation 1), as described by Ghernaout (2020), which considers the total potential energy function (V_T) as the sum of the three force: the attractive van der Waals force (V_A) (Equation 2), the potential energy attributed to the solvent (water) (V_s), and

the repulsive force due to the EDL (V_R) (Equation 3). The energy barrier that is derived from the sum of these forces prevents colloids from approaching each other if repulsive force dominate. The barrier aids in the dispersion of the colloids until their charges and the EDL is significantly diminished allowing effective coagulation and particle removal during the process of treating the water.

$$V_T = V_R + V_A + V_S \quad (1)$$

$$V_A = A / 12\pi D^2 \quad (2)$$

$$V_R = 2\pi\varepsilon\alpha\, \xi^2 e^{-kD} \quad (3)$$

were A is the Hamaker constant, D is the distance between particles, ε is the solvent permeability, α is the particle radius, ξ is the zeta potential and K is the function of the ionic composition.

In water treatment, the EDL is compressed when a coagulant is applied to water and interacts with the charged particles. Particles assemble more easily because of this compression which lessens the repulsive forces between them forming large flocs that settle out of the water.

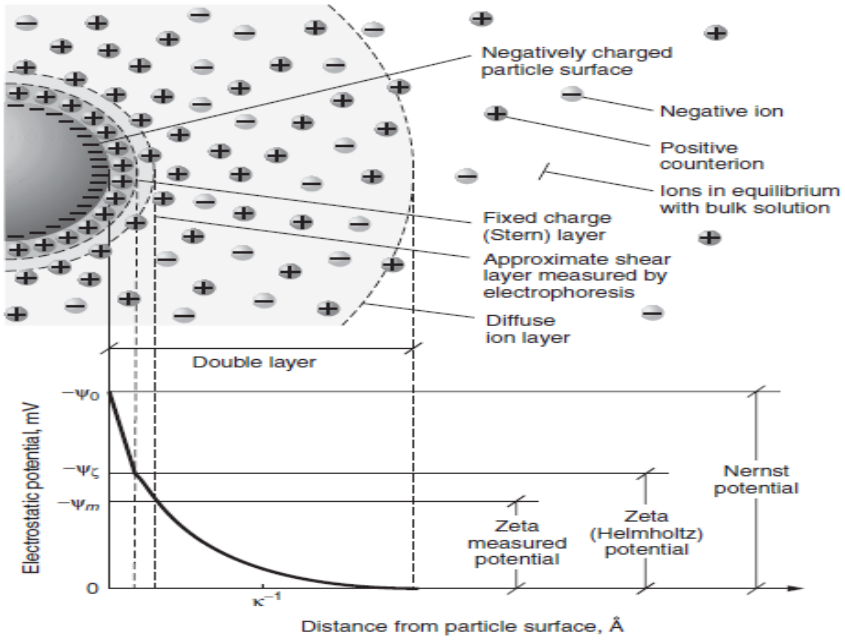

Figure 2 The structure of the electrical double layer includes the potential measured at the shear plane, which is referred to as the zeta potential. This shear plane is usually located within the diffuse layer (Crittenden et al., (2012)

4.1.8.1.1.2.1.2 Adsorption And Charge Neutralization

Particle adsorption and charge neutralization is also a significant mechanism in chemical coagulation. It involves the destabilization of particles through the adsorption of oppositely charged ions onto a particle surface making them more likely to aggregate. Most particles in natural waters like clay, humic acid and bacteria are negatively charged especially in a neutral pH range. On the surfaces of these particles, coagulants can adsorb and neutralize the charges by forming hydrolyzed or prehydrolyzed metal salts and cationic polymers. This process is driven by various forces including Van der Waal forces, electrostatic interactions and chemical bonding. The negatively charged particle surface is covered with the coagulant (Figure 2) neutralizing the charged particle. Cationic organic polymers often used in conjunction with inorganic coagulants can effectively neutralize the negative charge on particles leading to the formation of flocs. The optimum coagulant dose is typically reached

when the particle surface is partially covered, usually less than 50 %. Polymers with high charge density and moderate molecular weights adsorb on the particle surface, creating a patch that facilitates charge neutralization and subsequent floc formation.

4.1.8.1.1.2.1.3 Aggregation and Interparticle Bridging

Coagulants not only neutralize the surface charge of the particles but also promote aggregation of the particles by means of interparticle bridging. Coagulants have the tendency to create bridges between particles by adhering to their surfaces and strengthening the aggregates stability (Ghernaout, 2020; Wang et al., 2021) (Figure 3). The creation of bigger flocs that easily settle or filter out of the water is encouraged by these bridges. Interparticle bridging is a key factor in raising the effectiveness of chemical coagulation (Figure 3). This enhances the overall effectiveness of water treatment by causing the production of more stable and bigger flocs that can be easily removed from the water.

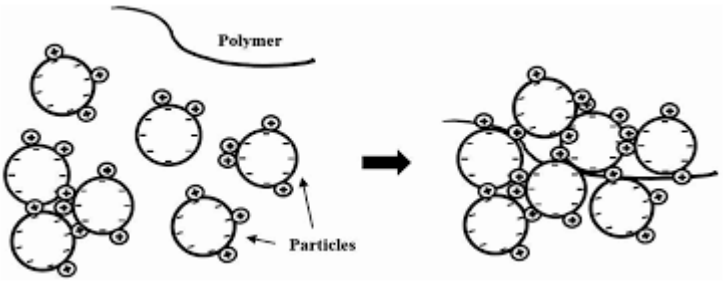

Figure 3 Diagram of polymer based bridging model of interparticle bridging of flocs (Ho et al., 2020)

4.1.8.1.1.2.1.4 Enmeshment In a Precipitate (Sweep Floc / colloidal entrapment)

The process that can result in the entanglement of particles inside the precipitate structure is an occurrence known as the sweep floc. Coagulants react in water to generate insoluble hydroxide precipitates which occur at a pH between the ranges of 6.8 to 8.2 which can

capture dissolved components, colloids and smaller particles to remove them from water (Crittenden et al. 2012), Ghernaout 2020). In water treatment procedures, sweep floc mechanism improves the removal of impurities, hence augmenting the overall efficacy of the chemical coagulation.

4.1.8.1.1.3 Limitation Of Chemical Coagulation and Flocculation in MPs and NPs Removal

Chemical coagulation has been an established technique for removing suspended particles, organic matter, and other contaminants from water. Removal of MPs using CCF has been met with mixed results (Table 1). Lapointe et al. (2020) using jar tests and natural surface water examined the removal efficiency of CCF on PE and PS microspheres and PEST microfibers. The pristine PE microspheres (15 and 140 µm) demonstrated a removal efficiency of 82% due to their homogeneous and inert surfaces which limits their ability to interact with the aluminum coagulant. In contrast, the weathered PE had 99% removal efficiency. Weathering of the MPs, caused by UV radiation, and the presence of organic matter raised the surface roughness and functional groups (hydroxyl, carboxyl, vinyl) on the MP, which enhanced contact with the coagulant. Showing similar removal efficiency as PE, PS microspheres removal efficiency depended on their surface properties. PEST fibers demonstrated the best removal efficiency (97%) with alum and aluminum chlorohydrate (ACH). PEST aggregation was through the bridging mechanism and the presence of the ester groups enhanced the fibers attachment to aluminum hydroxide species resulting in higher removal efficiency. The PEST fibers interacted with the coagulants more effectively than the microspheres due to their large surface area.

In contrast to Lapoint et al (2020), regardless of the sizes of PE bead (10 to 125 µm), Zhang et al. (2020) observed the maximum removal of 2 % (10-20 µm) using alum coagulant.

Addition of a coagulant aid improved removal of 45-53 µm fraction to 13.6 %. The coagulation efficiency increased to 16.5 % when the MPs (45-53 µm) were coated with a biofilm. Another research group (Zhang et al., 2022) reported removal of 86% of PS NPs (50 and 100 nm) and 89-91% for 1000 and 500 nm MP using Al chlorohydrate. The addition of a nonionic polymer (PAM) increased the removal of the 500 nm MP to 98.5%.

Wang et al. (2020) observed that the plastic type, size, and surface properties make CCF ineffective in a full-scale drinking water treatment plant. Coagulation and sedimentation in the water treatment plant had an overall removal efficiency of 82.1 % to 88.6 %. More specifically, the larger MP sizes (>10 µm) easily settled during sedimentation hence their higher removal efficiency. Nevertheless, MPs (1–10 µm) had a removal efficiency from 28.3 % to 47.5 %. As the plastic shape also is said to influence the removal efficiency, PET being fibrous in nature had a relatively high removal efficiency but the pristine plastics such as the PE showed low removal efficiency due to their surface properties. Summarized in Table 1 are some studies evaluating the removal efficiency of different polymers using coagulation and flocculation in water treatment. Polymers like PE and PS of varying sizes and conditions showed removal efficiencies ranging from 2 % to 99 %, depending on the coagulant used. Pristine and weathered plastics of varying sizes exhibited different removal efficiencies. Alum, PAM and PAC were either used individually which had low removal efficiency or were used in combination to achieve a much higher removal efficiency.

Table 1 Summary of MPs and NPs removal efficiency using chemical coagulation

Study	Polymer Type	Size Range	Coagulant and flocculant	Removal Efficiency (%)	Notes
Lapointe et al. (2020)	PE (Pristine) 500 particles/L	140 µm	Alum +Aluminum chlorohydrate+ Ballast medium+Polyacrylamid, Higher alum conc. (2.73 mg/L)	82%	The jar test simulates water treatment processes to evaluate coagulation and flocculation efficiency for removing MPs and other contaminants.
	PE (Pristine) 500 particles/L	15 µm		89%	
	Weathered PE			99%	
	PEST Fibers			99%	
	PS	140 µm (microspheres)		84%	
Zhang et al. (2020)	PE Bead (7000 particle/L)	10-20 µm	Alum	2%	The jar test simulates water treatment processes to evaluate coagulation and flocculation efficiency for removing MPs and other contaminants.
	PE Bead (2000 particle/L)	45-53 µm	Alum + Coagulant Aid	13.6%	
	PE Bead (2000 particle/L)	45-53 µm	Alum + Biofilm Coating	16.5%	
	PS NPs	50 and 100 nm	Al chlorohydrate	86.00%	
	PS MPs	1000 and 500 nm	Al chlorohydrate	89-91%	
Zhang et al. (2022)	PS NPs	50 nm	Polyaluminum chloride (PAC) (0.4 $g \cdot L^{-1}$) and polyacrylamide (PAM) (20 $mg \cdot L^{-1}$)	85.6 ± 0.2%	Coagulation tests conducted using a beaker test setup; evaluated removal efficiency through fluorescence spectrophotometry
	PS NPs	100 nm		86.3 ± 0.2%	
	PS MPs	500 nm		91.0 ± 0.7%	
	PS MPs	1 µm		89.3 ± 1.1%	
Wang et al. (2020)	PET, PP, PE	>10 µm	Polyaluminum chloride and polyacrylamide	82.1% to 88.6%	Full scale DWTP MP sizes (>10 µm) easily settled during sedimentation without filtration
	PET, PP, PE, PS	1–10 µm	Polyaluminum chloride and polyacrylamide	28.3% to 47.5%	
	PET	1– > 100	Polyaluminum chloride and polyacrylamide	87%	PET being fibrous had relatively high removal efficiency
	PE and others	Various	Polyaluminum chloride and polyacrylamide	81 % to 84 %	Pristine plastics showed less removal efficiency due to surface properties

4.1.9 Electrocoagulation

Electrocoagulation (EC) is a water treatment technology that has gained considerable attention in recent years due to its efficiency in the removal of contaminants from water, mostly wastewater (Akarsu & Deniz, 2021; Mahvi & Bazrafshan, 2007; Pawak et al., 2023; Shen et al., 2022). The EC process involves the application of electric current to electrodes immersed in the water, which subsequently leads to various electrochemical reactions to destabilize and aggregate contaminants, facilitating their removal from the water through processes such as coagulation, flocculation and precipitation. EC is used in the removal of metals, organics, suspended solids, MPs and NPs (Akarsu & Deniz, 2021; Mahvi & Bazrafshan, 2007; Pawak et al., 2023; Shen et al., 2022). EC application in the treatment of water for drinking is limited due to perceived high cost, infrastructure needs, and ongoing research needs about it benefits and capabilities compared to the conventional treatment methods (Chen et al., 2022; Harif et al., 2012; Shen et al., 2022).

4.1.9.1 Mechanisms of Electrocoagulation

The mechanism of both CCF and EC are similar. The slight difference include: possible flotation in EC and the mode of introducing the coagulant into the water. CCF uses chemical coagulant whereas EC produce metal ions in-situ through electrochemical reaction.

4.1.9.1.1 Metal Ion Formation:

The metal ions released from the electrodes during the EC process destabilizes the contaminants in the water through the same mechanisms as described for CCF. Aluminum or iron is commonly used as the anode due to their ability to generate trivalent metal ions (Al^{3+} and Fe^{3+}) (Figure 4). When the negatively charged species in the water comes into

contact with the metal ions or metal hydroxide (depending on solution pH), they agglomerate and form larger flocs which then can be easily removed through sedimentation. During the EC process the metal ions are released into the water, where coagulant formed, and bubbles generated aids in the pollutant removal through flotation as well (Figure 4). These are the essential mechanisms that leads to the destabilization, aggregation, and separation of contaminants (sedimentation and flotation) in the EC system. The primary reactions for aluminum are as follows.

Anode reaction (Oxidation):

Aluminum (Al)

$$Al(s) \rightleftharpoons Al^{3+}(aq) + 3e- \quad (4)$$

Cathode reaction (Reduction):

$$3H_2O + 3e- \rightleftharpoons 3/2H_2 + 3OH^- \quad (5)$$

The hydroxide ions generate at the cathode contribute to the neutralization and precipitation process.

The metals precipitation:

$$Al^{3+}(aq) + 3OH-(aq) \rightleftharpoons Al(OH)_3 \quad (6)$$

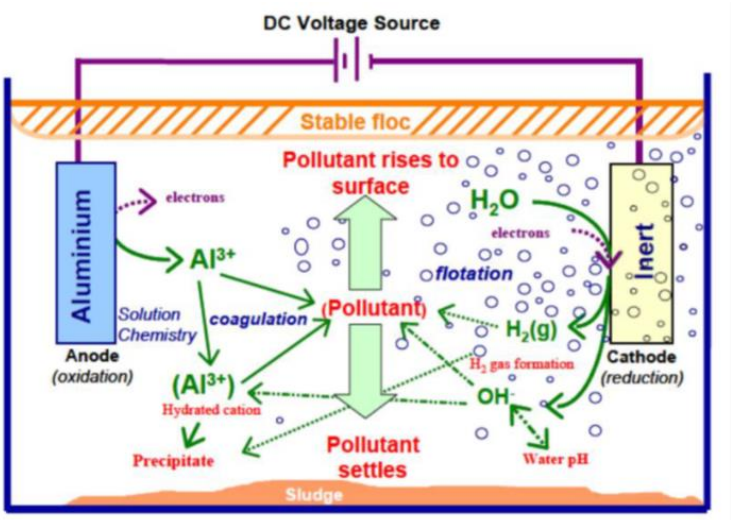

Figure 4 Reactions that take place inside an electrocoagulation reactor (Holt, 2002).

4.1.9.1.2 Hydrogen and Oxygen Evolution:

Akarsu et al. (2021), Holt (2002), Shen et al. (2022) and other researchers have investigated the EC process and its multifaceted effects. In addition to metal ion formation, EC induces the evolution of hydrogen gas at the cathode and oxygen gas at the anode (which competes with Al dissolution). During the EC process (Figure 4), H_2 gas is generated at the cathode, where electrons are transferred to water molecules, leading to the formation of hydrogen gas and hydroxide ions (Equation 5). At the anode, hydroxide ions can be oxidized to form oxygen gas and water (Equation 7), although is reaction is often not detected under relatively low cell potential (Holt 2002).

$$4OH^- \rightarrow O_2 + 2H_2O + 4e^- \qquad (7)$$

Furthermore, hydrogen and oxygen evolution play crucial roles in maintaining electrode stability and performance, preventing electrode passivation, and ensuring sustained treatment efficacy (Holt, 2002; Shen et al., 2022). However, Hossain et al. (2013) noted in their study on textile wastewater that higher current densities may escalate gas evolution

rates, albeit excessively high currents could lead to gas bubble accumulation and reduced treatment efficiency. Moreover, the choice of electrode material, pH, and electrolyte composition significantly influences gas evolution kinetics and treatment performance (Holt, 2002), emphasizing the importance of meticulous control and optimization in EC systems.

4.1.9.1.3 Floc Formation

As metal ions react with hydroxide, they form insoluble hydroxide precipitate, which further hetero-aggregate with suspended particles forming flocs. Research by Akarsu & Deniz (2021) and Pawak et al. (2023) support that floc formation emerges as a pivotal aspect of EC in NPs removal from synthetic wastewater. Through the agglomeration of coagulated particles, including NPs, into larger flocs, the process facilitates effective separation of solids from the solution.

In the study of Holt (2002), the process of floc formation during EC is intricately linked to the interactions between coagulants, pollutants, and electrolytic gas bubbles. The destabilization of colloidal particles occurs as metal cations are released from the sacrificial anode, leading to the neutralization of charged pollutants through mechanisms like charge neutralization, double layer compression, and sweep coagulation. These interactions promote the aggregation of particles into larger flocs. Factors such as the type of electrode, current density, pH, and mixing conditions play crucial roles in determining the characteristics of the formed flocs, including size, density, and structure. Optimal floc formation is essential for efficient pollutant removal, as larger and denser flocs settle more rapidly, aiding in the separation of contaminants from the treated water.

4.1.9.2 Electrocoagulation Advantages Over CCF

1. No application of chemical coagulant: coagulants are generated in-situ, and this eliminates the usage of chemical coagulant reducing the problem of chemical residue and handling (Akarsu et al., 2021; Akarsu & Deniz, 2021; Tsai et al., 2023).
2. Efficient contaminant removal: EC can achieve higher removal efficiency for various contaminants (Akarsu et al., 2021; Akarsu & Deniz, 2021; Shen et al., 2022).

4.1.9.3 Challenges and Limitations

1. Anode electrode passivation: the development of a passive coating on the surface of the electrode, which might hinder the dissolution of the electrode material and reduce the EC efficiency (Pawak et al., 2023; Shen et al., 2022).
2. Energy consumption: high energy consumption is a challenge especially in systems operating with a lower number of electrodes, since the amount of energy used is influenced by the number of electrodes (Shen et al., 2022).
3. pH and conductivity sensitivity: the performance of the EC process is largely influenced by factors such as pH, conductivity and water chemistry which requires careful control and operational conditions for an optimum performance (Akarsu et al., 2021; Akarsu & Deniz, 2021; Pawak et al., 2023; Shen et al., 2022).

4.1.9.4 Previous Applications of Electrocoagulation for MP and NP Removal from Water

Table 2 provides a summary of studies done using EC under various operating conditions, water chemistries and plastic types for the removal MPs and NPs from wastewater. Shen et al. (2022) systematically evaluated the effectiveness of EC in simulated wastewater altering the type of electrodes (Al-Cu vs Fe-Cu), initial pH (pH = 3-10), electrolyte concentration (sodium sulfate 0.01 to 0.1 M), applied voltage (5, 10, 15V), MPs types (PE,

polymethylmethacrylate (PMMA), cellulose acetate (CA), and PP) and concentration (0.05 to 1 g/L). Each parameter was altered individually holding all other variables under standard conditions of 0.5 g/L of the MPs, 0.05M sodium sulfate, pH of 7.2, applied voltage of 10 V. These plastics exhibited negative charge surfaces under neutral conditions which aids their interaction with the positively charged coagulant. The removal efficiencies were reported as 98.6% for PE, 99.1% for PMMA, 99.9% for CA, and 99.9% for PP under optimal conditions of pH of 7.2, Al electrode, applied voltage of 10 to 15V, and electrolyte concentration of 0.05M to 0.1M. Comparing granular MPs (PE and PMMA), and fiber MPs (CA and PP), the fibrous MPs showed greater removal efficiency. Using Fe-Cu electrode the removal efficiencies were 71.6% for PE, 58.6% for PMMA, 85.4% for CA, and 82.7% for PP.

Akarsu & Deniz (2021) using the EC /electroflotation (EF) process to remove COD, anionic surfactants, color, and MPs from laundry wastewater utilized a combination of electrodes (Al–Al, Al–Fe, Fe–Fe, and Fe–Al), initial pH (5–9), current intensity (0.54–2.16 A), and treatment duration (15–60 minutes). Seeking to optimize the process, the response surface methodology was used and was observed that with an initial pH of 9, reaction time of 60 minutes, current of 2.16 A, and the Fe–Al electrode combination resulted the best removal efficiency for COD, anionic surfactants, colour, and MPs were 91 %, 94 %, 100 %, and 98 %, respectively.

Akarsu et al. (2021) examined the effectiveness of EC/EF and membrane filtration processes in removing MPs from wastewater comparing laboratory-scale results with a full-scale operating treatment plant. Membrane filtration is a technique that uses a semi-permeable membrane in the filtration process, which filters out materials, molecules, or particles according to their charge, size, shape, or other characteristics removing bacteria, suspended

particles, and MPs. The study investigated the efficacy of different electrode combinations (Fe-Al and Al-Fe) in the EC/EF process and optimizing the parameters current density (10–20 A/m²), initial pH (4.0–10.0), and reaction time (0–120 minutes), to achieve maximum removal efficiency of PE (150 µm) and PVC (250 µm) particles in water. From their findings, the maximum removal efficiencies with membrane filtration recorded was 100 % for both polymer types and were achieved using the Al-Fe electrode combination, an initial pH of 7, a current density of 20 A/m², and a reaction time of 10 minutes. They also observed that the conventional full scale treatment plant showed variable MP removal efficiencies, ranging from 2% to 81.6%. The lower efficiency of the full-scale system being due to failure of the membrane in removing plastic fibers.

Tsai et al. (2023) studied the destabilization of PS-NPs with sizes of 90 nm, 200 nm and 500 nm (Table 3) using Fe EC. The study revealed varying removal efficiency with respect to size which was largely influenced by surface properties. In this study the PS-NPs were coated with surfactants Sodium Dodecyl Sulfate (SDS) which is negatively charged or Cetyltrimethylammonium Bromide (CTAB) which is positively charge. For the 90 nm PS-NPs, SDS coated had a removal efficiency of 85.3 % but only 1 % for the CTAB coated. For the 200 nm and 500 nm, their removal efficiencies were 82.8% and 74.7% respectively for SDS coated, 77.9 % and 54.8 % for CTAB coat respectively. The study revealed different removal mechanisms for SDS-NPs and CTAB-NPs during Fe EC. SDS-NPs were effectively removed through charge neutralization and adsorption onto the Fe flocs, achieving 85.3 % removal of 90 nm plastic particles. In contrast, CTAB-NPs was removed by the enmeshment mechanism with much lower removal efficiencies, thus less than 1 % for 90 nm and between 50 % to 76% for 200 nm and 500 nm. The presence of Fe floc was essential enhancing SDS-NP

removal while limiting CTAB-NP effectiveness due to the combination of charge repulsion and hydrophilic interactions.

Table 2 Summary of electrochemical treatment studies for MPs and NPs removal

Study	Electrode Material	Time	Electrode Distance (ED)	Current Density	Voltage (V)	Temperature	Current	Electrolyte (El)	Electrolyte Concentration	Electrical conductivity	Turbidity (NTU)	pH	Pollutant	Pollutant Concentration	Particle Size	Removal efficiency
Akarsu and Deniz. (2021)	Iron & Aluminium4	(0 - 60) min	2 cm	-	-	30 °C	0.54A - 2.16A	-	-	2.77 µS/cm	-	5, 7, 9	Organics, Microplastics	15802 MP/L (Microplastic, MP)		1. Chemical Oxygen Demand (COD): 91% 2. Color: 94% 3. Anionic Surfactant: 100% 4. Microplastics: 98%
Akarsu et al. (2021)	Iron & Aluminium	(0-120) min	2 cm	(10, 15, 20) (A/m²)	-	-	-	sodium chloride	-	3,000 + 50 µs/cm	-	4, 7, 10	Microplastics (PVC, PE)	0.2 MPs/mL		
Pawak et al. (2023)	Aluminium	(0 - 20) min (V & El, dependent) (0 - 5) hrs (No El, ED, dependent) (0 - 20) min (El, ED, dependent)	1 cm and 2cm	-	5, 10,15	(15 - 25) °C	-	sodium chloride	(10, 30, 50) mM	-	-	7.2 ± 0.3	Nanoplastics	0.35 (mg/L)		**1. Electrolyte Concentration:** 10 mM NaCl: 1.11% to 94.5% after 3 to 20 30 mM NaCl: 81.0% to 94.5% after 3 to 20 min 50 mM NaCl: 87.2% to 95.6% after 3 to 20 min **2. Applied Voltage:** 5 V: 18.7% to 96.6% after 3 to 20 min 10 V: 77.0% to 90.15% after 3 to 20 min 15 V: 87.2% to 95.6% after 3 to 20 min **3. Electrode Spacing:** 1 cm: 65.7% to 95.1% after 1 to 5 hrs 2 cm: 40.8% to 93.3% after 1 to 5 hrs
Shen et al. (2022)	Iron & Aluminium	(0 - 6) hrs	-	-	5, 10,15	(15 - 25) °C	350 mA, 600 mA, 1.52 A, 2.56 A	sodium sulfate (Na2SO4)	(0.01, 0.02, 0.05, 0.1) M	-	-	3, 5, 8, 10	Microplastics (PPMA, CA, PP, PE)	0.05 g/L, 0.1 g/L, 0.2 g/L, 0.5 g/L, 0.8 g/L, 1 g/L,	1. Polyethylene (PE): approximately 286.7 µm. 2. Polymethylmethacrylate (PMMA): approximately 6.3 µm 3. Cellulose acetate (CA) and Polypropylene (PP): The fibrous	For PE: 98.6%. For PMMA: 99.1% For CA: 99.9% For PP: 99.9%.
Tsai et al. (2023)	Iron	(0 - 30) min	1 cm	1		(15 - 25) °C	10mA	-	-	600 µS/cm	-	7.2 ± 0.2	Polystyrene Nanoplastics (surface coated with SDS-NPs or CTAB-NPs)	10 mg/L	90 nm, 200 nm, and 500 nm	1. Effect of pH : For SDS-NPs: pH 7: 85.3% for small-size (90 nm), 82.8% for mid-size (200 nm), 74.7% for large-size (500 nm) SDS-NPs. pH 5: 53% for SDS-NPs. For CTAB-NPs: pH 7: 53% for CTAB-NPs. pH 5 and other pH levels:

Table 3 Impact of particle size and surface charge on removal efficiency at pH 7.2 (Tsai et al., 2023)

Particle Size	90 nm	200 nm	500 nm	90 nm	200 nm	500 nm
Surface Coating	SDS-NPs	SDS-NPs	SDS-NPs	CTAB-NPs	CTAB-NPs	CTAB-NPs
Removal Efficiency (%)	85.3	82.8	74.7	<1	77.9	54.8

4.1.9.5 Factors Influencing MPs and NPs Removal by Electrocoagulation

Effectiveness of EC is dependent on electrode material, current density, voltage, pH, electrical conductivity. Again, Table 2 provides a summary of studies done using EC for the removal MPs and NPs from wastewater

4.1.9.5.1 Electrochemical Conditions

Current, current density and voltage are the driving force of the EC process since they determine the rate at which the coagulant is generated. Increasing the current, current density and voltage impacts the removal efficiency (Pawak et al., 2023). But it should be noted that excessive increase in these parameters causes electrode passivation.

4.1.9.5.2 Electrocoagulation Reactor Design at Lab-Scale

4.1.9.5.2.1 Component of the Reactor

4.1.9.5.2.1.1 Electrode:

4.1.9.5.2.1.1.1 Material Selection:

The core of the EC process is the type of electrode used for the process. The type of electrode material selected influences the EC performance and efficiency. In a review by Nidheesh et al. (2022) several electrodes including aluminum, iron, graphite, and stainless

steel were evaluated. Others research also explore different electrode materials impact the EC process (Bazrafshan et al., 2006; Mahvi & Bazrafshan, 2007; Shen et al., 2022). The conductivity of the electrode material controls how well electric current passes through it. A higher conductivity usually enables a more uniform current distribution which enhances the EC's process uniformity. In the water medium, mostly wastewater, the metal ions are released into the water as the electrodes undergo electrochemical reaction when an electric current is introduced (Akarsu et al., 2021; Akarsu & Deniz, 2021; Shen et al., 2022). The current through the electrodes during the EC process subjects the electrodes to wear and corrosion. To ensure a long operational lifespan and lower maintenance requirement, the electrode material's stability and durability are essential. Different materials offer their unique advantages and considerations. Al and Fe are the most used electrodes in the EC process. Al electrodes are widely used in the EC process due to their high coagulation potential and cost effectiveness (Akarsu et al., 2021). Similar to Al electrodes in terms of coagulation capabilities, Fe electrodes can likewise be utilized for EC process. Fe electrodes, however, can cause treated water to have greater residual Fe concentrations which might be problematic for some applications. Outlined are some of the reasons why Al electrodes are preferred over Fe electrodes

1. **Higher Performance:** Al electrodes removal efficiencies of MPs was within the ranges of 92 % to 99.9% whereas Fe electrodes the efficiencies was 58 % to 98% (Shen et al., 2022).
2. **Lower Energy Consumption**: Al electrodes often require less energy than Fe electrodes which contributes to increased efficiency and cost saving (Akarsu & Deniz, 2021).

3. **Faster Coagulant Formation**: EC process can remove pollutants more quickly when Al ions are released from the Al electrodes (Shen et al., 2022).
4. **Consistent Performance**: Al electrodes compared to Fe electrodes provided consistent performance during the EC process resulting in steady treatment results (Shen et al., 2022).
5. **Reduced Settled NPs Production**: The use of Al electrodes results in lower settled NPs production compared to Fe electrodes, simplifying settled NPs handling and disposal processes (Shen et al., 2022).
6. **Corrosion Resistance**: Al electrodes are more corrosion-resistant than Fe electrodes, especially in aggressive water chemistry or high chloride concentrations, contributing to longer electrode lifespan and system reliability as reported by Nidheesh et al. (2022).

4.1.9.5.2.1.1.2 Configuration

After the selection of an electrode material, its configuration also influences the removal efficiency. Electrode types, as reviewed by Nidheesh et al. (2022), can come in various forms which includes flat or plates-like, tubular or cylindrical or rod-like in shape and can also be in a mesh or perforated forms. The parallel plate is the most widely used because its set up is easy and straight forward. To ensure a uniform distribution of current, the plates are arranged parallel to each other. Tubular or cylindrical shaped electrodes configurations are used in certain reactor designs particularly in continuous flow systems to improve contact with the water. Mesh or perforated electrodes increase the surface area available for reaction and potentially enhance the efficiency of coagulation but may require a maintenance practise.

4.1.9.5.2.1.2 Maintenance Practise

1. **Cleaning**: To prevent passivation where a non-conductive layer forms on the electrode surface, reducing its efficiency, the electrodes must be cleaned regularly. This can be done mechanically (scrubbing) or chemically (acid washed) (Shen et al., 2022).
2. **Replacement:** To maintain the efficiency of and ensure a consistent coagulation performance, the electrodes must be periodically changed since the electrodes gradually dissolve over time.

4.1.9.5.2.2 Power Supply

4.1.9.5.2.2.1 Power Supply Types

The EC process is not effective without an electric power source or supply. A pivotal factor in the EC process is voltage applied. It significantly influences the removal efficiency and kinetics. Altering the voltage has a direct effect on the current density, electrolysis rate and the coagulant generation. In Nidheesh et al. (2022) review, three types of power supply were discussed. Direct current (DC), pulsed DC and alternating current (AC). The DC is the most used power source for the EC process because it provides a constant current, ensuring the stable production of coagulants. However, this power source accelerates the depletion of the electrodes. The pulse DC type of power supply alternates between the on and off state which reduces the rate of electrode passivation thereby prolonging the electrode lifespan and improving efficiency. The AC application in the EC process is less used due to the lower efficiency in coagulant generation. AC applications can be beneficial in certain applications to reduce the fouling of electrode.

Altering the voltage has a direct effect on the current density, electrolysis rate and the coagulant generation. To achieve the desired removal efficiencies and to optimize the treatment conditions, this parameter's impact on the EC process must be understood. Pawak et al. (2023) examined the effect of applied voltages (V), 5V, 10V, 15V on removal efficiency, alternating the voltages in an experiment but keeping other operating parameters constant. The outcome of the experiment showed an increase in voltage increased the removal efficiency of the NPs. Over a 20-minute reaction period, the removal efficiency was 18.7 % to 95.8 for 5 V, 77.0 % to 90.15% for 10 V and 87.2 % to 95.6 % for 15 V.

Shen et al. (2022) also investigated the impact of varying voltages (5 V, 10 V, and 15 V) on removal efficiency of MPs, specifically PE, PMMA, CA, and PP. The concentration of the four MPs were maintained at 0.5 g/L, pH of 7.2 and electrolyte concentration of 0.05 M Na_2SO_4. Removal efficiency of the MPs increased with increasing voltage. The removal efficiency for plastic types recorded were 34.3% to 73.8% for PE, 29.6% to 61.8% for PMMA, 42.6% to 71.2% for CA, and 44.4% to 73.8% for 5V and 15V, respectively, for PP after 1 hour of electrocoagulation with an Al anode and Cu anode. Furthermore, the removal efficiency was enhanced when the reaction time was extended from 4 to 6 hours.

4.1.9.5.2.2.2 Current Density

The current density applied to the electrodes influences the rate of coagulant generation and particle destabilization. Higher current densities generally result in faster coagulation kinetics but may also increase energy consumption and electrode wear. The current density influenced the removal efficiency of MPs in wastewater influent (Figure 5) (Akarsu et al., 2021), with 100 % removal with current density of 15 and 20 A/m^2. Furthermore, at the

lowest current density, it was noted that the flocs were destabilized due to insufficient ionization of aluminum. Perren et al. (2018) (Figure 6) used current densities of 11, 15, 19, and 23 A/m^2 for the removal of MPs but reported that the there was no statistically significant effect; sufficient coagulant was produced by the Al electrode under all current densities tested. The Akarsu study provides no statistical analysis of their data.

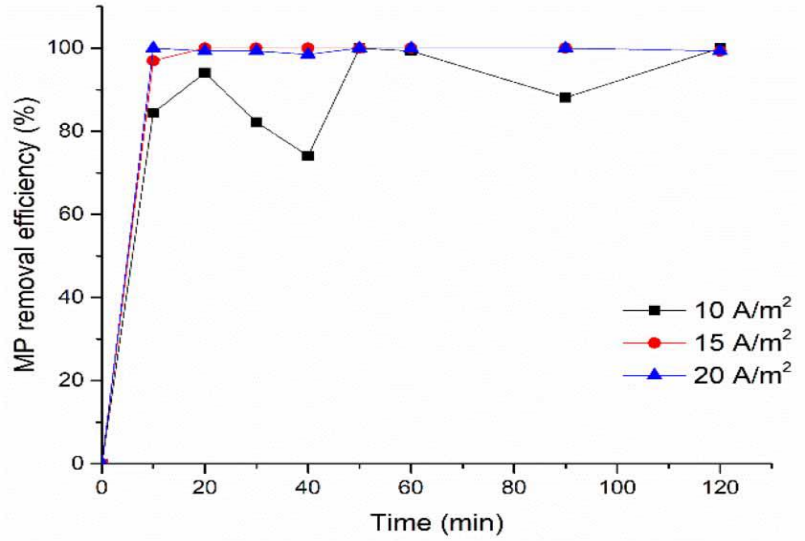

Figure 5 Impact of current density on the removal efficiency of MPs over time using Al-Fe electrodes, pH 7 (Akarsu et al., 2021)

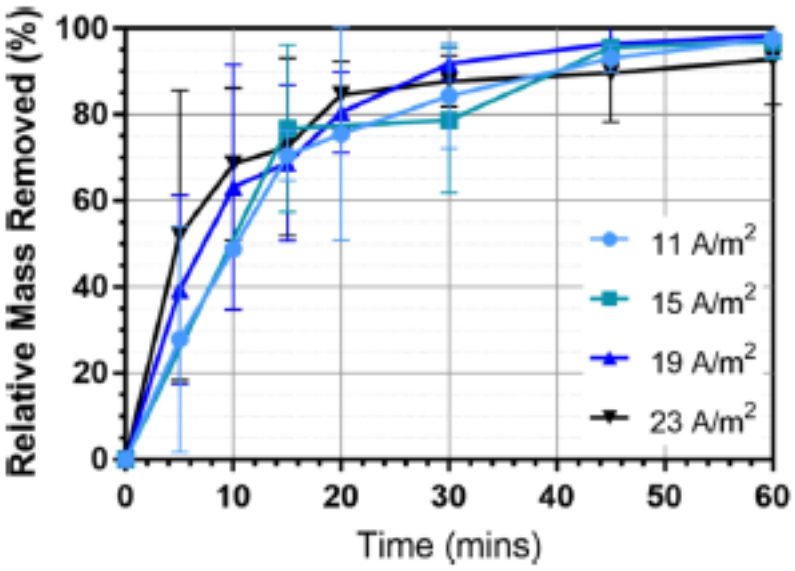

Figure 6 Impact of current density on the removal of MPs beads using Al-Al electrodes (Perren et al 2018)

4.1.9.5.2.3 Reactor Configuration

1. **Batch reactor** is a closed vessel system that is usually ideal for lab-scale experiment where the water is treated in a single batch with electrodes placed within the reactor. This allows for the precise control cover the treatment time but may not be a representation of the real environment scenario.
2. **Continuous flow reactors (CFR)** are designed to treat water continuously allowing a steady flow of water into the reactor. This type of reactor enables a continuous EC process. Nidheesh et al. (2022) reviewed the application of CFR in the treatment of wastewater for a rice processing plant as studied by Abbasi et al. (2022)

4.1.9.5.2.4 Electrode Spacing

The distance between the electrodes impacts the electric field strength which in turn influences the rate at which the coagulants are being generated. In the study of Pawak et al. (2023) the impact of the spacing of electrode was explore in the removal of NPs from

wastewater using Al electrode with varying the distance of the electrodes from 1 cm and 2 cm. A higher removal efficiency occurred when the space between the electrodes was reduced, particularly in the initial 3 hours of the study due to the electrostatic effects and higher ion movement. Removal efficiency was higher at 1 cm spacing (up to 95.1 %) compared to 2 cm (93.3 %) over 5 hours of reaction time without electrolytes. The removal efficiency for both spacing increased significantly recording over 95 % NP removal within 15 minutes when an electrolyte concentration of 50 mM sodium chloride (NaCl) was added.

4.1.9.5.2.5 Reaction Time

Sufficient time is required to ensures enough contact time with coagulant species promoting an effective formation of floc. The studies done by Akarsu et al. (2021), Akarsu & Deniz (2021), Pawak et al. (2023) and Shen et al. (2022) have shown that the efficiency for MPs removal tends to improve as the reaction or coagulation time increases, although the optimal reaction time varies across different experiments. For instance, Akarsu et al. (2021) found that the maximum removal efficiency occurred within 10 minutes, 60 minutes was reported as optimal by the study of Akarsu and Deniz (2021). Shen et al. (2022) from their study used 4 hours. Additionally, Pawak et al. (2023) noted that in the absence of electrolyte, 3 hours is required for an efficient removal but when electrolytes are present, 5 minutes is required for and efficient removal. The variation in these results is due to different experimental setups used in each study.

4.1.9.5.2.6 Effect of Water Quality Parameters On EC

4.1.9.5.2.6.1 Operational Factors

4.1.9.5.2.6.1.1 Water pH

The metal hydroxide stability, the formation of the coagulant, and efficiency of the EC process in its entirety, is influenced by the pH of the water (Akarsu & Deniz, 2021). The electrode material and the type of contaminant in the water also plays a vital role in determining the optimal pH level for efficient contaminant removal. The solubility diagram for Al $(OH)_3$, focusing on mono nuclear Al species, is shown in Figure 7. The solubility of Al species varies with pH, suggesting metal hydroxide production is essential for the agglomeration, and removal of pollutants in EC process is highly pH dependent.

Akarsu & Deniz (2021) using wastewater from a laundry facility with initial pH adjusted from 5 to 9 (the pH of the wastewater), observed a removal efficiency of 98 % of the plastics at pH 9 using Fe-Al electrodes. Shen et al. (2022) used four common MPs with Al-Cu electrode combination observed the highest removal efficiency for the various MPs (93.2% for PE, 91.7% for PMMA, 98.2% for CA, and 98.4% for PP) at a pH of 7.2. Akarsu et al. (2021) focused on the removal of MP (PE and PVC) from wastewater by EC - EF at initial pH values of 4, 7, and 10 (Figure 8). They reported a 100 % removal with an initial pH of 7 using an electrode combination (Al-Fe) however they did not report final pH values (Figure 8). The reaction kinetics was slowed at lower initial pH values since the production of OH was limited (Figure 8) but the final pH was sufficient for 90 % removal even with a starting pH of 4. These three studies started EC experiments at the cited initial pH values, but the pH was not controlled during the reaction nor was the final pH values reported. The authors of these articles also do not provide any indication of error in their analyses so the significance

of difference in response to initial pH cannot be fully evaluated. Perren et al (2018) did tracked pH changes during EC process using Al electrodes for removal of MPs using initial pH values from 3 to 10 **(**Figure 9**)**. Regardless of the initial pH all systems increased in pH due to the formation of hydroxide ions as the reaction progressed resulting in greater than 90% removal of MPs **(**Figure 10**)**. The pH of the water is a key factor in influencing the efficient removal of MPs and NPs but unless the water to be treated is highly buffered the EC reactions increase pH to levels for effective removal of MPs. An optimal pH range between 6.5 and 8.0 is crucial for maximizing the removal efficiency.

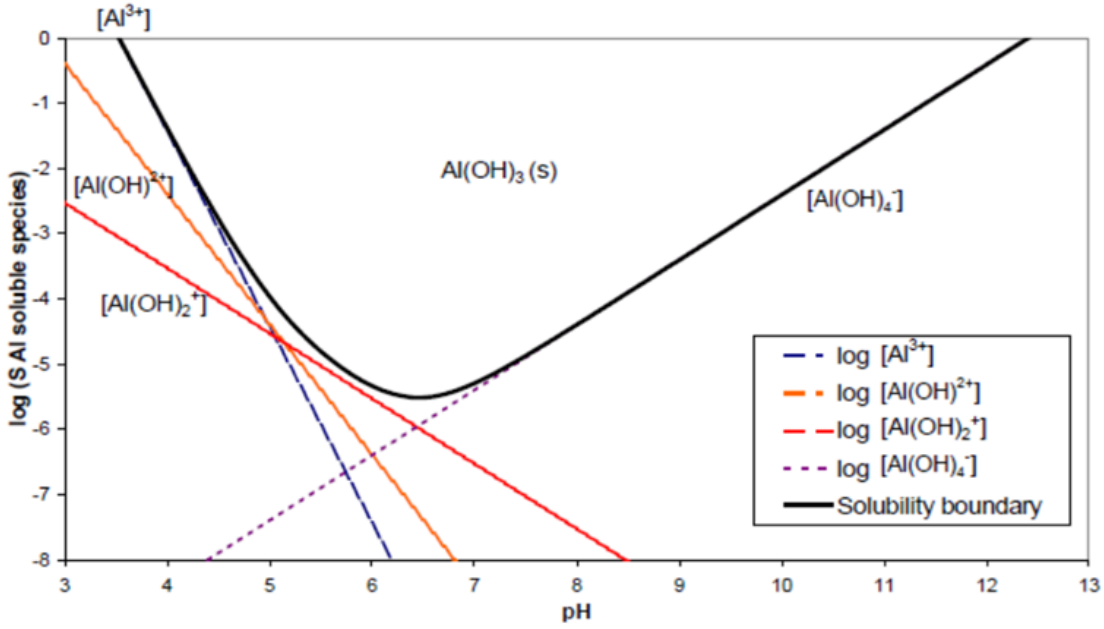

Figure 7 Solubility chart illustrating the solubility of aluminum hydroxide Al (OH)3(s), focusing solely on mononuclear aluminum species

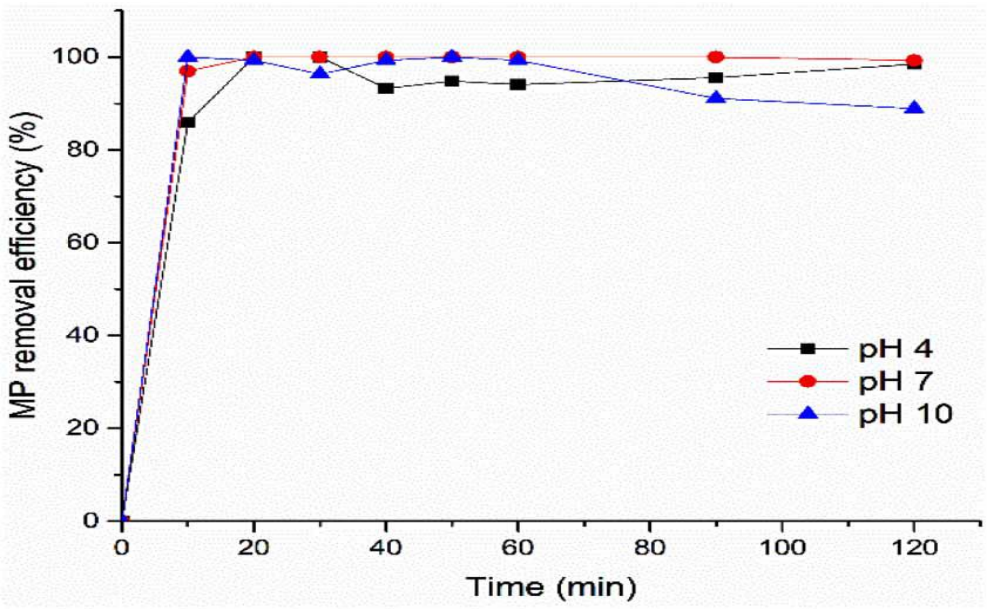

Figure 8 Impact of pH on the Removal efficiency of MPs removal over time Al-Fe electrodes (Akarsu et al., 2021)

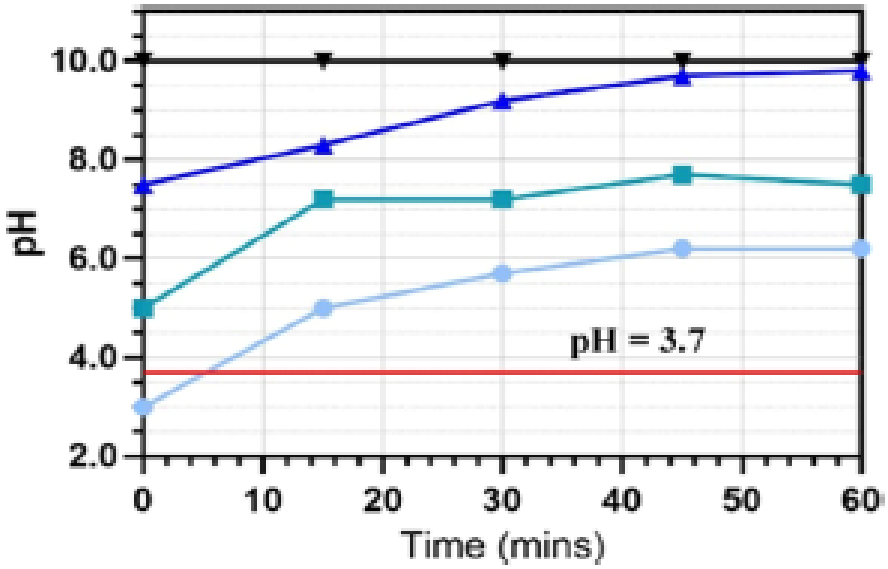

Figure 9 Change in pH over 60-minute EC reaction time. All initial pH values increased to values greater than 3.7 (red line) where Al(OH)3 is the dominant species B. Removal efficiency of MP as influenced by the initial pH. (Perren et al 2018)

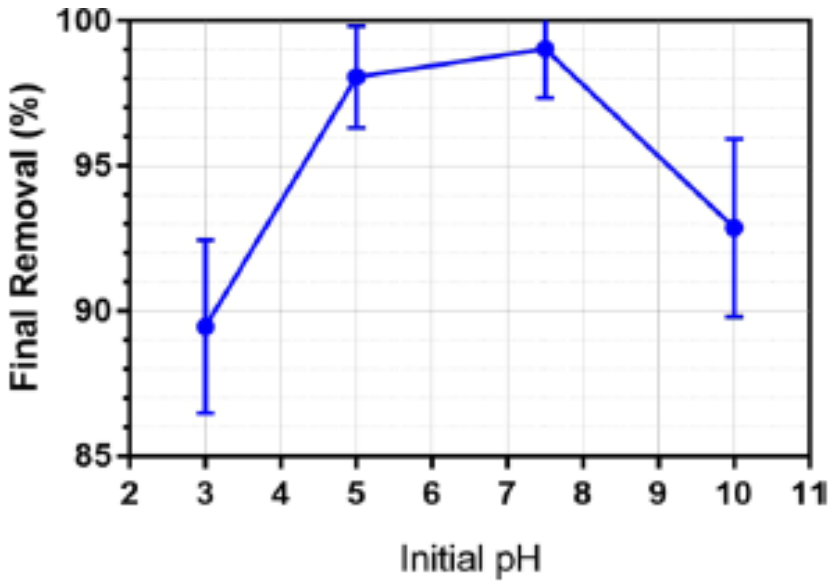

Figure 10 Removal efficiency after 60 min of EC at different initial pH values (Perren et al. 2018)

4.1.9.5.2.6.1.2 Electrolyte Type and Concentration

The type and the concentration of electrolytes used during the EC process influences the removal of efficiency MPs and NPs from the water solution and the overall reaction kinetics. Shen et al. (2022), used sodium sulfate (Na_2SO_4) as the background electrolyte with different concentration from 0.01 M to 0.1 M. After an hour of the EC process using an electrolyte concentration of 0.01 M, the removal efficiencies of 35.4% for PE, 39.4% for PMMA, 51.2% for CA, and 52.2% for PP were reported. As the concentration increased to 0.1 M, the removal efficiencies improved significantly, reaching up to 72.1% for PE, 68.4% for PMMA, 70.4% for CA, and 70.8% for PP. Perren et al. (2018) used NaCl as the background electrolyte also observed an increase in removal efficiencies as the electrolyte dose increased from 2 g/l (85 % removal) to 8 g/l (99 % removal). Pawak et al. (2023), using lower concentrations of NaCl (10 mM, 30 mM, and 50 mM) than Perren et al (2018), again reported higher removal of PS-NPs with increased ionic strength. These results

demonstrate that increasing electrolyte concentration enhances the removal efficiency by increasing the electrical conductivity of the solution. The size of the NPs also contributes to the removal efficiency. In the study of Shen et al. 2022, they indicated 98% removal efficiency for fibrous MPs (Cellulose Acetate (CA) and Polypropylene (PP)) was significantly higher than that for the granular MPs (Polyethylene (PE) and Polymethylmethacrylate (PMMA)) (**Error! Reference source not found.**). In their study also, they observed an increased removal efficiency of PE microgranules (286.7 µm) as compared to PMMA (6.3 µm) with makes it easier to be trapped the Fe flocs formed during the EC process.

Table 4 Removal efficiency of various plastics based on shape, size, and surface characteristics (Shen et al 2023)

Plastic Type	Shape	Size	Surface Type	Removal Efficiency (%)
Polyethylene (PE)	Granular	286.7 µm	Smooth/ pristine	93.2
Polymethylmethacrylate (PMMA)	Granular	6.3 µm	Smooth/ pristine	91.7
Cellulose Acetate (CA)	Fibrous	1–2 mm	Smooth/ pristine	98.2
Polypropylene (PP)	Fibrous	1–2 mm	Smooth/ pristine	98.4

4.1.9.5.2.6.1.3 Characterization of Plastics

As discussed in CCF, the effectiveness of EC will be influenced by the size, shape, surface properties, and type of MPs or NPs. Search of the literature however did not identify studies that directly explore how different surface properties such as surface charge influence the removal efficiency of EC in the context of MPs and NPs. Tsai et al (2023) as stated in section 4.1.9.4, reported that the negatively coated NPs (SDS-NPs) demonstrated better stabilization and removal efficiency as compared to the positively charged (CTAB) coated NPs due to electrostatic attraction (**Error! Reference source not found.**). Implications of surface coatings with natural organic matter (NOM), weathering of MP, NP etc. are needed studies that will help understand the stability and removal efficiency of NPs in various environmental matrices, especially when interacting with NOM.

5 Experimental Design

The objective of this experiment was to build a robust lab-scale EC reactor for removing NPs from water. Preliminary experiments were conducted in a 200 ml beaker using ring stand and clamps to hold the electrodes. It was difficult to position the electrodes precisely and consistently. A new design for consistent placement of the electrodes is presented. Experiments were run at 5V with 5, 10 and 25 mA. Experiments were performed in triplicate. The same conditions were repeated but with the new electrode holder design.

6 Materials and Methods

6.1 Materials

6.1.1 Chemicals Used

Sulfuric acid (0.05M) was used to clean the electrodes. 5 mM sodium chloride was used as the background electrolyte in the reactors. Nitric acid (10%) was used to dissolve aluminium hydroxide in the foam and settled NPs samples to eliminate the contribution of $Al(OH)_3$ to turbidity. Acid treatment should also have been applied to the water column and supernatant samples to again dissolved $Al(OH)_3$ but was not performed in this study.

6.1.2 Electrodes

The electrodes used were made of aluminum (Eisco aluminum electrodes, 100 x 19 mm) due to the effectiveness of this material. This electrode size was appropriate for the size of the reactor and provided a suitable surface area for the electrochemical reactions.

6.1.3 Reactor Vessel

Non-reactive borosilicate glass beakers (200 ml) were used as the reactor ensuring no interference with the EC process.

6.1.4 Power Supply

A variable DC power supply (EXTECH 382200 and SKYTOPPOWER STP 3005) capable of delivering up to 30 V and 10 A was used to control the current t and voltage applied to the electrodes.

6.1.5 NPs Samples

Pristine PS-NPs were laboratory prepared using the emulsion polymerization method (Feng et al., 2018). The PS-NPs were spherical with an average diameter of 246.50 ± 16.12 (std.

error) nm, a zeta potential of -30.51 ± 5.70 (std. error) mV and were prepared at a concentration of 31.7 g/L. Although the size of the particle technically exceeds the conventional definition of nano sized plastics, they exhibit the characteristics of the conventional nano size plastics such as the high surface area to volume ratio, adsorption potential and enhanced mobility in water. This size allows for a more manageable and a realistic investigation into the NPs removal from water by EC. Data on the characterization of the PS-NP using a Brookhaven NanoBrook 90PlusPALS are available in Appendices B and C.

6.1.6 Analytical Instruments

Hach 2100N turbidimeter was used to measure the turbidity of the water samples. pH was measured using Accumet excel (XL25) dual channel pH / ion meter. The electrical conductivity was measured using Accumet conductivity meter (model 30) and Brookhaven instrument NanoBrook 90PlusPALS was used to measure the particle size and zeta potential (surface charge) of the PS-NPs. An AstroAI multimeter was used to measure the current and a calibrated ruler or calliper was used to measure the distance of the electrodes.

6.2 Methods

6.2.1 Reactor Design and Configuration

Aluminium electrodes were configured in a vertically parallel manner with the aid of electrode holders specifically designed and made with an adjustable bar to hold the electrodes in precise, measurable vertical positions (Figures 11 and 12). The electrode holders with a total dimension of 7 cm X 4 cm were printed in 3D using Acrylonitrile Butadiene Styrene (ABS) filament (1.75 mm) at the USU Idea Factory. ABS was used because of its strength.

Preliminary studies were conducted using ring stands, burette holders and paper clips for the electrodes, but this configuration could not hold the electrodes in a vertical and parallel manner which influenced the results at the end of the process (Figure 14). Results from the preliminary experiments showed large variance especially with 5V, 10 mA and the data from 25 mA and 50 mA connecting letter from Tukey were statistically the same (Figure 14). The objective of this study was to design and manufacture a better electrode holder to hold the electrode in place (vertical and parallel).

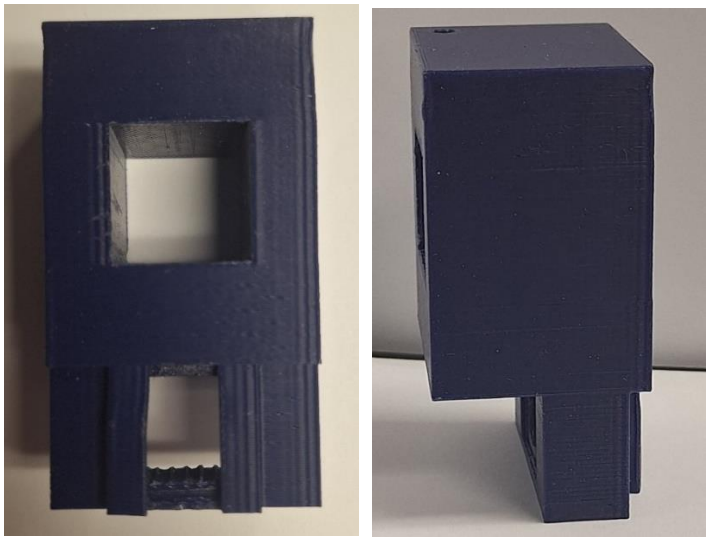

Figure 11 3D printed electrode holder

Figure 12 Electrode holders on its designed adjusting bars

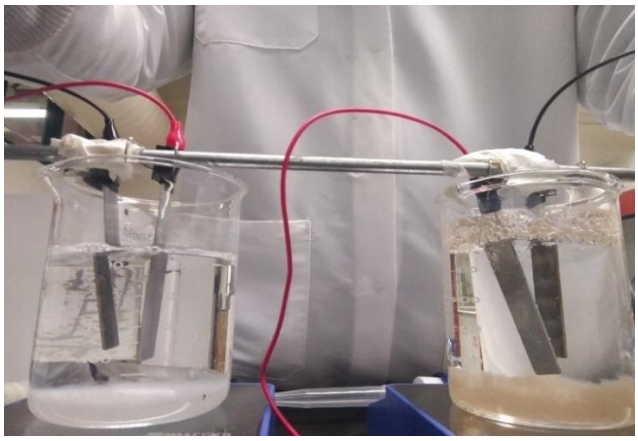

Figure 13 Electrode setup for previous reactor with paper clips

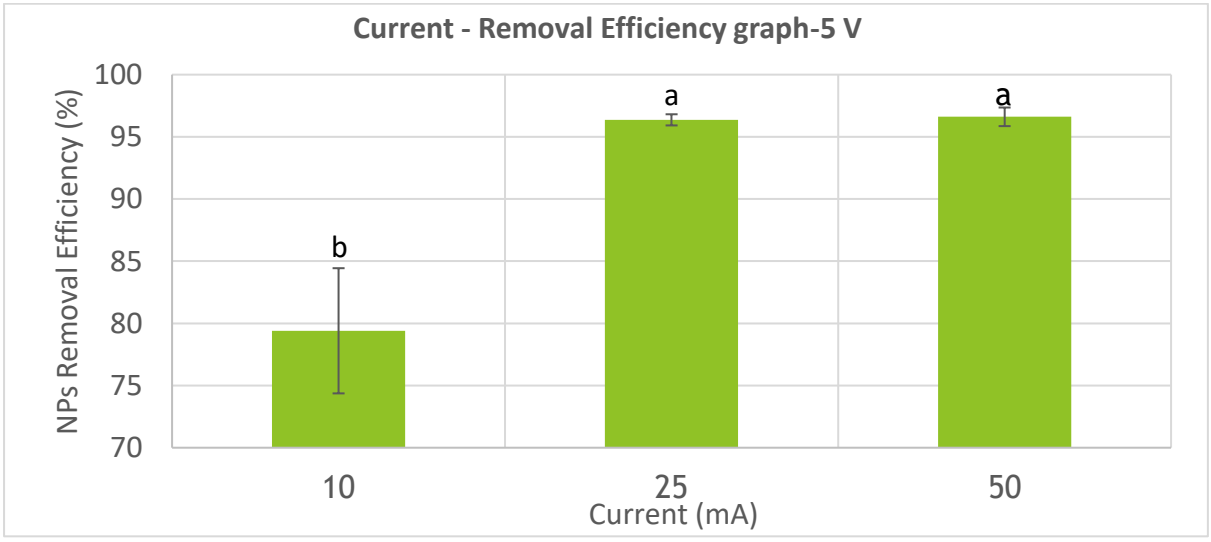

Figure 14 Results from data of previous reactor experiments (Figure 13).

6.2.2 Preparation Of Water Sample

Synthetic water samples were prepared by dosing 2000 ml of deionized water with 0.1 ml PS-NP stock solution (31.7 g /L) which yielded a final concentration of 1.585 mg / L to achieve a turbidity of 20 + 0.5 NTU. 199 ml of the prepared PS-NP solution was measured using a graduated cylinder and poured into a 200 ml beaker and the conductivity was modified by dosing 1.0 ml of 1 M NaCl into the solution to make a total volume of 200 ml. The concentration of the electrolyte was 5 mM NaCl. Without adjusting the pH of the solution, the initial pH of the solution was recorded.

6.2.3 Operational Parameters

A DC power supply and multimeter were used to control voltage and current during the EC process. The system operated under a constant voltage of 5V, with varying currents of 10 mA, 25 mA and 50 mA with electrodes spaced at 5.4 cm, 2 cm, and 1 cm. ~~which had~~The active surface areas (electrode area in contact with water~~),~~) were 1.0×10^{-3} m² , 1.0×10^{-3} m² and 1.13×10^{-3} m² for the respective currents. The current density applied was mathematically obtained using Equation 8.

$$J = \frac{I}{A} \qquad (8)$$

where J = Current density (A/m^2), I = Current (A) and A = Cross-sectional area of the electrode (m^2).

In the previous reactor's electrode holder, which was a paper clip, the current was achieved by adjusting the paper clip with masking tape to hold the electrode in place which most of the time, the distance between the electrode above the water differs from the distance of the electrode in the water solution which gives a false reading. With the designed electrode

holder on the adjusting bar, the electrodes are vertical and parallel and the measured distance above is equal to the electrode distance in the water.

The experiments were conducted over a period of 4 hours. The first 2 hours were for the EC reaction time and the final 2 hours were for settling and final turbidity measurement to assess the PS-NP removal efficiency.

6.2.4 Analytical Techniques

The turbidimeter was first calibrated using the Hach turbidimeter calibration solution. Although the initial concentration of NPs in the solution is known, the turbidity of the solution before and after the treatment was measured using a turbidimeter to determine the removal efficiency. Calibration curves were generated to determine the relationship between the measured turbidity and concentration of the NPs in solution. The initial solution with a concertation of 1.585 and turbidity of 20 NTUs was diluted to generate three additional concentrations of NPs, and their turbidities were recorded. Calibration curves were prepared in both DI water and in 10% nitric acid. The relationship was the same for the two matrices.

Turbidity (NTU) = Concentration of PS_NPs mg/L * 12.618 (9)

The particle size and the surface charge of the plastic particle analysis were determined before and after the reaction (Brookhaven NanoBrook 90PlusPALS). The final pH of the solution is also measured.

6.2.4.1 EC Process for the Removal of PS-NPs

The previous reactor setup and the current reactor design followed the same protocol. The aluminium electrodes were first rinsed with deionized water and then were soaked into 0.05

M H_2SO_4 for 20 minutes to prevent the passivation of electrodes. Shen et al. (2022) soaked electrodes for 30 minutes in 1 M H_2SO_4. After soaking the electrodes were rinsed well under running tap water and finally with Type I for 2- 3 minutes. The electrodes were then dried and inserted into the electrode holder. The electrode holders were then inserted into the adjusting bar and finally fixed on a ring stand (Figure 12). The initial turbidity was measured followed by the measurement of the electrical conductivity and the pH. The beaker containing the solution was then place on a Thermolyne Mirak Hotplate magnetic stirrer. With the aid of a 25 mm magnetic stirrer, the solution was stirred at a speed of 200 revolution per minute (rpm). The electrodes were then inserted into the solution and the power supply was switched on. With aid of the multimeter, the current to be examine was set by adjusting the electrode holder to the desired spaces between them with a given current allowance of ± 0.5 mA. The EC process lasted for 2 hours after which the stirring and the power supply was switched off.

6.2.4.2 NPs Concentration Determination

With the analysis of plastics in the foam, settled NPs and water column, a mass balance was calculated. After the EC process, the foam formed on the surface of the water was collected into a graduated cylinder using a stainless-steel spoon. The sample in the beaker was then allowed to settle for 2 additional hours after which 15 ml – 20 ml of the water was sampled from the midpoint of the beaker using a 10 ml pipet and was transferred to a vial and the final turbidity was measured. The rest of the water sample was removed leaving about 45 ml to 50 ml of the water in the beaker which contains the settled NPs and aluminum hydroxide. Both the foam and settled NPs samples were centrifuged at 10000 rpm for 25 minutes. The supernatant was removed. 20 ml of 10% nitric acid was added to dissolve the

$Al(OH)_3$. Turbidity was then determined on these solutions. Using Equation 9, the concentration of the NPs in the solutions were determined, and hence the mass of the NPs in the solution. Measuring all phases allowed for a mass balance calculation by conversating concentration to mass.

6.2.5 Statistical Method (Data Analysis)

The experimental data compiled was analysed using one-way analysis of variance (ANOVA) using JMP 8 statistical software, and when significant a Tukey's honestly significant difference test (Tukey HSD). These tests compared removal efficiencies, change in pH, and production of foam and settled NPs as affected by the applied current.

6.2.6 Quality assurance and consistency

For data reliability and reproducibility, the experiments were performed in triplicate and were repeated three times.

7 Results and Discussion

7.1 Characterization of PS-NP

The particle size initially measured before commencing the EC process for all the experiments 10 mA, 25 mA and 50 mA for the PS-NP measured an average of size of 246.50 ± 16.12 (std. error) (n=27**)**. The zeta potential of the NPs measured to determine the surface charge of the NPs since it also impacts its removal efficiency. For all the experiments, the NPs exhibited an average zeta potential measurement of the PS-NP of -30.51 ± 5.7 (std. error) (n=27). Appendix B shows the individual data for each set of the experiment.

Table 5 Particle size of PS-NP before the EC process for 10 mA, 25 mA, 50 mA

Sample ID	Eff. Diam. (nm)	Polydispersity	Baseline Index	Count Rate (kcps)	Data Retained (%)	Diffusion Coeff. (cm^2/s)	pH
PS-NP SAMP BF EC	246.50	0.18	3.69	490.19	97.64	0.00	5.48
Std Err (n=27):	16.12	0.02	0.47	46.67	0.32	0.00	0.03

Table 6 Surface charge of PS-NP before the EC process for 10 mA, 25 mA, 50 mA

Sample ID	Eff. Diam. (nm)	Polydispersity	Baseline Index	Count Rate (kcps)	Data Retained (%)	Diffusion Coeff. (cm^2/s)	pH
PS-NP SAMP BF EC	-30.51	-2.38	1,397.66	602.24	1,198.32	0.05	5.48
Std Err (n=27):	5.70	0.45	48.79	63.22	31.84	0.00	0.03

The particle size of the PS-NP after the EC process revealed significant changes. Appendix C shows all the detailed data of the measured samples after the EC process. The measurement was done after 2 hours of settling by sampling water from the mid-point with a 10 ml pipette in the reactor and the measuring of the micro sizes can be attributed to the continuous aggregation and settling of the plastics facilitated by the EC process. The particle size measured after the EC process for all the experiments 10 mA, 25 mA and 50 mA for the PS-NP measured an average of size of 49,294.27 ± 18,046.09 nm (std. error) (n=9), 46,947.72 ± 9,134.21 nm (std. error) (n=9), 25,735.18 ± 4,529.11 nm (std. error) (n=9) (Table 7) respectively. The zeta potential of the NPs was measured to determine the surface charge of the NPs since it also impacts its removal efficiency. For all the experiments, 10 mA, 25 mA and 50 mA, the NPs exhibited an average zeta potential of 21.70 ± 4.48 (std. error) (n=9),

29.14 ± 1.76 (std. error) (n=9), 23.41 ± 3.17 (std. error) (n=9) (Table 8) respectively. This increase in the surface charge can be attributed to the adsorption of positively charged aluminum hydroxide formed during the electrocoagulation process, which neutralizes the initial negative charges of the NPs. Additionally, the compression of the double layer by aluminum ions enhances this adsorption, further shifting the surface charge from negative to positive as the pH increases.

Table 7 Particle size of PS-NP After the EC process for 10 mA, 25 mA, 50 mA

Sample ID	Eff. Diam. (nm)	Polydispersity	Baseline Index	Count Rate (kcps)	Data Retained (%)	Diffusion Coeff. (cm^2/s)	pH
PS-NP SAMP AFEC 10 mA (n=9)	49,294.27	2.13	0.06	103.95	92.81	0.00	8.04
Std Err (n=9):	18,046.09	1.02	0.05	42.80	1.12	0.00	0.03
PS-NP SAMP AFEC 25 mA (n=9)	46,947.72	0.61	0.01	265.64	91.69	0.00	8.29
Std Err (n=9):	9,134.21	0.38	0.01	92.38	1.11	0.00	0.04
PS-NP SAMP AFEC 50 mA (n=9)	25,735.18	0.44	0.56	687.90	94.42	0.00	8.48
Std Err (n=9):	4,529.11	0.04	0.37	336.16	1.34	0.00	0.06

Table 8 Surface charge of PS-NP After the EC process for 10 mA, 25 mA, 50 mA

Sample ID	Zeta Potential (mV)	Mobility (µ/s)/(V/cm)	Conductance (µS)	Sample Count Rate (kcps)	Ref. Count Rate (kcps)	RMS Residual	pH
PS-NP SAMP AFEC 10 mA (n=9)	21.70	1.70	1,464.41	1,278.00	1,058.89	0.03	8.04
Std Err (n=9):	4.48	0.35	23.87	478.18	77.41	0.00	0.03
PS-NP SAMP AFEC 25 mA (n=9)	29.14	2.28	1,534.30	1,513.89	1,033.00	0.03	8.29
Std Err (n=9):	1.76	0.35	8.47	745.14	93.07	0.00	0.04
PS-NP SAMP AFEC 50 mA (n=9)	23.41	1.83	1,839.81	1,633.33	1,066.00	0.03	8.48
Std Err (n=9):	3.17	0.25	303.25	1,066.64	71.52	0.00	0.06

7.2 NPs Removal Efficiency (Impact of Current)

The EC process was evaluated for the PS-NP removal efficiency from water under varying current 10 mA, 25 mA, 50 mA at a constant 5 V. The turbidity before and after the reaction was used to determine the removal efficiency. All raw data are presented in Appendix A.

Initial turbidity readings although consistent but not statistically the same (Figure 15). The final turbidity readings showed effective removal by the EC process in reducing the turbidity and by extension NPs from the water column (Figure 15). The low variance across replicates confirms the robustness of the EC reactor. There were differences in the extent of NP removal with the highest applied current having the best removal.

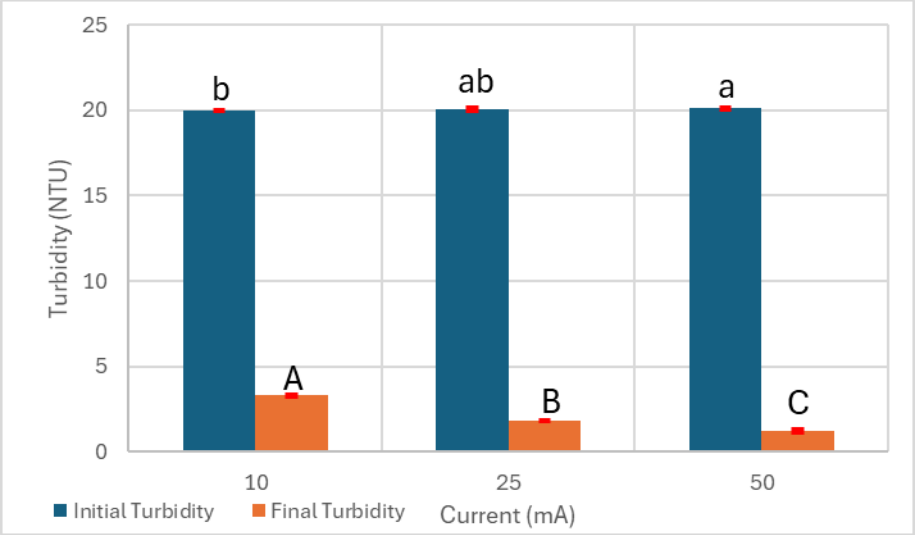

Figure 15 Effect of current on turbidity at 5V. Error bar is 95 % confidence interval ($p < 0.05$) for final turbidity and ($p > 0.05$). Differing letters above columns represents a significant difference based on Tukey HSD ($p<0.05$). Small letters for one way ANOVA for initial conditions and capital letters for final readings.

The data are also expressed as removal efficiency (Figure 16) displaying increase in removal with increasing applied current. Figure 16 also displayed the low variance in the data with this new design compared to the high variability in the data with the original method for holding the electrodes (Figure 14).

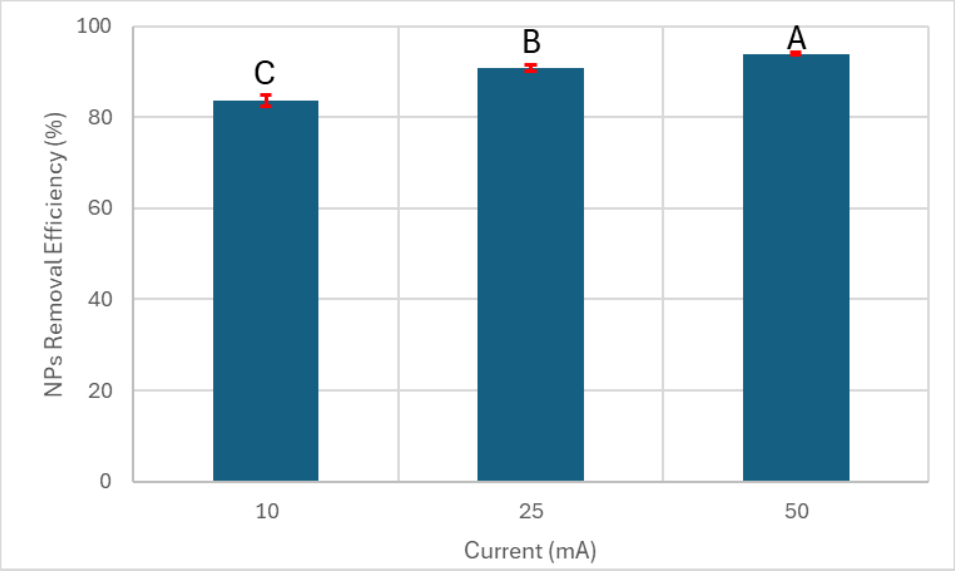

Figure 16 Removal efficiency of various current at 5V. Error bar is 95 % confidence interval. Differing letters above columns represents a significant difference based on Tukey HSD ($p<0.05$).

The new data aligned with findings from other studies that, as the current or current density increases, the removal efficiency also increases (Akarsu et al., 2021; Akarsu & Deniz, 2021). Akarsu & Deniz (2021) reported increased removal efficiency from 66 % to 81 % with increasing applied current from 0.54 A to 2.16 A in wastewater under alkaline condtions after one hour EC process. Akarsu et al. (2021) observed a higher removal efficiency of 100 % with their experiment highest current density 20 A/m^2 after 10 minutes of reaction time.

7.3 pH of the solution

Conventional water treatment is pH dependent, so is EC. But in the conventional water treatment, the pH must be adjusted (more addition of chemicals) to achieve an efficient removal. During the EC process, without the addition of any chemical to adjust the pH, the pH increased from a 5.3 to 8.5 (Figure 17). The initial pH of the solution recoded before the EC process were between 5.3 to 5.5 making the solution slightly acidic which favours the dissolution of the aluminium electrode at the anode. The Al^{3+} released into the solution

serves as the coagulant to initiate the coagulation process. At the aluminium electrode as the cathode, water is reduced by releasing hydrogen gas (H_2) and hydroxide ions (OH^-) (Equation 3). As the EC reaction is initiated, the pH increased over the reaction period (Figure 17) and the $Al(OH)_3$ produced forms flocs and other steps of the coagulation process are initiated which is the adsorption and charge neutralization and the formation of the gelatinous aluminium hydroxide to initiate the sweep floc process which removes the NPs from the water and causes the turbidity of the solution to reduce which was the determinant of the NPs removal from the water as shown in Figure 15. It can be inferred that the EC process promotes pH conditions that are conducive for maintaining Al hydroxide formation and coagulation. The increase in pH to sufficient values to promote floc formation has been reported by Perren et al. 2018. They illustrated the impact of initial pH on the MPs removal efficiency during the EC process. Their study used four initial pH values (3, 5, 7.5 and 10). All pH values increased, with the exception of pH 10, over the 60-minute EC process to values that promoted formation of coagulant and removal of MPs.

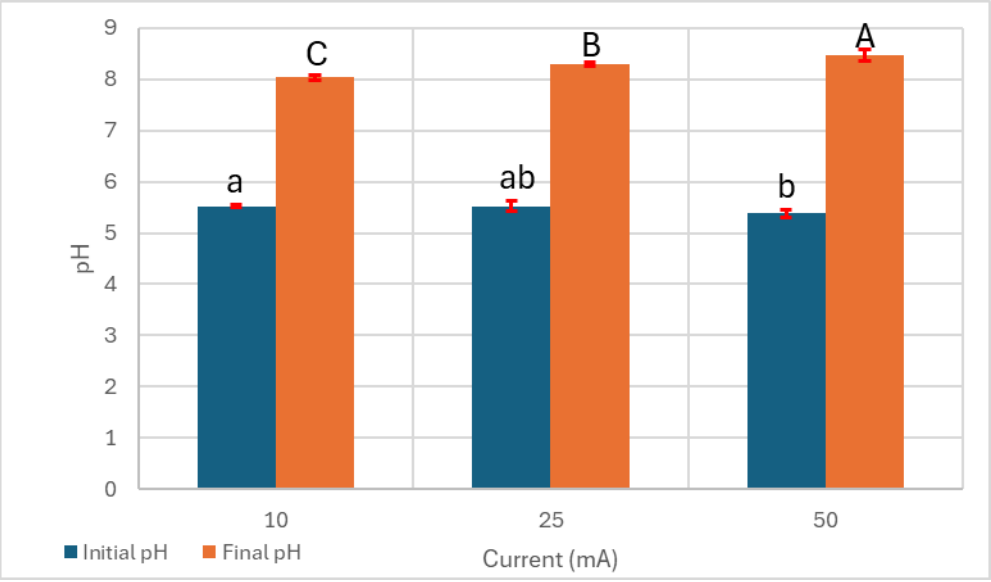

Figure 17 Increasing pH over the reaction time. Error bar is 95 % confidence interval. ($p < 0.05$. Differing letters above columns represents a significant difference based on Tukey HSD

(p<0.05). Small letters for one way ANOVA for initial conditions and capital letters for final readings

7.4 Foam, Water column and Settled NPs

As the Al hydroxide formed acts as a coagulant, neutralizing the charge on the NPs facilitates its aggregation into larger flocs causing the removal of the NPs by settling and some through flotation. From the new reactor design, the distribution of NPs in the foam, water column and settled NPs (Figure 18) were analysed to understand EC's effectiveness to optimize the process. Statistical analysis (Figure 19) showed that the foam volume increased as the current increased. For all applied current most of the NP mass was in the settled solids (Figures 20, 21, 22). The two higher currents (25 and 50 MA) produced more foam (Figure 19) and more of the NPs were distributed into the foam compared to the water column (Figure 21, 22). More of the NP was distributed into the foam with increasing current due to the increase in H_2 bubbles which attaches to the flocs formed during the EC process which also facilitates the removal of the NPs from the water.

Figure 18 Foam formation after EC process for all three experimented currents

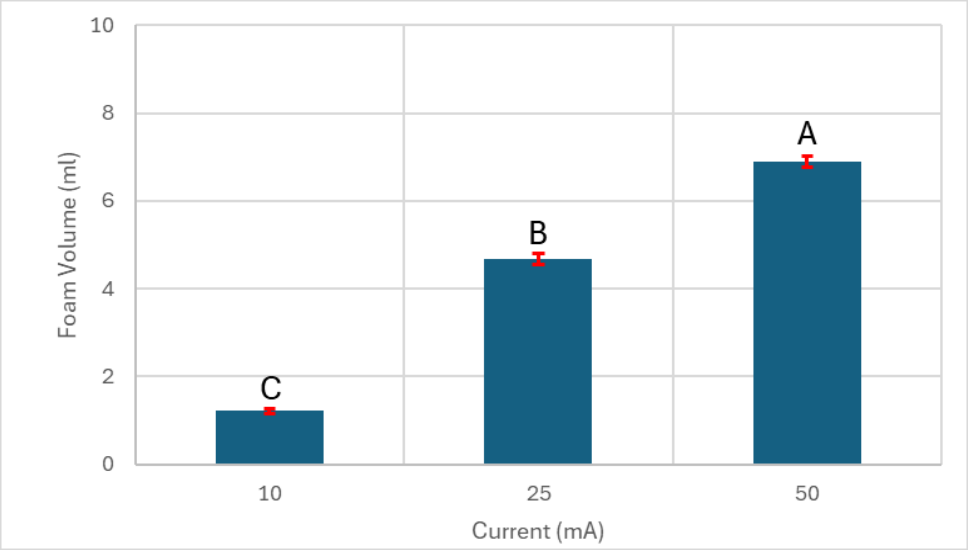

Figure 19 Foam Volume graph. Error bar 95 % confidence interval. ($p < 0.05$). Differing letters above columns represents a significant difference based on Tukey HSD ($p<0.05$).

Figures 20 to 22 demonstrated the mass of NPs in the various segments in the reactor according to the current applied. Figures 23 to 25 compared the NPs mass in the foam, water columns and in the settled solids across the experimented currents. The mass of NPs in the settled solids was the same regardless of applied current (Figure 25). While the applied current affected the distribution of NPs between the foam and the water column, higher currents of 25 mA or 50 mA led to larger mass of NPs in the foam (Figure 23) than that with current of 10 mA, further increasing from 25 mA to 50 mA did not show significant effect. With lower applied current (10 mA), more NPs remained in the wate column (Figure 24).

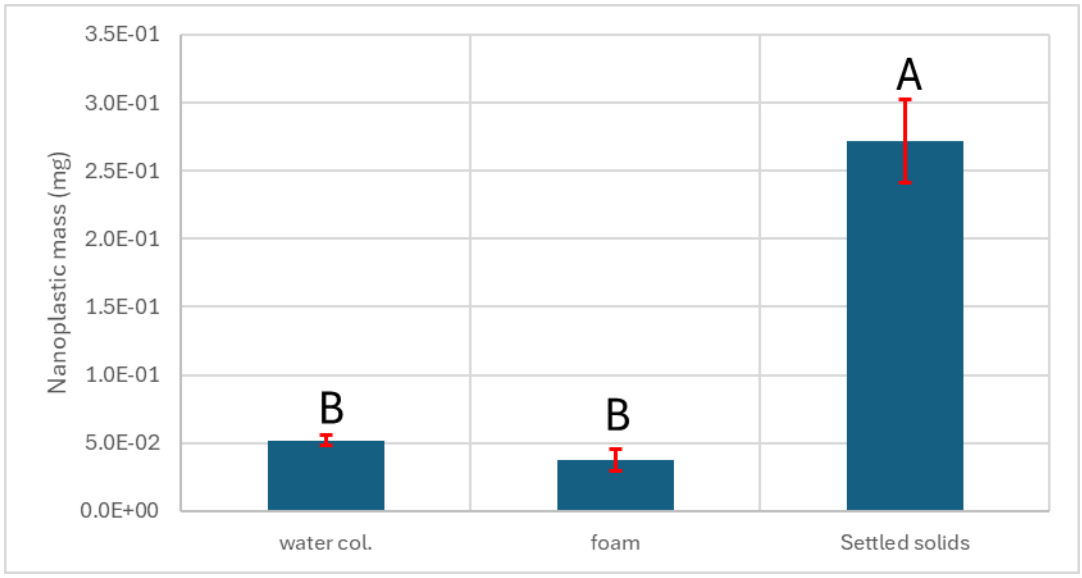

Figure 20 10 mA (0.01 A) NP distribution after the EC Process. Error bar 95 % confidence interval. ($p < 0.05$). Differing letters above columns represents a significant difference based on Tukey HSD ($p<0.05$).

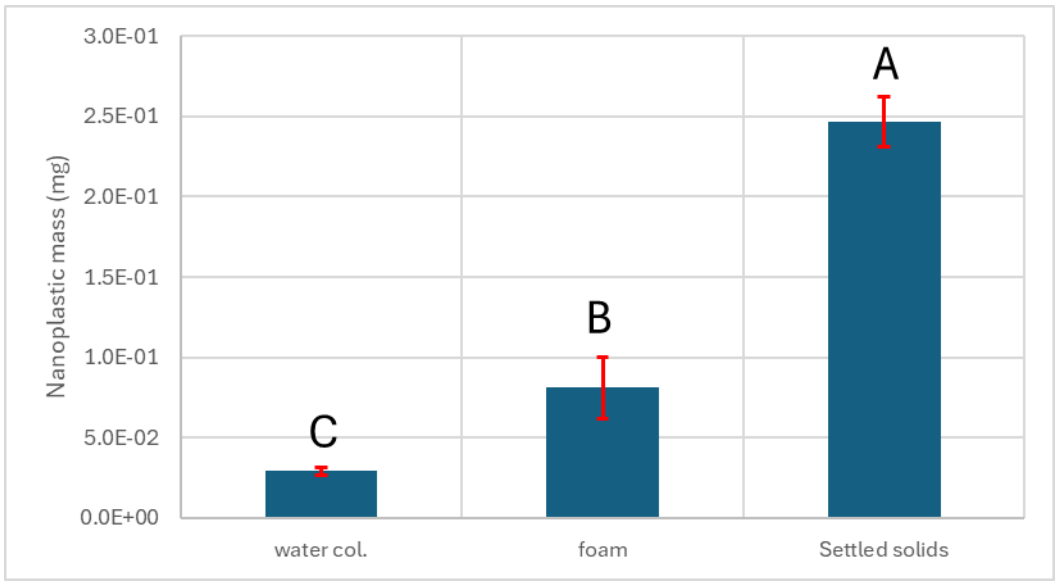

Figure 21 25 mA (0.025 A) NP distribution after the EC Process. Error bar 95 % confidence interval. ($p > 0.05$). Differing letters above columns represents a significant difference based on Tukey HSD ($p<0.05$).

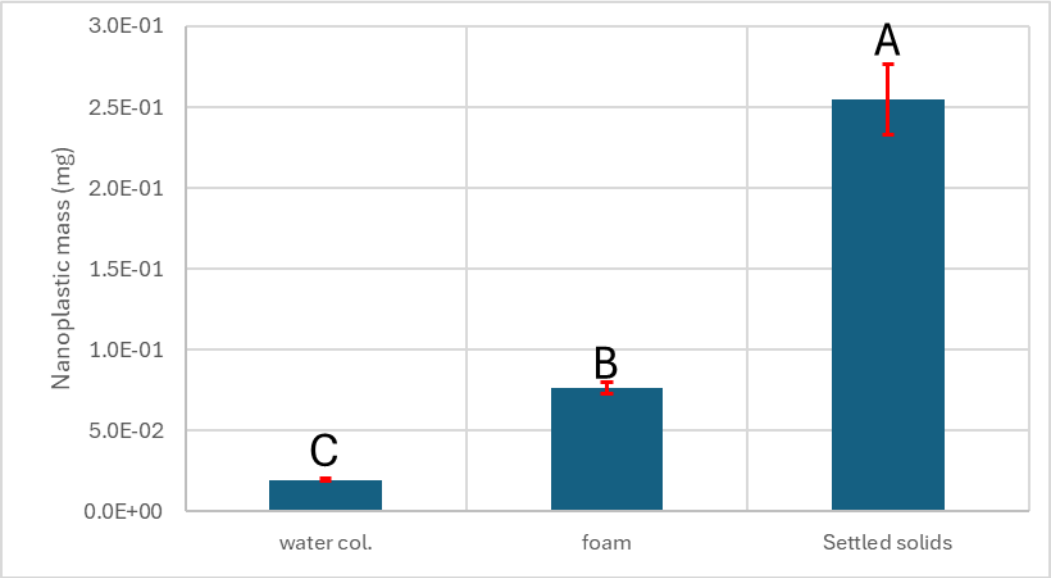

Figure 22 50 mA (0.05 A) NP distribution after the EC process. Error bar 95 % confidence interval. ($p < 0.05$). Differing letters above columns represents a significant difference based on Tukey HSD ($p<0.05$).

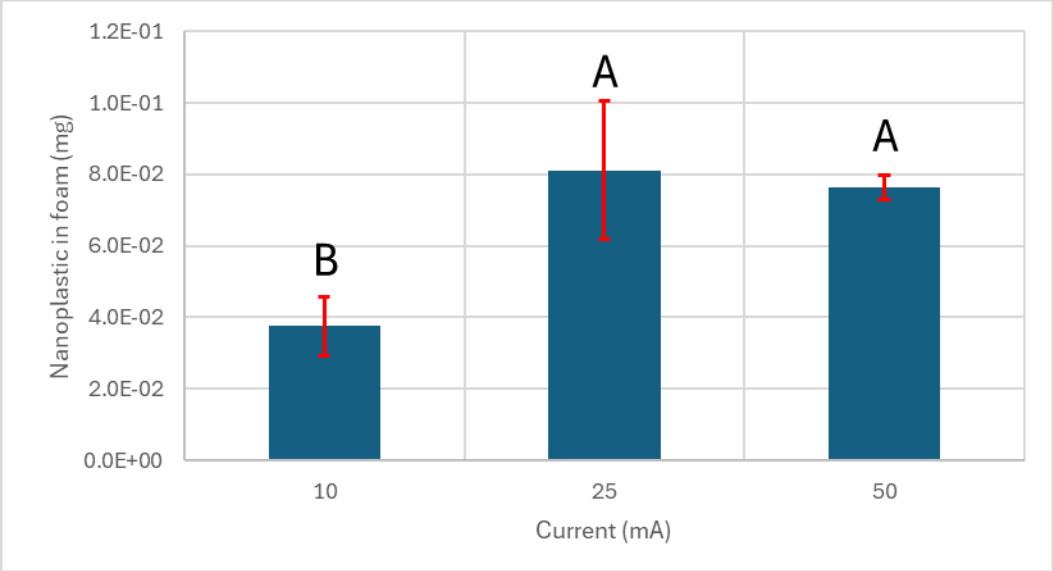

Figure 23 Impact of current on NPs accumulation in foam. Error bar 95 % confidence interval. ($p < 0.05$). Differing letters above columns represents a significant difference based on Tukey HSD ($p<0.05$). Differing letters above columns represents a significant difference based on Tukey HSD ($p<0.05$).

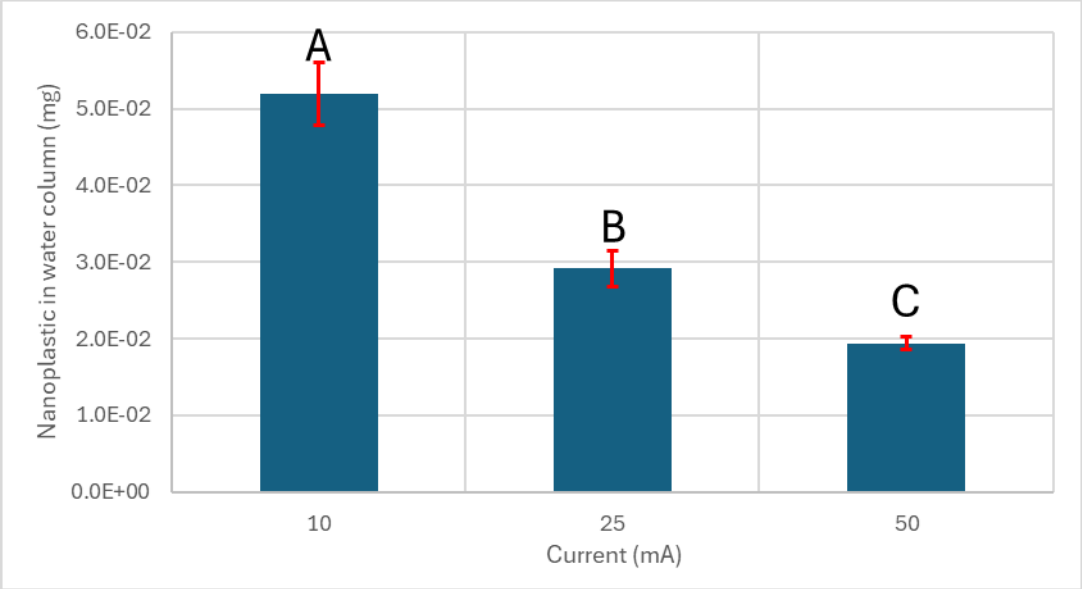

Figure 24 Impact of current on NPs accumulation in the water column. error bar 95 % confidence interval. ($p < 0.05$). Differing letters above columns represents a significant difference based on Tukey HSD ($p<0.05$).

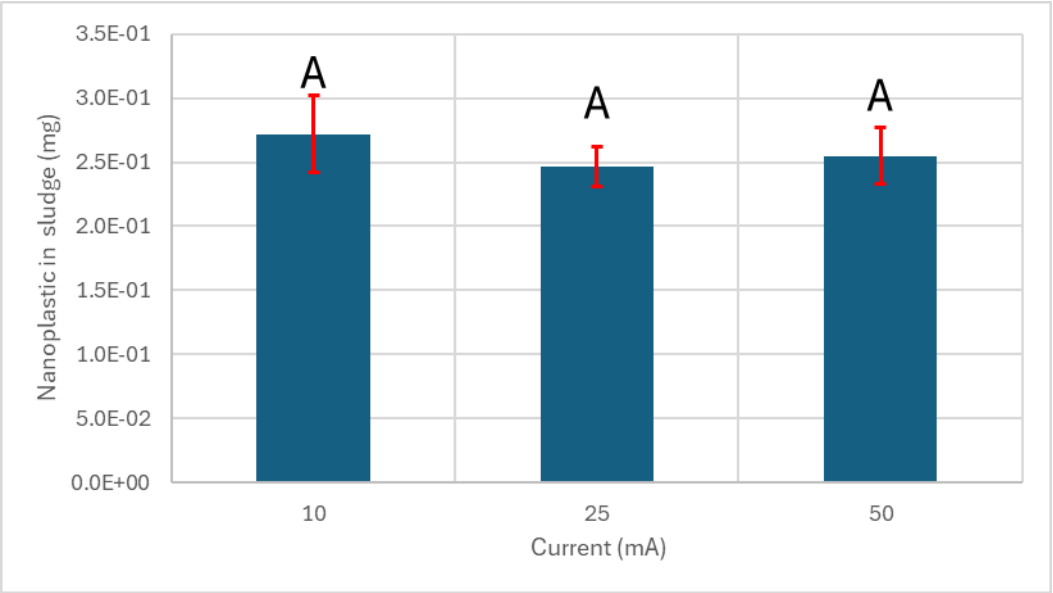

Figure 25 Impact of current on NPs accumulation in settled matter. Error bar 95 % confidence interval. ($p < 0.05$). The mass of NPs in the settled solids was the same regardless of the applied current.

Mass balance calculations were performed to ensure a full accounting of the mass distribution of NPs within the different phases. Percent recoveries ranged from 111 % to 115% with standard errors between 2.8% and 5.2% (**Error! Reference source not found.**). The recoveries were systematically high due to not adding 10% nitric acid to the water column and the supernatant samples to dissolve any aluminum hydroxide in them. Highly turbidity reading may have resulted from not removing all the $Al(OH)_3$ associated with these samples. Figure 26 shows a graphical representation of the mass balance recovery percentage data and from the graph, the percentage recovery across the currents are statistically not significant. This mass balance data implies that results of NPs distribution in final water column, foam, and settlements are reliable.

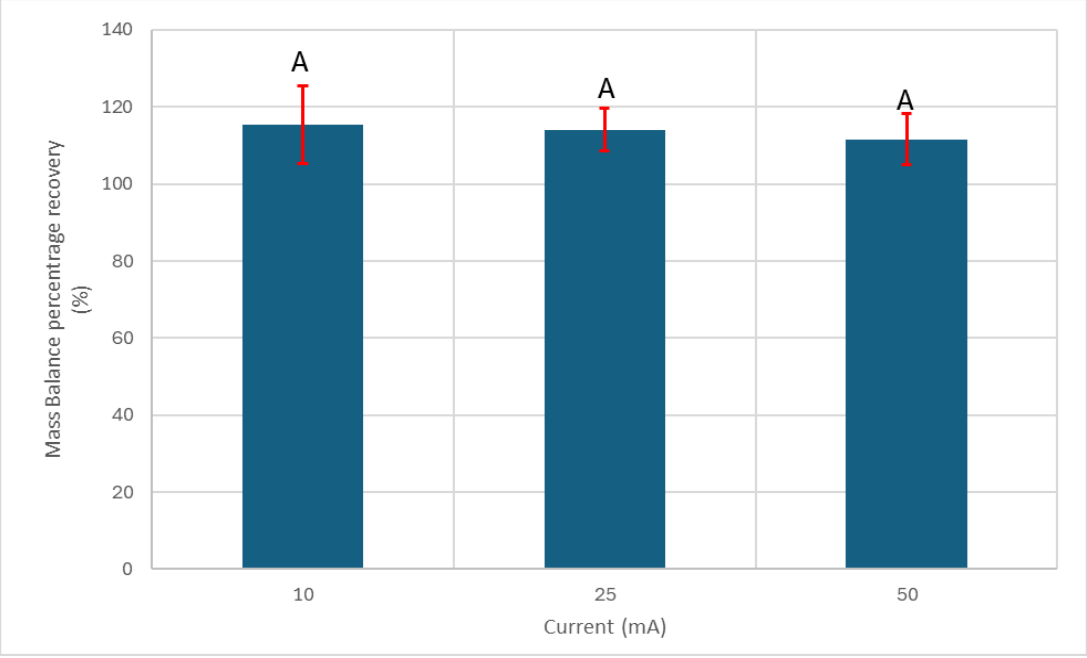

Figure 26 Mass balance percentage recovery of the EC data. Error bar 95 % confidence interval. ($p < 0.05$)

8 Conclusion

The pollution of the various drinking water sources especially surface waters with the MPs and NPs, has become an environmental and public health concern as the conventional pretreatment of drinking water have proven to be not effective in handling MPs and NPs necessitating the need for an advanced treatment method. This report focused on the design of a laboratory-scale EC reactor to provide a stable platform to evaluate the removal of NPs from drinking water sources. The rigid placement of the electrodes with the design system provided reproducible results so that differences in treatment can be discerned.

The EC process demonstrated a higher removal efficiency for NPs at higher current (50 mA) at a cell voltage of 5 V, indicated by the lower turbidity in water column. The volume of foam produced is influenced by the applied current. The NPs contained in the foam increased when the applied current was increased from 10 to 25 mA, while the total mass of NPs in settlements produced at different currents did not show significant difference. It is also noteworthy that the pH increases from an initial value of 5.5 to be buffered at and optimum pH of 8 to 8.5 without the need to add chemicals for pH adjustment.

Further studies could delve into using different water qualities (different electrolytes at varying concentrations, type and concentration of natural organic matter, pH buffered systems), different plastic types (with varying surface types, shape and size at varying concentrations, weathered versus pristine plastics) for a comprehensive understanding on the effectiveness of EC for removing NPs from water.

Other studies should focus on the effect of the applied current on the distribution of NPs between the foam and settled NPs. Since NPs are so small, their removal may be more

effective by increasing the production H_2 bubbles which may facilitate the removal of NPs into the foam layer.

9 Recommendation

Designing a lab-scale EC reactor for the effective removal of NPs from drinking water showing a good removal efficiency without the use of extra coagulants and flocculants will serve as reliable system for evaluating various paraments know to effect NP removal. Aluminium electrode would be recommended but the aluminium electrode configuration must be designed based on the volume of water to be treated and the reaction period. As plastic pollution is an environmental menace and the world is seeking to go green and clean to save lives of all various organisms in their respective environments, further studies should be done on the foam and settled NPs NPs to determine how these waste or by-products can be used for the benefit of the environment.

10 Engineering significance

The conventional procedure for the treatment of water faces a series of difficulties as a result of environmental pollution from NPs. The designing of a robust lab-scale EC reactor for removing NPs from drinking water sources is crucial for advancing water treatment technologies. As NPs are increasingly being produced and used by various industries due to their unique properties and plastic waste is not properly handled degrading into micro and nano sizes, drinking water sources are likely to continue to be polluted. Understanding the fate of NPs in drinking water bodies is crucial as the traditional water treatment methods often fall short in removing NPs which has the tendency of carrying harmful chemicals and pathogens posing significant risks if ingested. The design of EC reactor will enhance the

coagulation process leading to higher removal efficiencies compared to the conventional treatment method as the in-situ generation of coagulant reduces the need for more application of chemical coagulants making the EC process an environmentally friendly one. More so, an optimized EC system translates to lower cost of operation making EC an economically viable option for a large-scale operation

This lab-scale design of the EC reactor ensures that the developed technology is not only efficient, effective, and sustainable but also can adapt to the various real-world challenges in water and the successful implementation of this technology can lead to advancements in the water treatment significantly contributing to a clean and safe environment.

11 References

Akarsu, C., & Deniz, F. (2021). Electrocoagulation/Electroflotation Process for Removal of Organics and Microplastics in Laundry Wastewater. *Clean - Soil, Air, Water*, *49*(1). https://doi.org/10.1002/clen.202000146

Akarsu, C., Kumbur, H., & Kideys, A. E. (2021). Removal of microplastics from wastewater through electrocoagulation-electroflotation and membrane filtration processes. *Water Science and Technology*, *84*(7), 1648–1662. https://doi.org/10.2166/wst.2021.356

Allen, S., Allen, D., Karbalaei, S., Maselli, V., & Walker, T. R. (2022). Micro(nano)plastics sources, fate, and effects: What we know after ten years of research. *Journal of Hazardous Materials Advances*, *6*, 100057. https://doi.org/10.1016/j.hazadv.2022.100057

Baldwin, A. K., Spanjer, A. R., Rosen, M. R., & Thom, T. (2020). Microplastics in Lake Mead National Recreation Area, USA: Occurrence and biological uptake. *PLoS ONE*, *15*(5). https://doi.org/10.1371/journal.pone.0228896

Bank Editor, M. S. (n.d.). *Environmental Contamination Remediation and Management Microplastic in the Environment: Pattern and Process*. http://www.springer.com/series/15836

Bazrafshan, E., Mahvi, A. H., Nasseri, S., Mesdaghinia, A. R., Vaezi, F., & Nazmara, S. (2006). REMOVAL OF CADMIUM FROM INDUSTRIAL EFFLUENTS BY ELECTROCOAGULATION PROCESS USING IRON ELECTRODES. In *J. Environ. Health. Sci. Eng* (Vol. 3, Issue 4).

Browne, M. A., Niven, S. J., Galloway, T. S., Rowland, S. J., & Thompson, R. C. (2013). Microplastic moves pollutants and additives to worms, reducing functions linked to health and biodiversity. *Current Biology*, *23*(23), 2388–2392. https://doi.org/10.1016/j.cub.2013.10.012

Chae, Y., & An, Y. J. (2017). Effects of micro- and nanoplastics on aquatic ecosystems: Current research trends and perspectives. *Marine Pollution Bulletin*, *124*(2), 624–632. https://doi.org/10.1016/j.marpolbul.2017.01.070

Chen, Z., Shi, X., Zhang, J., Wu, L., Wei, W., & Ni, B. J. (2023). Nanoplastics are significantly different from microplastics in urban waters. *Water Research X*, *19*. https://doi.org/10.1016/j.wroa.2023.100169

Chen, Z., Wei, W., Liu, X., & Ni, B. J. (2022). Emerging electrochemical techniques for identifying and removing micro/nanoplastics in urban waters. *Water Research*, *221*. https://doi.org/10.1016/j.watres.2022.118846

Chowdhury, S. R., Razzak, S. A., Hassan, I., Hossain, S. M. Z., & Hossain, M. M. (2023). Microplastics in Freshwater and Drinking Water: Sources, Impacts, Detection, and Removal Strategies. In *Water, Air, and Soil Pollution* (Vol. 234, Issue 11). Institute for Ionics. https://doi.org/10.1007/s11270-023-06677-y

Cole, M., Lindeque, P., Halsband, C., & Galloway, T. S. (2011). Microplastics as contaminants in the marine environment: A review. In *Marine Pollution Bulletin* (Vol. 62, Issue 12, pp. 2588–2597). https://doi.org/10.1016/j.marpolbul.2011.09.025

Crittenden, J. C. (John C., & Montgomery Watson Harza (Firm). (2012). *MWH's water treatment : principles and design.* John Wiley & Sons.

Feng, L. J., Wang, J. J., Liu, S. C., Sun, X. D., Yuan, X. Z., & Wang, S. G. (2018). Role of extracellular polymeric substances in the acute inhibition of activated sludge by polystyrene nanoparticles. *Environmental Pollution*, *238*, 859–865. https://doi.org/10.1016/j.envpol.2018.03.101

Gao, L., Fu, D., Zhao, J., Wu, W., Wang, Z., Su, Y., & Peng, L. (2021). Microplastics aged in various environmental media exhibited strong sorption to heavy metals in seawater. *Marine Pollution Bulletin*, *169*. https://doi.org/10.1016/j.marpolbul.2021.112480

Ghernaout, D. (2020). Water Treatment Coagulation: Dares and Trends. *OALib*, *07*(08), 1–18. https://doi.org/10.4236/oalib.1106636

Hakizimana, J. N., Gourich, B., Chafi, M., Stiriba, Y., Vial, C., Drogui, P., & Naja, J. (2017). Electrocoagulation process in water treatment: A review of electrocoagulation modeling approaches. In *Desalination* (Vol. 404, pp. 1–21). Elsevier B.V. https://doi.org/10.1016/j.desal.2016.10.011

Harif, T., Khai, M., & Adin, A. (2012). Electrocoagulation versus chemical coagulation: Coagulation/flocculation mechanisms and resulting floc characteristics. *Water Research*, *46*(10), 3177–3188. https://doi.org/10.1016/j.watres.2012.03.034

Holt, P. (2002). *Electrocoagulation: unravelling and synthesising the mechanisms behind a water treatment process*. *(Doctoral dissertation, University of New South Wales)* http://hdl.handle.net/2123/624

Hossein Mahvi, A., & Bazrafshan, E. (2007). Removal of Cadmium from Industrial Effluents by Electrocoagulation Process Using Aluminum Electrodes. *World Applied Sciences Journal*, *2*(1), 34–39.

Kiran, B. R., Kopperi, H., & Venkata Mohan, S. (2022). Micro/nano-plastics occurrence, identification, risk analysis and mitigation: challenges and perspectives. In *Reviews in Environmental Science and Biotechnology* (Vol. 21, Issue 1, pp. 169–203). Springer Science and Business Media B.V. https://doi.org/10.1007/s11157-021-09609-6

Koelmans, A. A., Besseling, E., Foekema, E., Kooi, M., Mintenig, S., Ossendorp, B. C., Redondo-Hasselerharm, P. E., Verschoor, A., Van Wezel, A. P., & Scheffer, M. (2017). Risks of Plastic Debris: Unravelling Fact, Opinion, Perception, and Belief. *Environmental Science and Technology*, *51*(20), 11513–11519. https://doi.org/10.1021/acs.est.7b02219

Kudzin, M. H., Piwowarska, D., Festinger, N., & Chruściel, J. J. (2024). Risks Associated with the Presence of Polyvinyl Chloride in the Environment and Methods for Its Disposal and Utilization. In *Materials* (Vol. 17, Issue 1). Multidisciplinary Digital Publishing Institute (MDPI). https://doi.org/10.3390/ma17010173

Kundu, A., Shetti, N. P., Basu, S., Raghava Reddy, K., Nadagouda, M. N., & Aminabhavi, T. M. (2021). Identification and removal of micro- and nano-plastics: Efficient and cost-effective methods. *Chemical Engineering Journal*, *421*. https://doi.org/10.1016/j.cej.2021.129816

Lapointe, M., Farner, J. M., Hernandez, L. M., & Tufenkji, N. (2020). Understanding and Improving Microplastic Removal during Water Treatment: Impact of Coagulation and Flocculation. *Environmental Science and Technology*, *54*(14), 8719–8727. https://doi.org/10.1021/acs.est.0c00712

Lin, H. T., Schneider, F., Aziz, M. A., Wong, K. Y., Arunachalam, K. D., Praveena, S. M., Sethupathi, S., Chong, W. C., Nafisyah, A. L., Parthasarathy, P., Chelliapan, S., & Kunz, A. (2024). Microplastics in Asian rivers: Geographical distribution, most detected types, and inconsistency in methodologies. In *Environmental Pollution* (Vol. 349). Elsevier Ltd. https://doi.org/10.1016/j.envpol.2024.123985

Marine Debris Program, N. (2015). *Laboratory Methods for the Analysis of Microplastics in the Marine Environment: Recommendations for quantifying synthetic particles in waters and sediments*.

Mason, S. A., Daily, J., Aleid, G., Ricotta, R., Smith, M., Donnelly, K., Knauff, R., Edwards, W., & Hoffman, M. J. (2020). High levels of pelagic plastic pollution within the surface waters of Lakes Erie and Ontario. *Journal of Great Lakes Research*, *46*(2), 277–288. https://doi.org/10.1016/j.jglr.2019.12.012

Mason, S. A., Garneau, D., Sutton, R., Chu, Y., Ehmann, K., Barnes, J., Fink, P., Papazissimos, D., & Rogers, D. L. (2016). Microplastic pollution is widely detected in US municipal wastewater treatment plant effluent. *Environmental Pollution*, *218*, 1045–1054. https://doi.org/10.1016/j.envpol.2016.08.056

Mason, S. A., Welch, V. G., & Neratko, J. (2018). Synthetic Polymer Contamination in Bottled Water. *Frontiers in Chemistry*, *6*. https://doi.org/10.3389/fchem.2018.00407

Nath, J., De, J., Sur, S., & Banerjee, P. (2023). Interaction of Microbes with Microplastics and Nanoplastics in the Agroecosystems—Impact on Antimicrobial Resistance. In *Pathogens* (Vol. 12, Issue 7). Multidisciplinary Digital Publishing Institute (MDPI). https://doi.org/10.3390/pathogens12070888

Nidheesh, P. V., Oladipo, A. A., Yasri, N. G., Laiju, A. R., Cheela, V. R. S., Thiam, A., Asfaha, Y. G., Kanmani, S., & Roberts, E. (Ted) P. L. (2022). Emerging applications, reactor design and recent advances of electrocoagulation process. In *Process Safety and Environmental Protection* (Vol. 166, pp. 600–616). Institution of Chemical Engineers. https://doi.org/10.1016/j.psep.2022.08.051

Pawak, V. S., Loganathan, V. A., & Sabapathy, M. (2023). *Efficient removal of nanoplastics from synthetic wastewater using electrocoagulation*. http://arxiv.org/abs/2302.08451

Perren, W., Wojtasik, A., & Cai, Q. (2018). Removal of Microbeads from Wastewater Using Electrocoagulation. *ACS Omega*, *3*(3), 3357–3364. https://doi.org/10.1021/acsomega.7b02037

A.T. Pruter, Sources, quantities and distribution of persistent plastics in the marine environment, Marine Pollution Bulletin, Volume 18, Issue 6, Supplement B, 1987, Pages 305-310. https://doi.org/10.1016/S0025-326X(87)80016-4.

Sankar Sana, S., Kumar Dogiparthi, L., Gangadhar, L., Chakravorty, A., & Abhishek, N. (n.d.). *Effects of microplastics and nanoplastics on marine environment and human health*. https://doi.org/10.1007/s11356-020-10573-x/Published

Shen, M., Zhang, Y., Almatrafi, E., Hu, T., Zhou, C., Song, B., Zeng, Z., & Zeng, G. (2022). Efficient removal of microplastics from wastewater by an electrocoagulation process. *Chemical Engineering Journal*, *428*. https://doi.org/10.1016/j.cej.2021.131161

Shen, M., Zhu, Y., Zhang, Y., Zeng, G., Wen, X., Yi, H., Ye, S., Ren, X., & Song, B. (2019). Micro(nano)plastics: Unignorable vectors for organisms. *Marine Pollution Bulletin*, *139*, 328–331. https://doi.org/10.1016/j.marpolbul.2019.01.004

Thomas, A., Marchand, J., Schwoerer, G. D., Minor, E. C., & Maurer-Jones, M. A. (2024). Size Distributions of Microplastics in the St Louis Estuary and Western Lake Superior. *Environmental Science and Technology*, *58*(19), 8480–8489. https://doi.org/10.1021/acs.est.3c10776

Tsai, M. H., Chao, S. J., Chung, K. H., Hua, L. C., & Huang, C. (2023). Destabilization of polystyrene nanoplastics with different surface charge and particle size by Fe electrocoagulation. *Science of the Total Environment*, *872*. https://doi.org/10.1016/j.scitotenv.2023.162254

Wang, L., Wu, W. M., Bolan, N. S., Tsang, D. C. W., Li, Y., Qin, M., & Hou, D. (2021). Environmental fate, toxicity and risk management strategies of nanoplastics in the environment: Current status and future perspectives. *Journal of Hazardous Materials*, *401*. https://doi.org/10.1016/j.jhazmat.2020.123415

Wang, Z., Lin, T., & Chen, W. (2020). Occurrence and removal of microplastics in an advanced drinking water treatment plant (ADWTP). *Science of the Total Environment*, *700*. https://doi.org/10.1016/j.scitotenv.2019.134520

Wright, S. L., Thompson, R. C., & Galloway, T. S. (2013). The physical impacts of microplastics on marine organisms: a review. In *Environmental pollution (Barking, Essex : 1987)* (Vol. 178, pp. 483–492). https://doi.org/10.1016/j.envpol.2013.02.031

Yee, M. S. L., Hii, L. W., Looi, C. K., Lim, W. M., Wong, S. F., Kok, Y. Y., Tan, B. K., Wong, C. Y., & Leong, C. O. (2021). Impact of microplastics and nanoplastics on human health. In *Nanomaterials* (Vol. 11, Issue 2, pp. 1–23). MDPI AG. https://doi.org/10.3390/nano11020496

Zhang, Y., Diehl, A., Lewandowski, A., Gopalakrishnan, K., & Baker, T. (2020). Removal efficiency of micro- and nanoplastics (180 nm–125 µm) during drinking water treatment. *Science of the Total Environment*, *720*. https://doi.org/10.1016/j.scitotenv.2020.137383

12 Appendices

12.1 Appendix A

The experiment number (Exp #) on the table denotes a unique identifier for each set of experimental condition. Experiments 1 to 3 (Tables 9 – 11) are experiments run at 10 mA, experiments 4 to 6 (Tables 12 – 14), 25 mA, and experiments 7 to 9 (Tables 15 – 17), 50 mA. All experimental were performed at 5 V.

Table 9 First set of triplicates at 10 mA, 5V

			Exp 1	AVG.	STD	CI
Sample ID	A1.1	A1.2	A1.3			
Initial Turbidity (NTU)	20	20	20	20.0	0.00	0.00
Initial pH	5.52	5.55	5.47	5.5	0.04	0.05
Temperature (˚C)	24.3	22.1	23.2	23.2	1.10	1.24
Electrical conductivity (µS/cm)	833	824	836	831.0	6.24	7.07
Electrode Number (E#)						
Electrode spacing (cm)	5.5	5.5	5.4	5.5	0.06	0.08
Electrode Area in water (m2)	0.0010	0.0010	0.0010	0.0	0.00	0.00
Volts (V)	5	5	5			
Current (A)	0.01	0.01	0.01			
Current density (A/m2)	10.53	10.53	10.53	10.5	0.00	0.00
Final pH	8.04	8.09	8.12	8.1	0.04	0.06
Final turbidity (NTU)	3.63	3.42	3.12	3.4	0.26	0.36
Removal %	81.85	82.90	84.40	83.1	1.28	1.78
Foam Volume (F.V)	1.20	1.30	1.15		0.08	0.11

Table 10 Second set of triplicates at 10 mA, 5V

			Exp 2	AVG.	STD	CI
Sample ID	A2.1	A2.2	A2.3			
Initial Turbidity (NTU)	20	20	20	20.0	0.00	0.00
Initial pH	5.5	5.49	5.56	5.5	0.04	0.05
Temperature (˚C)	23.1	22.8	22.9	22.9	0.15	0.21
Electrical conductivity (µS/cm)	831	849	837	839.0	9.17	12.70
Electrode Number (E#)						
Electrode spacing (cm)	5.3	5.4	5.4	5.4	0.06	0.08
Electrode Area in water (m2)	0.0010	0.0010	0.0010	0.0	0.00	0.00
Volts (V)	5	5	5			
Current (A)	0.01	0.01	0.01			
Current density (A/m2)	10.53	10.53	10.53	10.5	0.00	0.00
Final pH	7.99	8.08	8.13	8.1	0.07	0.10
Final turbidity (NTU)	3.01	3.62	2.82	3.2	0.42	0.58
Removal %	84.95	81.90	85.90	84.3	2.09	2.90

Foam Volume (F.V)	1.30	1.10	1.23	1.21	0.10	0.14

Table 11 Third set of triplicates at 10 mA, 5V

			Exp 3	AVG.	STD	CI
Sample ID	A3.1	A3.2	A3.3			
Initial Turbidity (NTU)	20	20	20	20.0	0.00	0.00
Initial pH	5.48	5.55	5.61	5.5	0.07	0.09
Temperature (˚C)	22.1	22.1	22.1	22.1	0.00	0.00
Electrical conductivity (µS/cm)	803	813	807	807.7	5.03	6.98
Electrode Number (E#)						
Electrode spacing (cm)	5.5	5.5	5.4	5.5	0.06	0.08
Electrode Area in water (m2)	0.0010	0.0010	0.0010	0.0	0.00	0.00
Volts (V)	5	5	5			
Current (A)	0.01	0.01	0.01			
Current density (A/m2)	10.53	10.53	10.53	10.5	0.00	0.00
Final pH	8.09	7.89	7.94	8.0	0.10	0.14
Final turbidity (NTU)	3.33	2.71	3.86	3.3	0.58	0.80
Removal %	83.35	86.45	80.70	83.5	2.88	3.99
Foam Volume (F.V)	1.20	1.30	1.10	1.20	0.10	0.14

Table 12 First set of triplicates at 25 mA, 5V

			Exp 4	AVG.	STD	CI
Sample ID	B1.1	B1.2	B1.3			
Initial Turbidity (NTU)	20	20	20	20.0	0.00	0.00
Initial pH	5.55	5.65	5.58	5.6	0.05	0.06
Temperature (C)	22.1	21.8	22.1	22.0	0.17	0.20
Electrical conductivity (µS/cm)	901	835	874	870.0	33.18	37.55
Electrode Number (E#)						
Electrode spacing (cm)	2	2	2	2.0	0.00	0.00
Electrode Area in water (m2)	0.0010	0.0010	0.0010	0.0	0.00	0.00
Volts (V)	5	5	5			
Current (A)	0.025	0.025	0.025			
Current density (A/m2)	23.92	24.37	23.92	24.1	0.26	0.35
Final pH	8.23	8.31	8.27	8.3	0.04	0.06
Final turbidity (NTU)	1.77	2.22	1.85	1.9	0.24	0.33
Removal %	91.15	88.90	90.75	90.3	1.20	1.66

Foam Volume (F.V)	4.38	4.75	4.55	4.56	0.19	0.26

Table 13 Second set of triplicates at 25 mA, 5V

			Exp 5	AVG.	STD	CI
Sample ID	B2.1	B2.2	B2.3			
Initial Turbidity (NTU)	20	20.3	20.1	20.1	0.15	0.21
Initial pH	5.44	5.25	5.35	5.3	0.10	0.13
Temperature (˚C)	22	21.7	21.8	21.8	0.15	0.21
Electrical conductivity (µS/cm)	862	820	854	845.3	22.30	30.91
Electrode Number (E#)						
Electrode spacing (cm)	2	2	2	2.0	0.00	0.00
Electrode Area in water (m2)	0.0010	0.0010	0.0010	0.0	0.00	0.00
Volts (V)	5	5	5			
Current (A)	0.025	0.025	0.025			
Current density (A/m2)	24.37	24.37	23.92	24.2	0.26	0.35
Final pH	8.38	8.35	8.29	8.3	0.05	0.06
Final turbidity (NTU)	1.73	1.58	1.61	1.6	0.08	0.11
Removal %	91.35	92.22	91.99	91.9	0.45	0.62

Foam Volume (F.V)	5.00	4.70	4.50	4.73	0.25	0.35

Table 14 Third set of triplicates at 25 mA, 5V

			Exp.6	AVG.	STD	CI
Sample ID	B3.1	B3.2	B3.3			
Initial Turbidity (NTU)	20	20	20.1	20.0	0.06	0.08
Initial pH	5.52	5.56	5.81	5.6	0.16	0.22
Temperature (˚C)	21.7	21.6	21.7	21.7	0.06	0.08
Electrical conductivity (µS/cm)	757	780	765	767.3	11.68	16.18
Electrode Number (E#)						
Electrode spacing (cm)	2	2	2	2.0	0.00	0.00
Electrode Area in water (m2)	0.0010	0.0010	0.0010	0.0	0.00	0.00
Volts (V)	5	5	5			
Current (A)	0.025	0.025	0.025			
Current density (A/m2)	23.92	23.92	24.37	24.1	0.26	0.35
Final pH	8.23	8.26	8.31	8.3	0.04	0.06
Final turbidity (NTU)	1.71	2.13	1.64	1.8	0.27	0.37
Removal %	91.45	89.35	91.84	90.9	1.34	1.86

Foam Volume (F.V)	4.80	4.60	4.90	4.77	0.15	0.21

Table 15 First set of triplicates at 50 mA, 5V

			Exp 7	AVG.	STD	CI
Sample ID	C1.1	C1.2	C1.3			
Initial Turbidity (NTU)	20.3	20	20.1	20.1	0.15	0.17
Initial pH	5.32	5.45	5.43	5.4	0.07	0.08
Temperature (˚C)	20.6	20.6	20.6	20.6	0.00	0.00
Electrical conductivity (µS/cm)	793	782	788	787.7	5.51	6.23
Electrode Number (E#)						
Electrode spacing (cm)	0.9	1	1	1.0	0.06	0.08
Electrode Area in water (m2)	0.0011	0.0011	0.0011	0.0	0.00	0.00
Volts (V)	5	5	5			
Current (A)	0.05	0.05	0.05			
Current density (A/m2)	43.86	43.86	43.86	43.9	0.00	0.00
Final pH	8.72	8.65	8.24	8.5	0.26	0.36
Final turbidity (NTU)	1.21	1.27	1.3	1.3	0.05	0.06
Removal %	94.04	93.65	93.53	93.7	0.27	0.37

Foam Volume (F.V)	6.80	7.10	6.90	6.93	0.15	0.21

Table 16 Second set of triplicates at 50 mA, 5V

			Exp 8	AVG.	STD	CI
Sample ID	C2.1	C2.2	C2.3			
Initial Turbidity (NTU)	20.2	20.3	20.2	20.2	0.06	0.08
Initial pH	5.54	5.43	5.38	5.5	0.08	0.11
Temperature (˚C)	20.5	20.7	20.5	20.6	0.12	0.16
Electrical conductivity (µS/cm)	796	798	798	797.3	1.15	1.60
Electrode Number (E#)						
Electrode spacing (cm)	1	0.9	1	1.0	0.06	0.08
Electrode Area in water (m2)	0.0011	0.0011	0.0011	0.0	0.00	0.00
Volts (V)	5	5	5			
Current (A)	0.05	0.05	0.05			
Current density (A/m2)	43.86	43.86	43.86	43.9	0.00	0.00
Final pH	8.65	8.49	8.41	8.5	0.12	0.17
Final turbidity (NTU)	1.19	1.34	1.1	1.2	0.12	0.17
Removal %	94.11	93.40	94.55	94.0	0.58	0.81

Foam Volume (F.V)	6.60	7.00	6.85	6.82	0.20	0.28

Table 17 Third set of triplicates at 50 mA, 5V

			Exp 9	AVG.	STD	CI
Sample ID	C3.1	C3.2	C3.3			
Initial Turbidity (NTU)	20	20	20	20.0	0.00	0.00
Initial pH	5.42	5.12	5.36	5.3	0.16	0.22
Temperature (˚C)	22.9	22.8	22.9	22.9	0.06	0.08
Electrical conductivity (µS/cm)	744	742	745	743.7	1.53	2.12
Electrode Number (E#)						
Electrode spacing (cm)	0.9	0.9	1	0.9	0.06	0.08
Electrode Area in water (m2)	0.0011	0.0011	0.0011	0.0	0.00	0.00
Volts (V)	5	5	5			
Current (A)	0.05	0.05	0.05			
Current density (A/m2)	45.37	45.37	43.86	44.9	0.87	1.21
Final pH	8.44	8.31	8.37	8.4	0.07	0.09
Final turbidity (NTU)	1.33	1.21	1.11	1.2	0.11	0.15
Removal %	93.35	93.95	94.45	93.9	0.55	0.76

Foam Volume (F.V)	7.20	6.80	7.00	7.00	0.20	0.28

12.2 Appendix B

The Brookhaven NanoBrook 90PlusPALS equipment was set to measure each sample three time hence the 1, 2, 3 comes after the sample name. An example is, for the first triplicates for 10 mA before and after EC is named PS-NP SAMP BF EC A1.1 – 1, A1.2 – 2, A1.3 – 3. And PS-NP SAMP AF EC A1.1 – 1, A1.2 – 2, A1.3 – 3 respectively. This naming style applies to the experiments run at 25 mA and 50 mA prefixed with “B” and “C” before the numerical values respectively.

The particle size graphs shown in odd numbered figures starting from 21 to 61 displays the distribution of particle sizes measured dynamic light scattering (DLS), where (Y-axis) is plotted against particle diameter in nanometers (X-axis) on a logarithmic scale. The dataset includes multiple samples, each represented by distinct curve identified by specific timestamps. The primary feature observed is a significant peak in the ranges around 100 nm and 350 nm on most curves, indicating that most particles in these samples have a diameter in that range. This peak suggests a relatively uniform and monodisperse distribution of the NPs, which is desirable characteristic in many applications.

However, for the measurement before EC, some of the curves show additional peaks at larger diameters ranging from 100 nm to 10000 nm. These secondary peaks indicate the presence of larger particles or aggregates within the sample. The sharp and well define primary peaks across most samples highlights the consistency in the particle size distribution, while the broader size distribution in one sample points to possible aggregation or polydispersity issues. And also, for measurements after EC process, the graphs suggest significant aggregation or presence of large particle clusters in the analysed sample. The

larger particle sizes across samples indicates the effect of aluminum coagulants produced during the EC process.

The zeta potential graphs shown in even numbered figures starting from 28 to 62 displays the illustrates phase versus time data for different analytical replicate samples with phase measured in radians over a time interval of 0 to 0.9 sec. The graph features multiple curves, each representing distinct analytical replication runs or samples differentiated by colour and timestamp. The phase values ranging from approximately -4 to 16 radians show periodic behaviour with each curve exhibiting distinct peak and troughs. The variations in peak heights, timing and overall shape suggests that the sample experienced differing phase shift overtime indicative of variations in their physical properties or interactions with their environment. The difference between the curves imply that the samples possess distinct characteristics possibly due to variation in particle size which is a critical factor under the investigation in this study.

Table 18 Particle size measurement for first set of triplicates at 10 mA, 5V before EC

Sample ID	Eff. Diam. (nm)	Polydispersity	Baseline Index	Count Rate (kcps)	Data Retained (%)	Diffusion Coeff. (cm^2/s)	pH
PS-NP SAMP BF EC A1.1 - 1	263.5	0.03	4.8	1,062.10	98.45	1.86E-08	5.52
PS-NP SAMP BF EC A1.1 - 2	252.55	0.046	7	1,091.60	96.44	1.94E-08	5.52
PS-NP SAMP BF EC A1.1 - 3	259.17	0.089	4.9	1,093.00	100	1.89E-08	5.52
PS-NP SAMP BF EC A1.2 - 1	284.38	0.082	0.6	419.4	96.85	1.73E-08	5.55
PS-NP SAMP BF EC A1.2 - 2	285.93	0.072	7.1	406.8	98.43	1.72E-08	5.55
PS-NP SAMP BF EC A1.2 - 3	275.22	0.119	4.6	403.7	91.73	1.78E-08	5.55
PS-NP SAMP BF EC A1.3 - 1	256.67	0.058	9.5	346.6	98.43	1.91E-08	5.47
PS-NP SAMP BF EC A1.3 - 2	814.74	0.204	0	348.5	100	6.02E-09	5.47
PS-NP SAMP BF EC A1.3 - 3	251.15	0.121	8.8	334.4	98	1.95E-08	5.47
Mean:	327.03	0.091	5.3	611.8	97.59	1.71E-08	5.51
Std Err:	61.12	0.017	1.1	118.1	0.83	1.42E-09	0.01

Table 19 Zeta potential measurement for first set of triplicates at 10 mA, 5V before EC

Sample ID	Zeta Potential (mV)	Mobility (µ/s)/(V/cm)	Conductance (µS)	Sample Count Rate (kcps)	Ref. Count Rate (kcps)	RMS Residual	pH
PS-NP SAMP BF EC A1.1 - 1	13.38	1.05	1,389	359	991	2.51E-02	5.52
PS-NP SAMP BF EC A1.1 - 2	14	1.09	1,397	359	991	3.88E-02	5.52
PS-NP SAMP BF EC A1.1 - 3	9.07	0.71	1,396	359	991	2.44E-02	5.52
PS-NP SAMP BF EC A1.2 - 1	36.48	2.85	1,392	308	1,085	4.83E-02	5.55
PS-NP SAMP BF EC A1.2 - 2	34.37	2.69	1,410	308	1,085	6.12E-02	5.55
PS-NP SAMP BF EC A1.2 - 3	33.92	2.65	1,408	308	1,085	5.47E-02	5.55
PS-NP SAMP BF EC A1.3 - 1	2.81	0.22	1,399	1,007	1,258	2.44E-02	5.47
PS-NP SAMP BF EC A1.3 - 2	3.03	0.24	1,405	1,007	1,258	2.73E-02	5.47
PS-NP SAMP BF EC A1.3 - 3	8.59	0.67	1,404	1,007	1,258	5.60E-02	5.47
Mean:	17.3	1.35	1,400	558	1,111	4.00E-02	5.51
Std Err:	4.59	0.36	2	113	39	5.08E-03	0.01

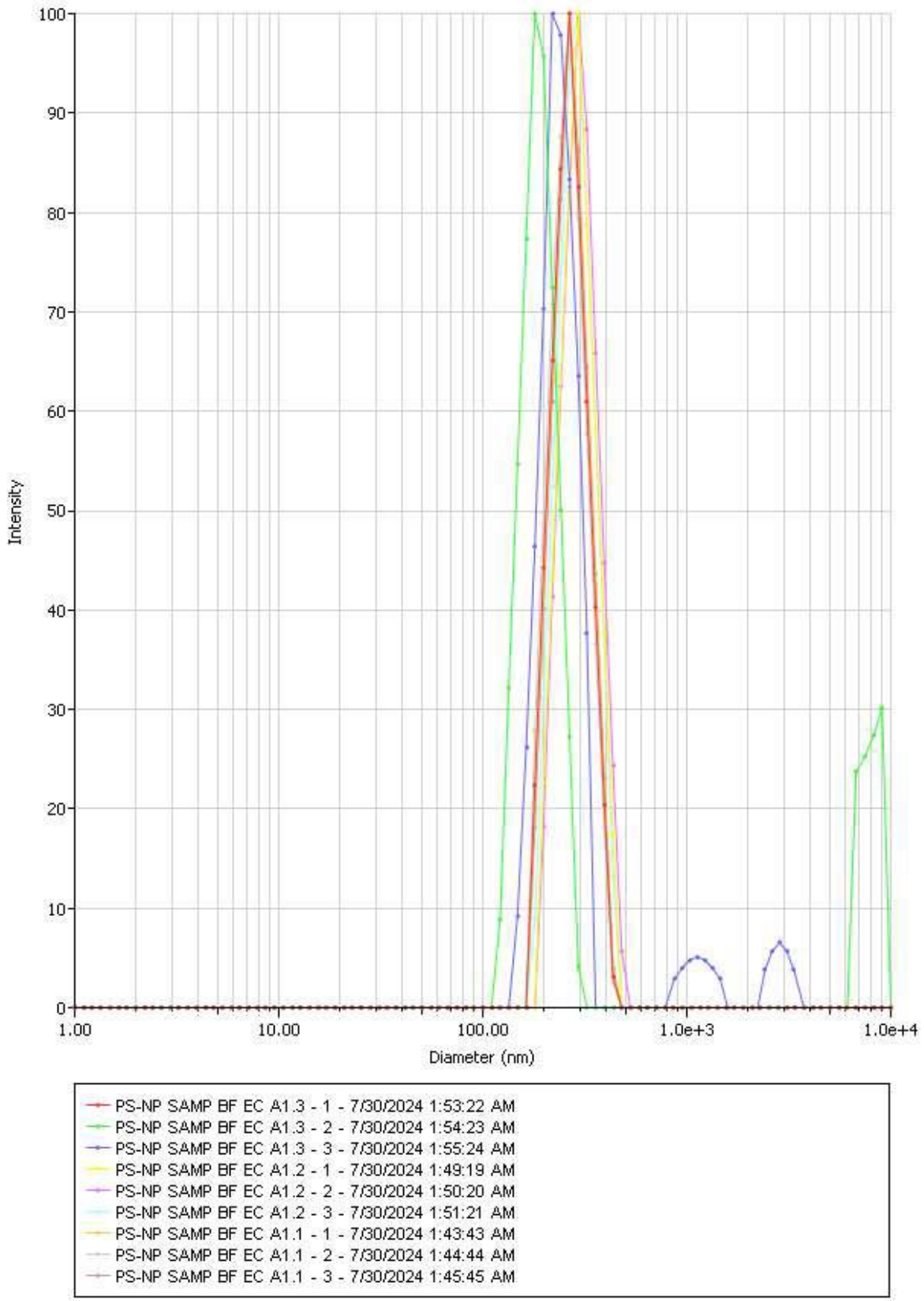

Figure 27 Particle size graph for first set of triplicates at 10 mA, 5V before EC

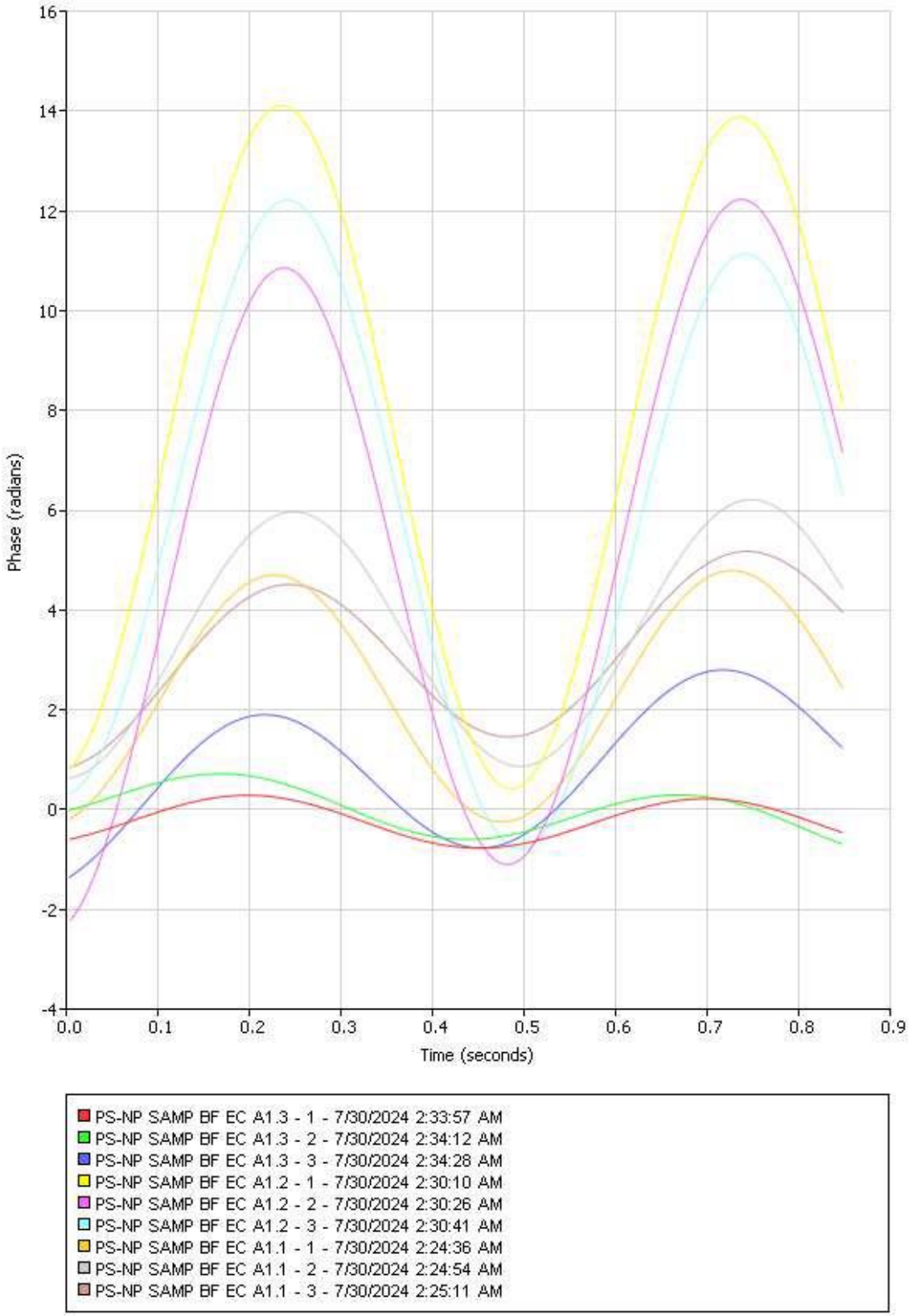

Figure 28 Zeta potential graph for first set of triplicates at 10 mA, 5V before EC

Table 20 Particle size measurement for second set of triplicates at 10 mA, 5V before EC

Sample ID	Eff. Diam. (nm)	Polydispersity	Baseline Index	Count Rate (kcps)	Data Retained (%)	Diffusion Coeff. (cm^2/s)	pH
PS-NP SAMP BF EC A2.1 - 1	257.7	0.006	0.1	224.8	98.85	1.90E-08	5.5
PS-NP SAMP BF EC A2.1 - 2	258.12	0.054	7.2	224.8	100	1.90E-08	5.5
PS-NP SAMP BF EC A2.1 - 3	250.03	0.193	4.5	222.2	98.11	1.96E-08	5.5
PS-NP SAMP BF EC A2.2 - 1	263.82	0.096	0	922.9	96.51	1.86E-08	5.49
PS-NP SAMP BF EC A2.2 - 2	254.23	0.056	5.8	905.5	100	1.93E-08	5.49
PS-NP SAMP BF EC A2.2 - 3	263.44	0.023	6	921.2	100	1.86E-08	5.49
PS-NP SAMP BF EC A2.3 - 1	261.49	0.047	3.7	921	98.45	1.88E-08	5.56
PS-NP SAMP BF EC A2.3 - 2	251.96	0.087	8.1	918	98.45	1.95E-08	5.56
PS-NP SAMP BF EC A2.3 - 3	252.3	0.034	6.3	911.8	95.35	1.95E-08	5.56
Mean:	257.01	0.066	4.6	685.8	98.41	1.91E-08	5.52
Std Err:	1.72	0.018	1	115.5	0.54	1.28E-10	0.01

Table 21 Zeta potential measurement for second set of triplicates at 10 mA, 5V before EC

Sample ID	Zeta Potential (mV)	Mobility (µ/s)/(V/cm)	Conductance (µS)	Sample Count Rate (kcps)	Ref. Count Rate (kcps)	RMS Residual	pH
PS-NP SAMP BF EC A2.1 - 1	34.75	2.72	1,415	446	1,192	7.33E-02	5.5
PS-NP SAMP BF EC A2.1 - 2	36.45	2.85	1,420	446	1,192	2.88E-02	5.5
PS-NP SAMP BF EC A2.1 - 3	20.52	1.6	1,422	446	1,192	6.01E-02	5.5
PS-NP SAMP BF EC A2.2 - 1	34.39	2.69	1,475	548	1,257	5.23E-02	5.49
PS-NP SAMP BF EC A2.2 - 2	37.84	2.96	1,477	548	1,257	5.96E-02	5.49
PS-NP SAMP BF EC A2.2 - 3	32.5	2.54	1,478	548	1,257	4.28E-02	5.49
PS-NP SAMP BF EC A2.3 - 1	11.09	0.87	1,435	264	1,270	4.52E-02	5.56
PS-NP SAMP BF EC A2.3 - 2	13.54	1.06	1,438	264	1,270	2.64E-02	5.56
PS-NP SAMP BF EC A2.3 - 3	11.88	0.93	1,434	264	1,270	2.36E-02	5.56
Mean:	25.88	2.02	1,444	419	1,240	4.58E-02	5.52
Std Err:	3.81	0.3	9	42	12	5.73E-03	0.01

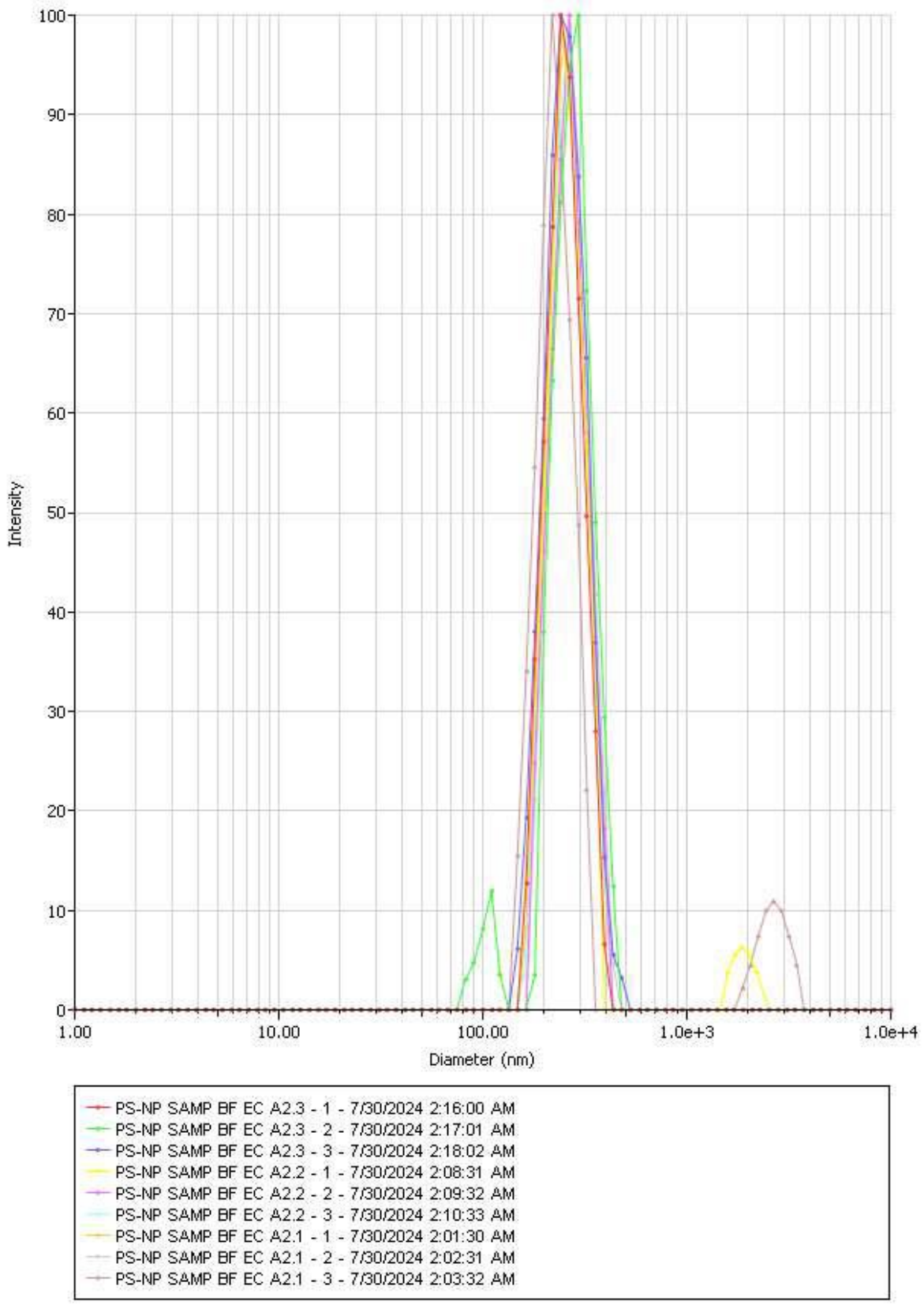

Figure 29 Particle size graph for second set of triplicates at 10 mA, 5V before EC

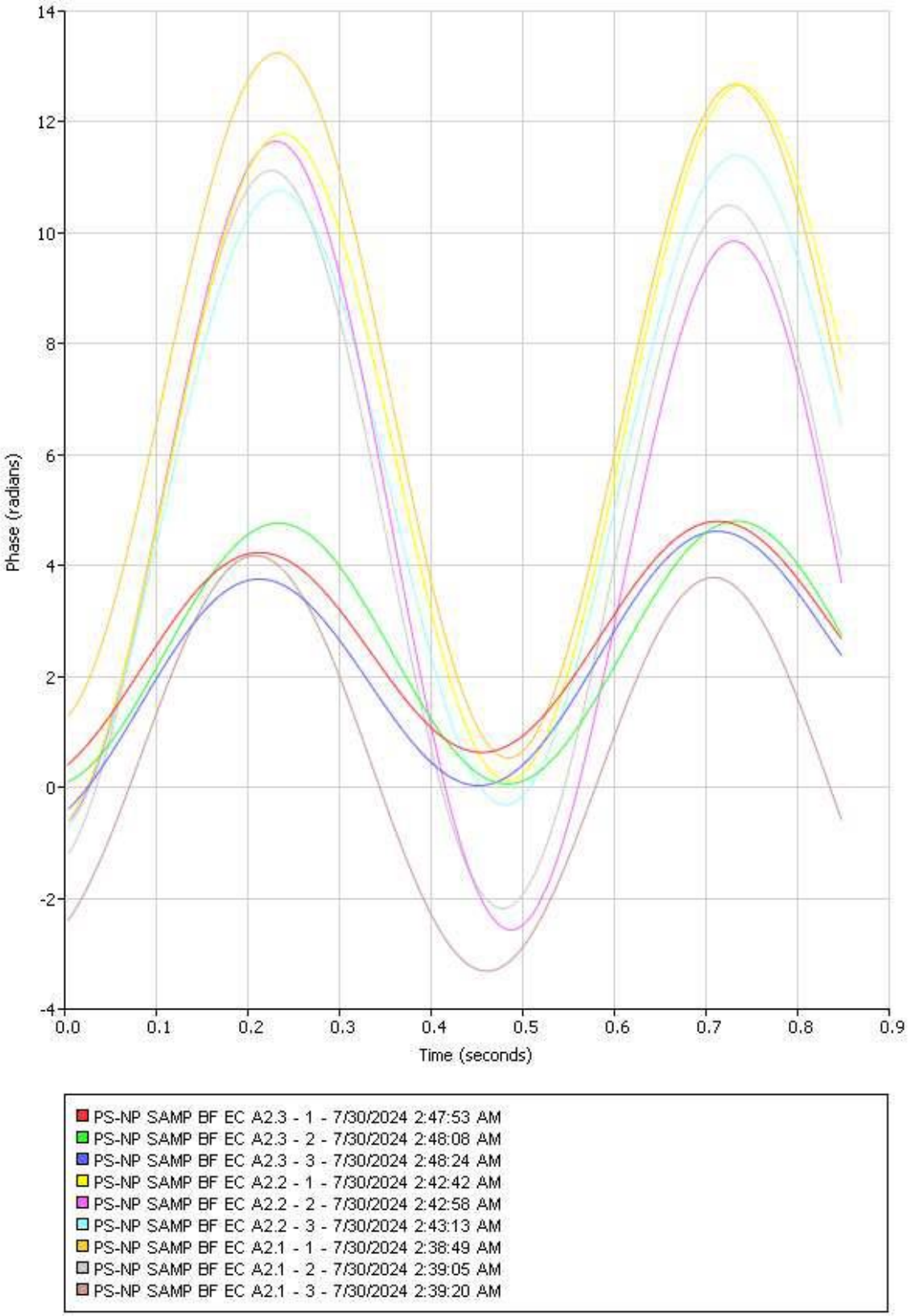

Figure 30 Particle size graph for second set of triplicates at 10 mA, 5V before EC

Table 22 Particle size measurement for third set of triplicates at 10 mA, 5V before EC

Sample ID	Eff. Diam. (nm)	Polydispersity	Baseline Index	Count Rate (kcps)	Data Retained (%)	Diffusion Coeff. (cm^2/s)	pH
PS-NP SAMP BF EC A3.1 - 1	208.84	0.279	0	33.1	96.53	2.35E-08	5.48
PS-NP SAMP BF EC A3.1 - 2	206.08	0.261	0	33.8	87.62	2.38E-08	5.48
PS-NP SAMP BF EC A3.1 - 3	201.57	0.267	2.8	34.1	93.38	2.44E-08	5.48
PS-NP SAMP BF EC A3.2 - 1	194.72	0.266	3.8	9.6	100	2.52E-08	5.55
PS-NP SAMP BF EC A3.2 - 2	183.97	0.191	0	9.7	97.12	2.67E-08	5.55
PS-NP SAMP BF EC A3.2 - 3	199.78	0.286	0	10.2	91.82	2.46E-08	5.55
PS-NP SAMP BF EC A3.3 - 1	268.81	0.092	0	491.7	96.47	1.83E-08	5.61
PS-NP SAMP BF EC A3.3 - 2	255.95	0.135	3	481.7	96.47	1.92E-08	5.61
PS-NP SAMP BF EC A3.3 - 3	253.65	0.137	0	486.6	96.8	1.94E-08	5.61
Mean:	219.26	0.213	1.1	176.7	95.13	2.28E-08	5.55
Std Err:	10.41	0.025	0.5	77.6	1.22	1.01E-09	0.02

Table 23 Zeta potential measurement for third set of triplicates at 10 mA, 5V before EC

Sample ID	Zeta Potential (mV)	Mobility (µ/s)/(V/cm)	Conductance (µS)	Sample Count Rate (kcps)	Ref. Count Rate (kcps)	RMS Residual	pH
PS-NP SAMP BF EC A3.1 - 1	-43.09	-3.37	1,466	1,008	508	8.30E-02	5.48
PS-NP SAMP BF EC A3.1 - 2	-55.12	-4.31	1,477	1,008	508	3.29E-02	5.48
PS-NP SAMP BF EC A3.1 - 3	-43.24	-3.38	1,477	1,008	508	5.12E-02	5.48
PS-NP SAMP BF EC A3.2 - 1	-32.9	-2.57	1,463	833	1,268	2.75E-02	5.55
PS-NP SAMP BF EC A3.2 - 2	-31.05	-2.43	1,470	833	1,268	3.54E-02	5.55
PS-NP SAMP BF EC A3.2 - 3	-40.68	-3.18	1,473	833	1,268	3.75E-02	5.55
PS-NP SAMP BF EC A3.3 - 1	-50.09	-3.91	1,506	414	1,220	3.95E-02	5.61
PS-NP SAMP BF EC A3.3 - 2	-40.58	-3.17	1,496	414	1,220	2.39E-02	5.61
PS-NP SAMP BF EC A3.3 - 3	-47.61	-3.72	1,510	414	1,220	3.97E-02	5.61
Mean:	-42.71	-3.34	1,482	752	999	4.12E-02	5.55
Std Err:	2.56	0.2	6	88	123	5.84E-03	0.02

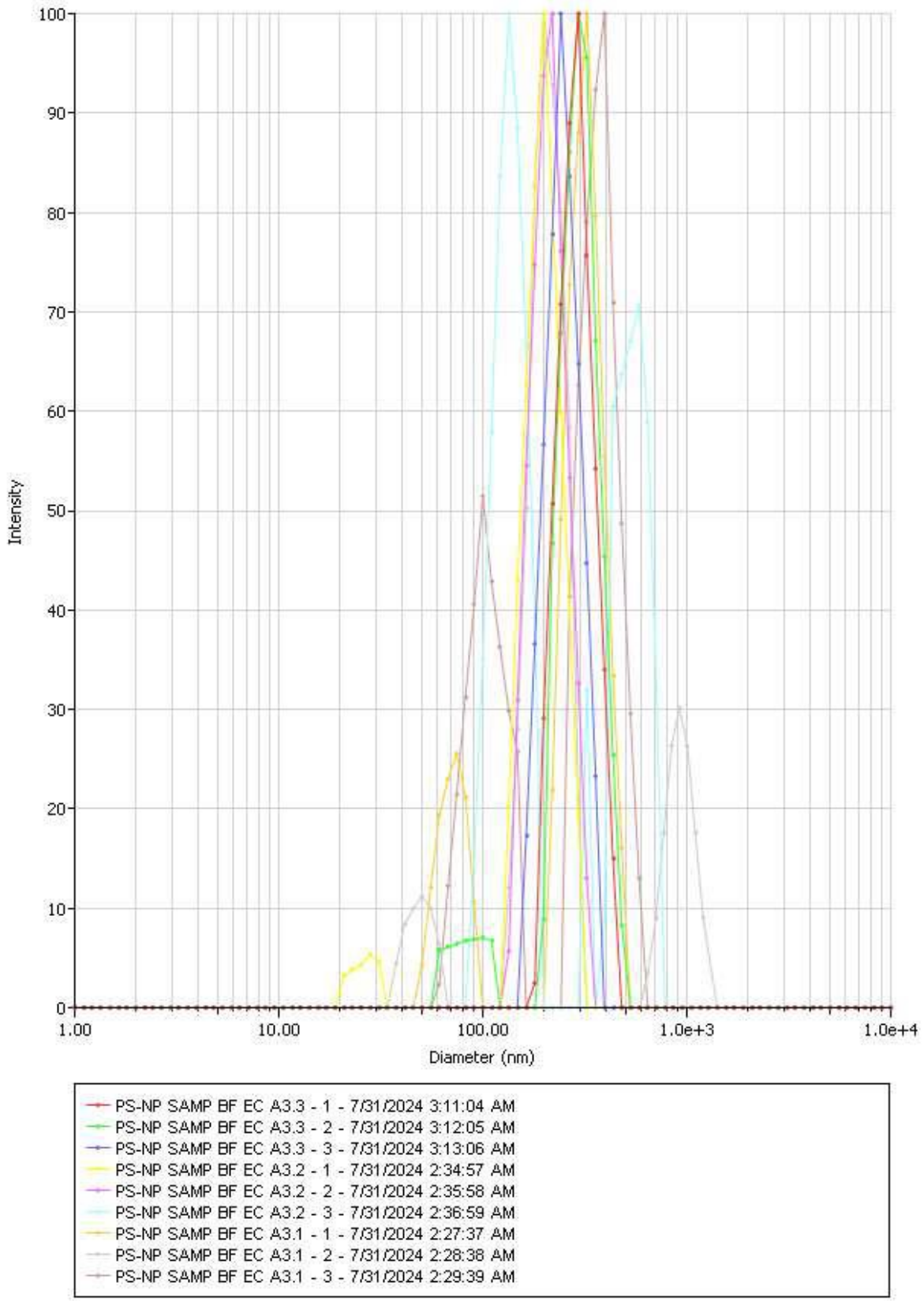

Figure 31 Particle size graph for third set of triplicates at 10 mA, 5V before EC

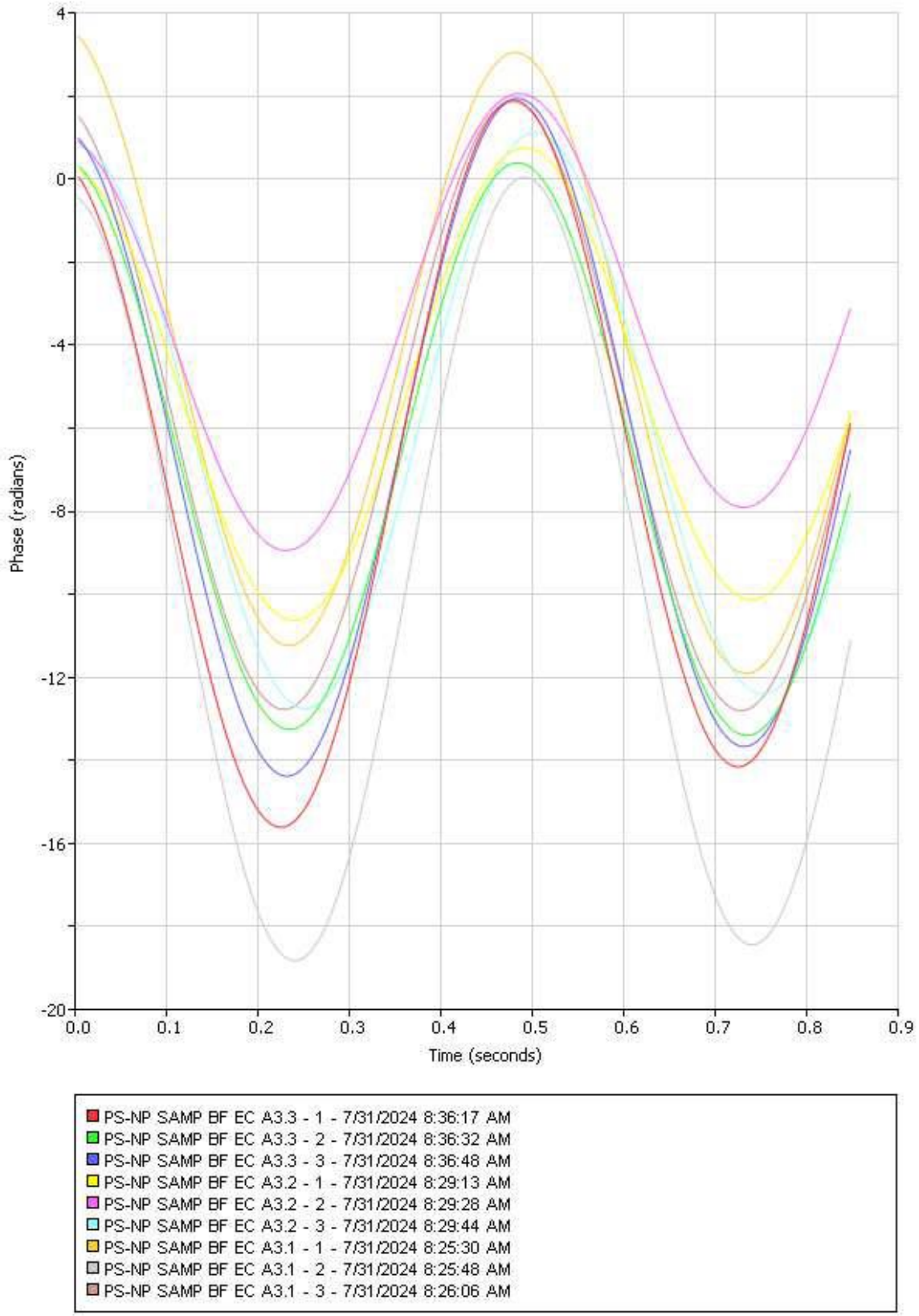

Figure 32 Zeta potential graph for third set of triplicates at 10 mA, 5V before EC

Table 24 Particle size measurement for first set of triplicates at 25 mA, 5V before EC

Sample ID	Eff. Diam. (nm)	Polydispersity	Baseline Index	Count Rate (kcps)	Data Retained (%)	Diffusion Coeff. (cm^2/s)	pH
PS-NP SAMP BF EC B1.1 - 1	209.4	0.234	1	606.8	100	2.34E-08	5.55
PS-NP SAMP BF EC B1.1 - 2	207.32	0.246	0	617.3	98.02	2.37E-08	5.55
PS-NP SAMP BF EC B1.1 - 3	213.21	0.24	0	628.1	98.41	2.30E-08	5.55
PS-NP SAMP BF EC B1.2 - 1	276.28	0.021	0	501.6	96.41	1.78E-08	5.65
PS-NP SAMP BF EC B1.2 - 2	272.06	0.036	0	508.7	94.9	1.80E-08	5.65
PS-NP SAMP BF EC B1.2 - 3	256.07	0.167	4.9	504.6	93.73	1.92E-08	5.65
PS-NP SAMP BF EC B1.3 - 1	210.64	0.246	7.7	506.9	91.5	2.33E-08	5.58
PS-NP SAMP BF EC B1.3 - 2	198.65	0.21	9.1	504	98.43	2.47E-08	5.58
PS-NP SAMP BF EC B1.3 - 3	198.79	0.23	2.4	500.1	96.41	2.47E-08	5.58
Mean:	226.94	0.181	2.8	542	96.42	2.20E-08	5.59
Std Err:	10.58	0.03	1.2	19	0.89	9.41E-10	0.01

Table 25 Zeta potential measurement for first set of triplicates at 25 mA, 5V before EC

Sample ID	Zeta Potential (mV)	Mobility (µ/s)/(V/cm)	Conductance (µS)	Sample Count Rate (kcps)	Ref. Count Rate (kcps)	RMS Residual	pH
PS-NP SAMP BF EC B1.1 - 1	-48.43	-3.78	1,494	950	1,184	5.22E-02	5.55
PS-NP SAMP BF EC B1.1 - 2	-44.78	-3.5	1,498	950	1,184	5.16E-02	5.55
PS-NP SAMP BF EC B1.1 - 3	-55.74	-4.36	1,497	950	1,184	4.71E-02	5.55
PS-NP SAMP BF EC B1.2 - 1	-24.54	-1.92	1,480	864	1,259	3.71E-02	5.65
PS-NP SAMP BF EC B1.2 - 2	-25.42	-1.99	1,486	864	1,259	6.83E-02	5.65
PS-NP SAMP BF EC B1.2 - 3	-26.73	-2.09	1,487	864	1,259	4.83E-02	5.65
PS-NP SAMP BF EC B1.3 - 1	-52.14	-4.07	1,509	775	1,284	4.22E-02	5.58
PS-NP SAMP BF EC B1.3 - 2	-44.41	-3.47	1,517	775	1,284	6.76E-02	5.58
PS-NP SAMP BF EC B1.3 - 3	-52.8	-4.13	1,516	775	1,284	6.82E-02	5.58
Mean:	-41.67	-3.26	1,498	863	1,242	5.36E-02	5.59
Std Err:	4.21	0.33	4	25	15	3.92E-03	0.01

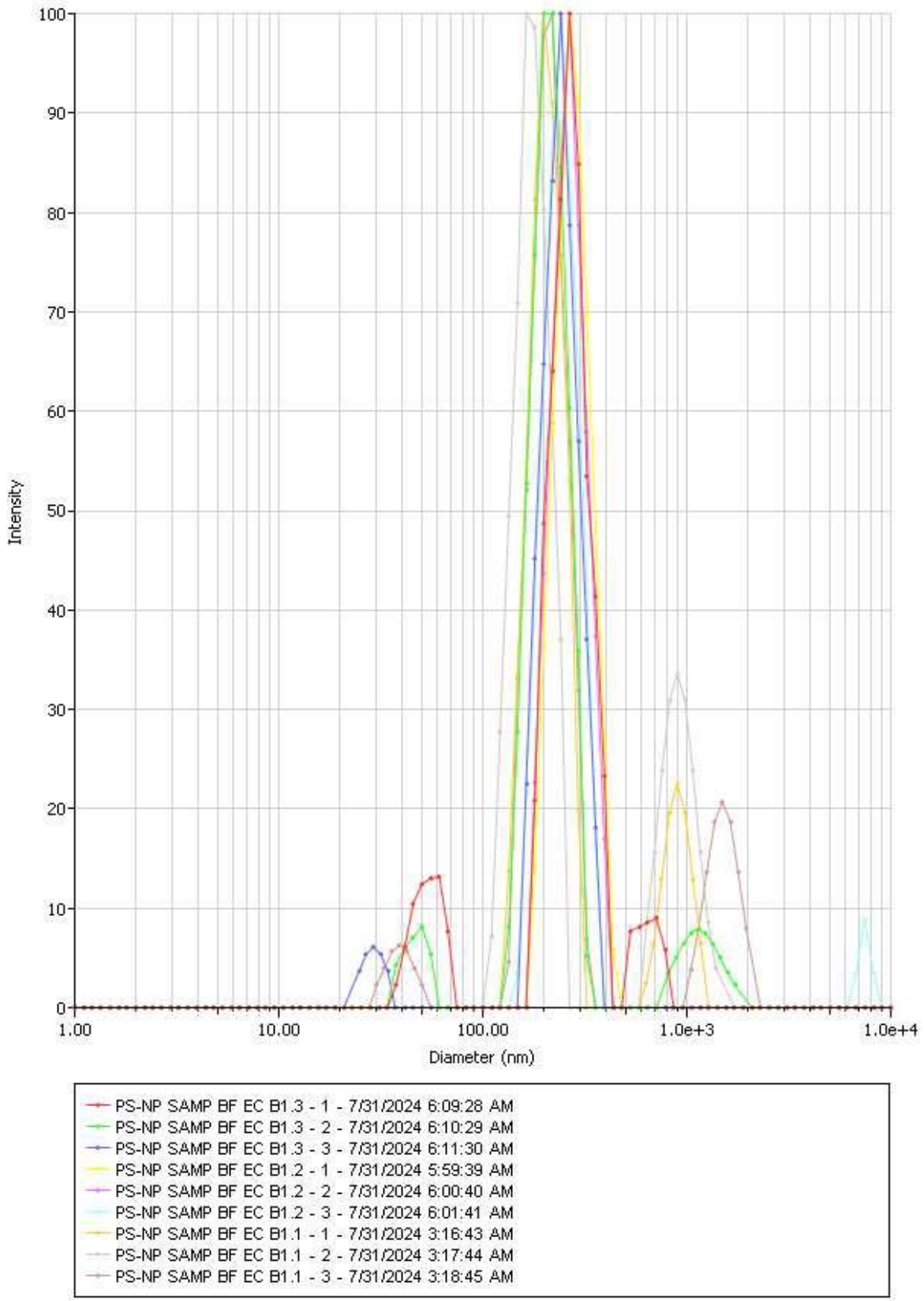

Figure 33 Particle size graph for first set of triplicates at 25 mA, 5V before EC

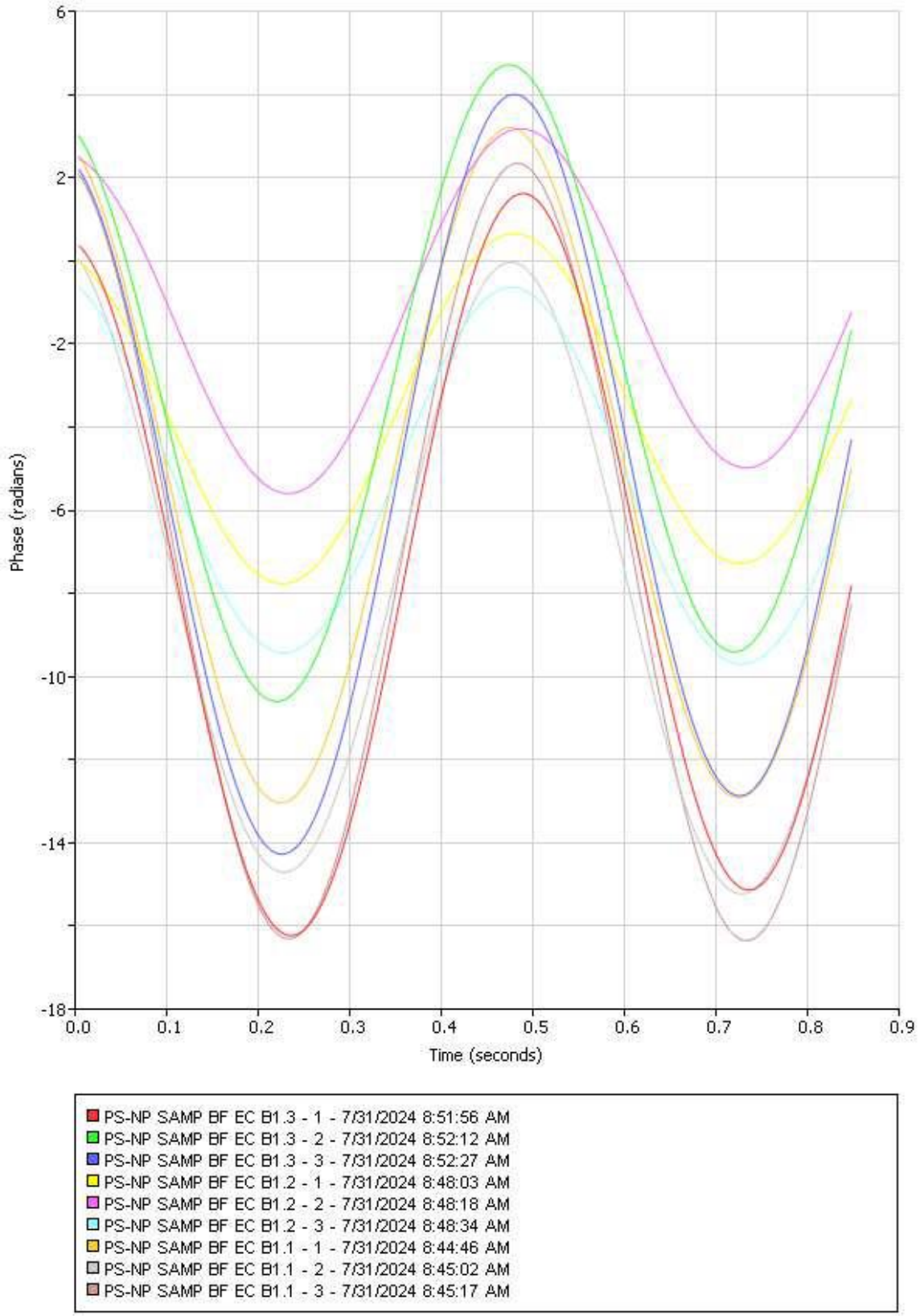

Figure 34 Zeta potential graph for first set of triplicates at 25 mA, 5V before EC

Table 26 Particle size measurement for second set of triplicates at 25 mA, 5V before EC

Sample ID	Eff. Diam. (nm)	Polydispersity	Baseline Index	Count Rate (kcps)	Data Retained (%)	Diffusion Coeff. (cm^2/s)	pH
PS-NP SAMP BF EC B2.1 - 1	193.34	0.238	9.8	517.6	98.43	2.54E-08	5.44
PS-NP SAMP BF EC B2.1 - 2	195.19	0.23	0	518	100	2.51E-08	5.44
PS-NP SAMP BF EC B2.1 - 3	187.54	0.204	0	516	100	2.62E-08	5.44
PS-NP SAMP BF EC B2.2 - 1	192.24	0.241	8.7	506.7	96.86	2.55E-08	5.25
PS-NP SAMP BF EC B2.2 - 2	189.05	0.18	3.6	502.8	96.86	2.60E-08	5.25
PS-NP SAMP BF EC B2.2 - 3	193.66	0.248	6.2	509	100	2.53E-08	5.25
PS-NP SAMP BF EC B2.3 - 1	204.28	0.259	7.5	492.8	100	2.40E-08	5.35
PS-NP SAMP BF EC B2.3 - 2	199.87	0.204	5.5	490	93.73	2.46E-08	5.35
PS-NP SAMP BF EC B2.3 - 3	199.84	0.259	6.8	488.6	98.04	2.46E-08	5.35
Mean:	195	0.229	5.3	504.6	98.21	2.52E-08	5.35
Std Err:	1.81	0.009	1.2	3.9	0.71	2.32E-10	0.03

Table 27 Zeta potential measurement for second set of triplicates at 25 mA, 5V before EC

Sample ID	Zeta Potential (mV)	Mobility (µ/s)/(V/cm)	Conductance (µS)	Sample Count Rate (kcps)	Ref. Count Rate (kcps)	RMS Residual	pH
PS-NP SAMP BF EC B2.1 - 1	-44.61	-3.49	1,520	627	1,171	6.25E-02	5.44
PS-NP SAMP BF EC B2.1 - 2	-57.15	-4.47	1,525	627	1,171	5.58E-02	5.44
PS-NP SAMP BF EC B2.1 - 3	-53.76	-4.2	1,524	627	1,171	5.69E-02	5.44
PS-NP SAMP BF EC B2.2 - 1	-39.59	-3.09	1,477	1,163	1,245	4.52E-02	5.25
PS-NP SAMP BF EC B2.2 - 2	-42.96	-3.36	1,478	1,163	1,245	3.97E-02	5.25
PS-NP SAMP BF EC B2.2 - 3	-35.69	-2.79	1,481	1,163	1,245	4.92E-02	5.25
PS-NP SAMP BF EC B2.3 - 1	-41.27	-3.22	1,484	694	1,320	5.72E-02	5.35
PS-NP SAMP BF EC B2.3 - 2	-58.39	-4.56	1,495	694	1,320	4.51E-02	5.35
PS-NP SAMP BF EC B2.3 - 3	-48.41	-3.78	1,498	694	1,320	3.06E-02	5.35
Mean:	-46.87	-3.66	1,498	828	1,245	4.91E-02	5.35
Std Err:	2.68	0.21	7	84	21	3.36E-03	0.03

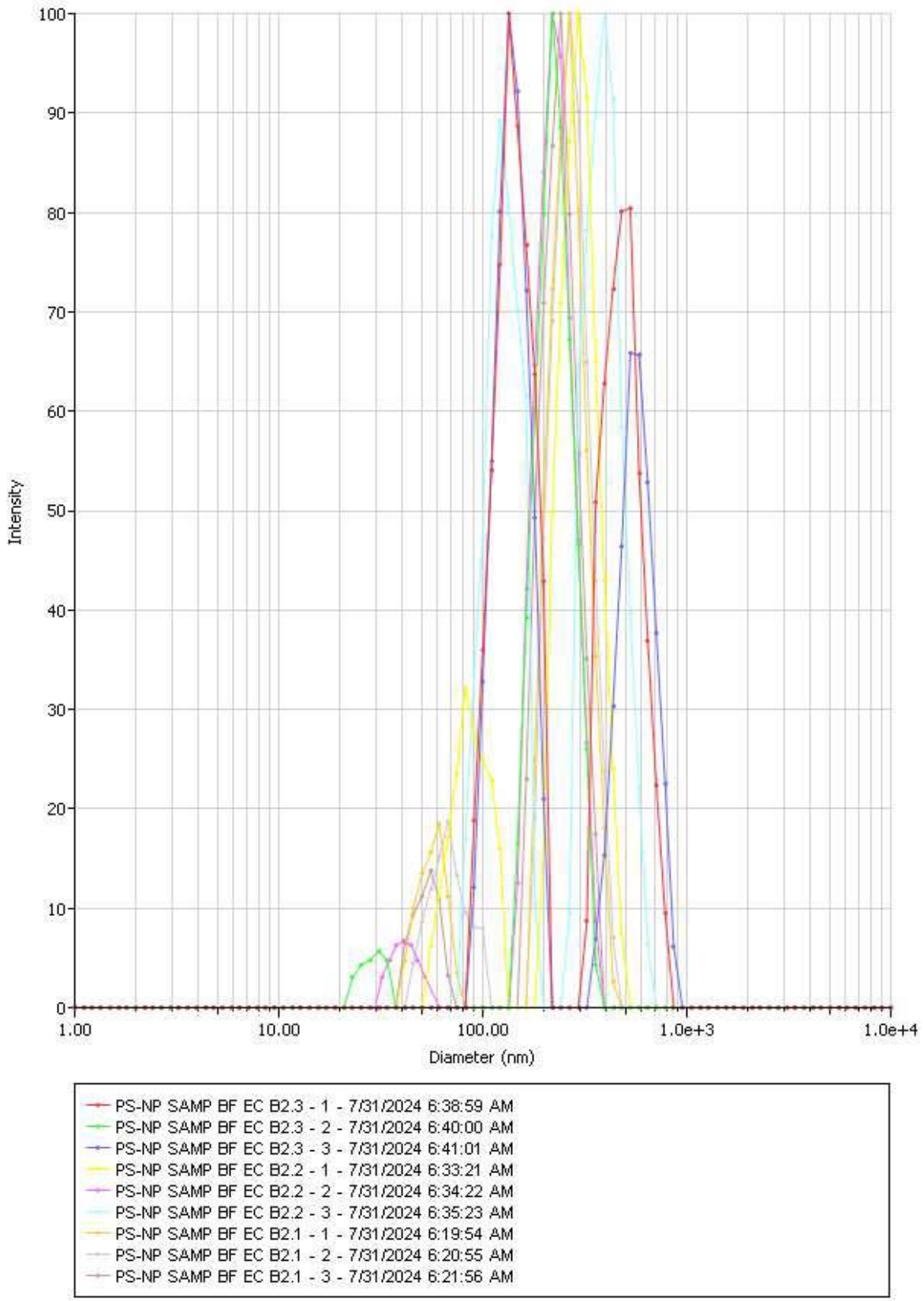

Figure 35 Particle size graph for Second set of triplicates at 25 mA, 5V before EC

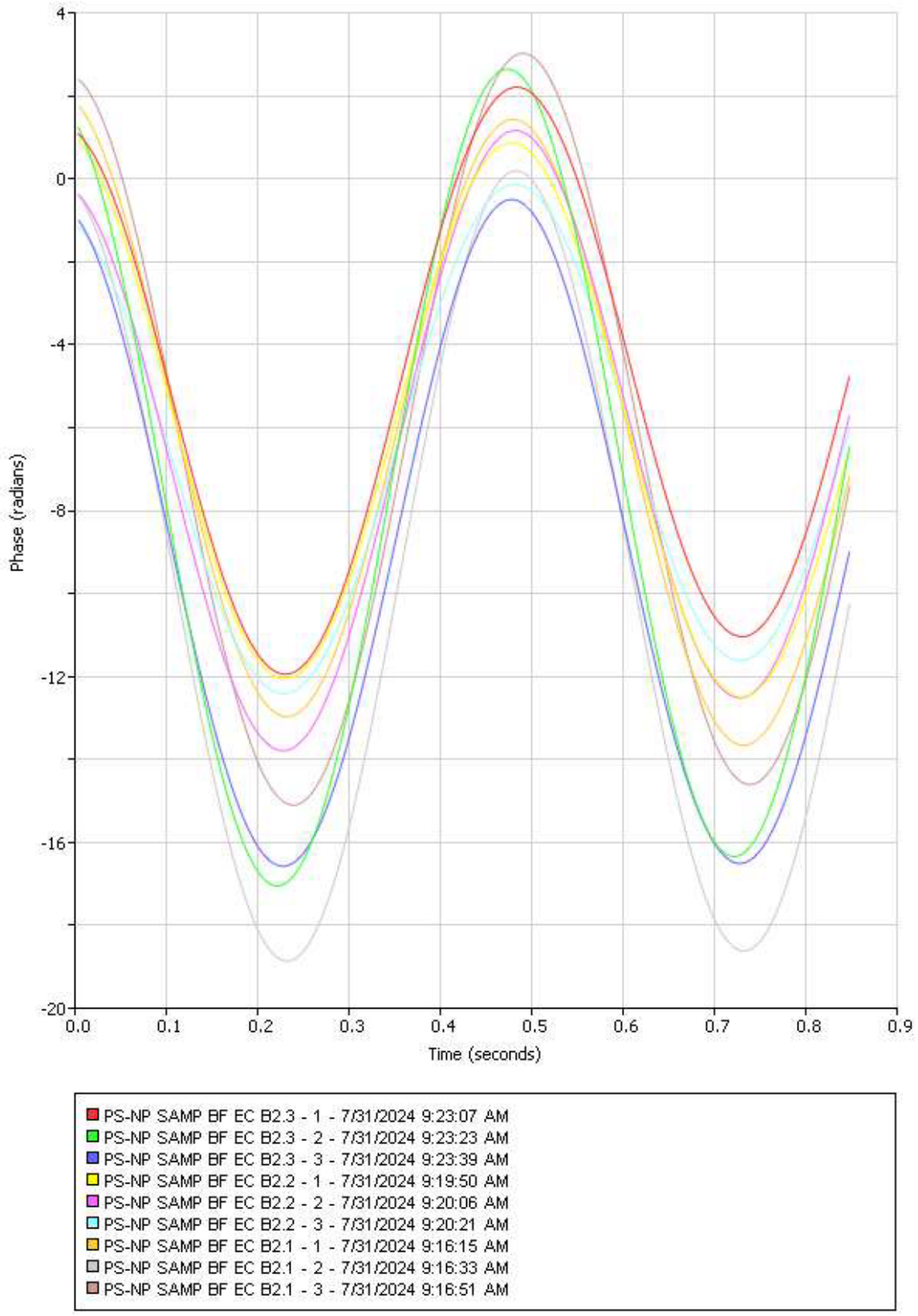

Figure 36 Zeta potential graph for Second set of triplicates at 25 mA, 5V before EC

Table 28 Particle size measurement for third set of triplicates at 25 mA, 5V before EC

Sample ID	Eff. Diam. (nm)	Polydispersity	Baseline Index	Count Rate (kcps)	Data Retained (%)	Diffusion Coeff. (cm^2/s)	pH
PS-NP SAMP BF EC B3.1 - 1	271.37	0.119	0.2	434.1	98.04	1.81E-08	5.52
PS-NP SAMP BF EC B3.1 - 2	261.16	0.079	0	429.1	96.86	1.88E-08	5.52
PS-NP SAMP BF EC B3.1 - 3	261.67	0.053	0	430.1	100	1.88E-08	5.52
PS-NP SAMP BF EC B3.2 - 1	190.93	0.214	4.9	523	96.86	2.57E-08	5.56
PS-NP SAMP BF EC B3.2 - 2	201.18	0.233	1.8	536.5	100	2.44E-08	5.56
PS-NP SAMP BF EC B3.2 - 3	197.32	0.216	0.7	526.4	97.21	2.49E-08	5.56
PS-NP SAMP BF EC B3.3 - 1	195.29	0.254	5.3	521.3	95.29	2.51E-08	5.81
PS-NP SAMP BF EC B3.3 - 2	191.97	0.263	9.7	514.9	98.43	2.56E-08	5.81
PS-NP SAMP BF EC B3.3 - 3	190.67	0.24	0	526.3	100	2.57E-08	5.81
Mean:	217.95	0.185	2.5	493.5	98.08	2.30E-08	5.63
Std Err:	11.79	0.027	1.1	15.7	0.56	1.13E-09	0.05

Table 29 Zeta potential measurement for third set of triplicates at 25 mA, 5V before EC

Sample ID	Zeta Potential (mV)	Mobility (µ/s)/(V/cm)	Conductance (µS)	Sample Count Rate (kcps)	Ref. Count Rate (kcps)	RMS Residual	pH
PS-NP SAMP BF EC B3.1 - 1	-42.11	-3.29	1,502	1,093	1,309	7.19E-02	5.52
PS-NP SAMP BF EC B3.1 - 2	-46.72	-3.65	1,506	1,093	1,309	3.33E-02	5.52
PS-NP SAMP BF EC B3.1 - 3	-46.42	-3.63	1,506	1,093	1,309	3.19E-02	5.52
PS-NP SAMP BF EC B3.2 - 1	-41.59	-3.25	1,507	282	1,086	4.70E-02	5.81
PS-NP SAMP BF EC B3.2 - 2	-48.31	-3.78	1,515	282	1,086	7.27E-02	5.81
PS-NP SAMP BF EC B3.2 - 3	-52.35	-4.09	1,514	282	1,086	3.90E-02	5.81
PS-NP SAMP BF EC B3.3 - 1	-37.21	-2.91	1,519	973	1,265	5.61E-02	5.56
PS-NP SAMP BF EC B3.3 - 2	-38.8	-3.03	1,521	973	1,265	4.16E-02	5.56
PS-NP SAMP BF EC B3.3 - 3	-42.03	-3.28	1,523	973	1,265	6.13E-02	5.56
Mean:	-43.95	-3.43	1,512	783	1,220	5.05E-02	5.63
Std Err:	1.62	0.13	3	126	34	5.22E-03	0.05

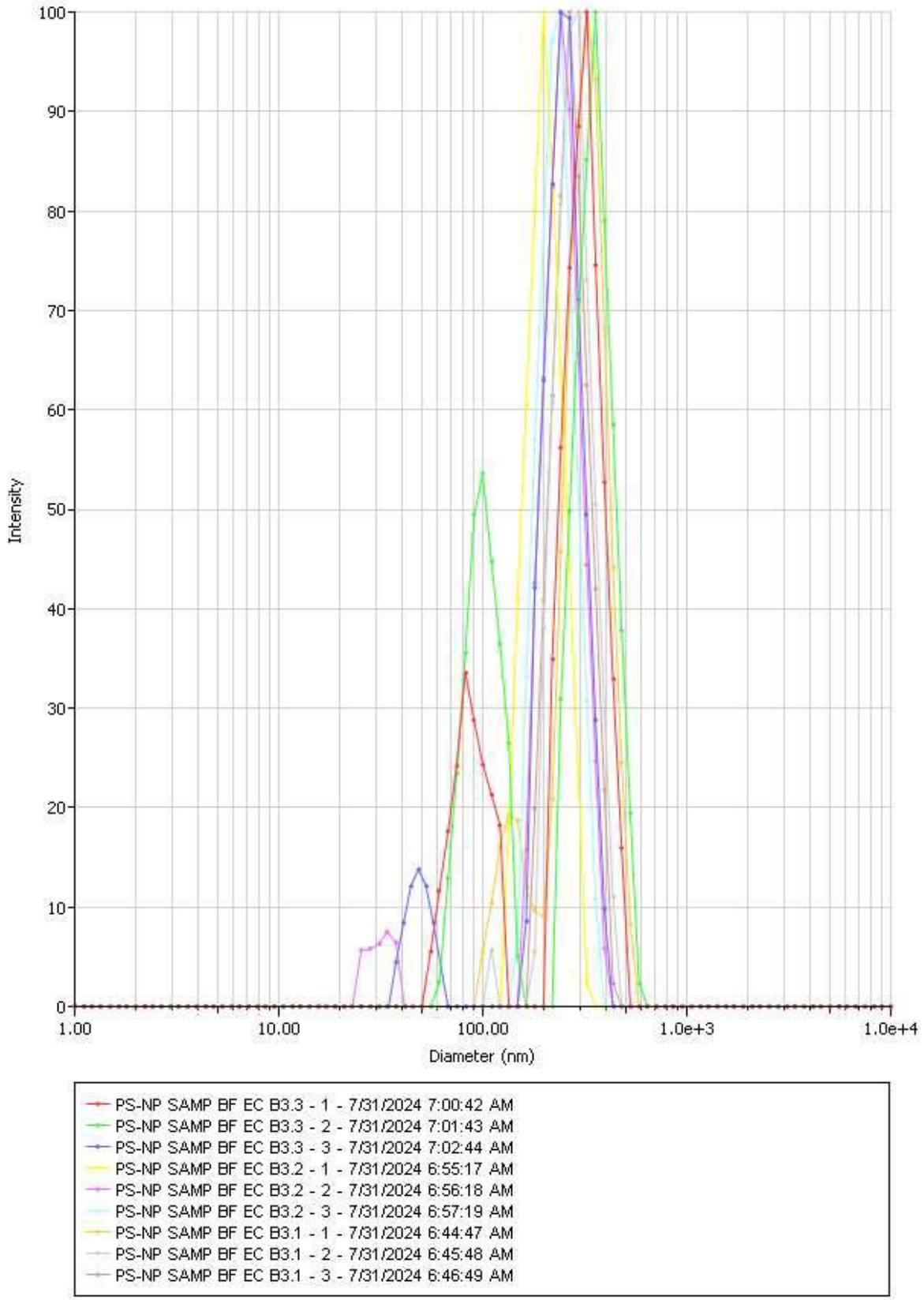

Figure 37 Particle size graph for third set of triplicates at 25 mA, 5V before EC

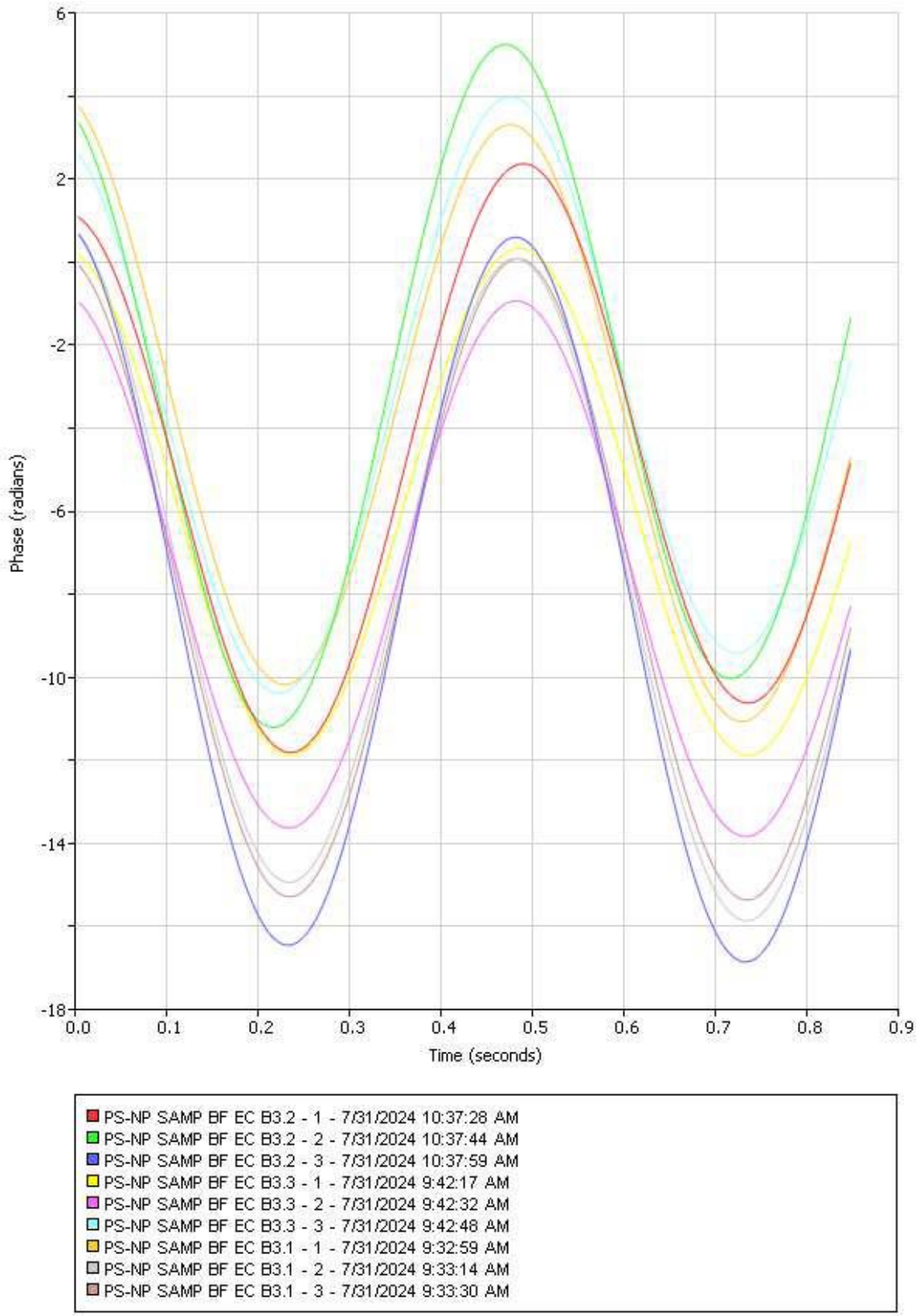

Figure 38 Zeta potential graph for third set of triplicates at 25 mA, 5V before EC

Table 30 Particle size measurement for first set of triplicates at 50 mA, 5V before EC

Sample ID	Eff. Diam. (nm)	Polydispersity	Baseline Index	Count Rate (kcps)	Data Retained (%)	Diffusion Coeff. (cm^2/s)	pH
PS-NP SAMP BF EC C1.3 - 1	195.5	0.236	0	537.1	98.43	2.51E-08	5.32
PS-NP SAMP BF EC C1.3 - 2	197.06	0.223	9.7	521.4	98.43	2.49E-08	5.32
PS-NP SAMP BF EC C1.3 - 3	191.61	0.197	0	516.3	94.9	2.56E-08	5.32
PS-NP SAMP BF EC C1.1 - 1	268.02	0.074	0	437.6	100	1.83E-08	5.45
PS-NP SAMP BF EC C1.1 - 2	263.79	0.192	1.4	436.4	95.29	1.86E-08	5.45
PS-NP SAMP BF EC C1.1 - 3	267.63	0.013	0	429.5	95.12	1.83E-08	5.45
PS-NP SAMP BF EC C1.2 - 1	200.58	0.237	0	549.9	100	2.45E-08	5.43
PS-NP SAMP BF EC C1.2 - 2	184.25	0.226	4.4	526.8	100	2.66E-08	5.43
PS-NP SAMP BF EC C1.2 - 3	189.76	0.232	2.6	539.7	100	2.59E-08	5.43
Mean:	217.58	0.181	2	499.4	98.02	2.31E-08	5.4
Std Err:	12.33	0.027	1.1	16.6	0.76	1.19E-09	0.02

Table 31 Zeta potential measurement for first set of triplicates at 50 mA, 5V before EC

Sample ID	Zeta Potential (mV)	Mobility (µ/s)/(V/cm)	Conductance (µS)	Sample Count Rate (kcps)	Ref. Count Rate (kcps)	RMS Residual	pH
PS-NP SAMP BF EC C1.1 - 1	-37.75	-2.95	317	689	1,437	2.43E-02	5.32
PS-NP SAMP BF EC C1.1 - 2	-38.73	-3.03	317	689	1,437	2.38E-02	5.32
PS-NP SAMP BF EC C1.1 - 3	-37.47	-2.93	317	689	1,437	2.38E-02	5.32
PS-NP SAMP BF EC C1.2 - 1	-48.98	-3.83	1,518	240	1,159	8.23E-02	5.45
PS-NP SAMP BF EC C1.2 - 2	-43.72	-3.42	1,520	240	1,159	3.87E-02	5.45
PS-NP SAMP BF EC C1.2 - 3	-43.61	-3.41	1,522	240	1,159	6.35E-02	5.45
PS-NP SAMP BF EC C1.3 - 1	-41.97	-3.28	1,522	160	1,314	6.98E-02	5.43
PS-NP SAMP BF EC C1.3 - 2	-49.93	-3.9	1,528	160	1,314	3.66E-02	5.43
PS-NP SAMP BF EC C1.3 - 3	-44.98	-3.51	1,535	160	1,314	4.59E-02	5.43
Mean:	-43.02	-3.36	1,122	363	1,303	4.54E-02	5.4
Std Err:	1.52	0.12	201	82	40	7.25E-03	0.02

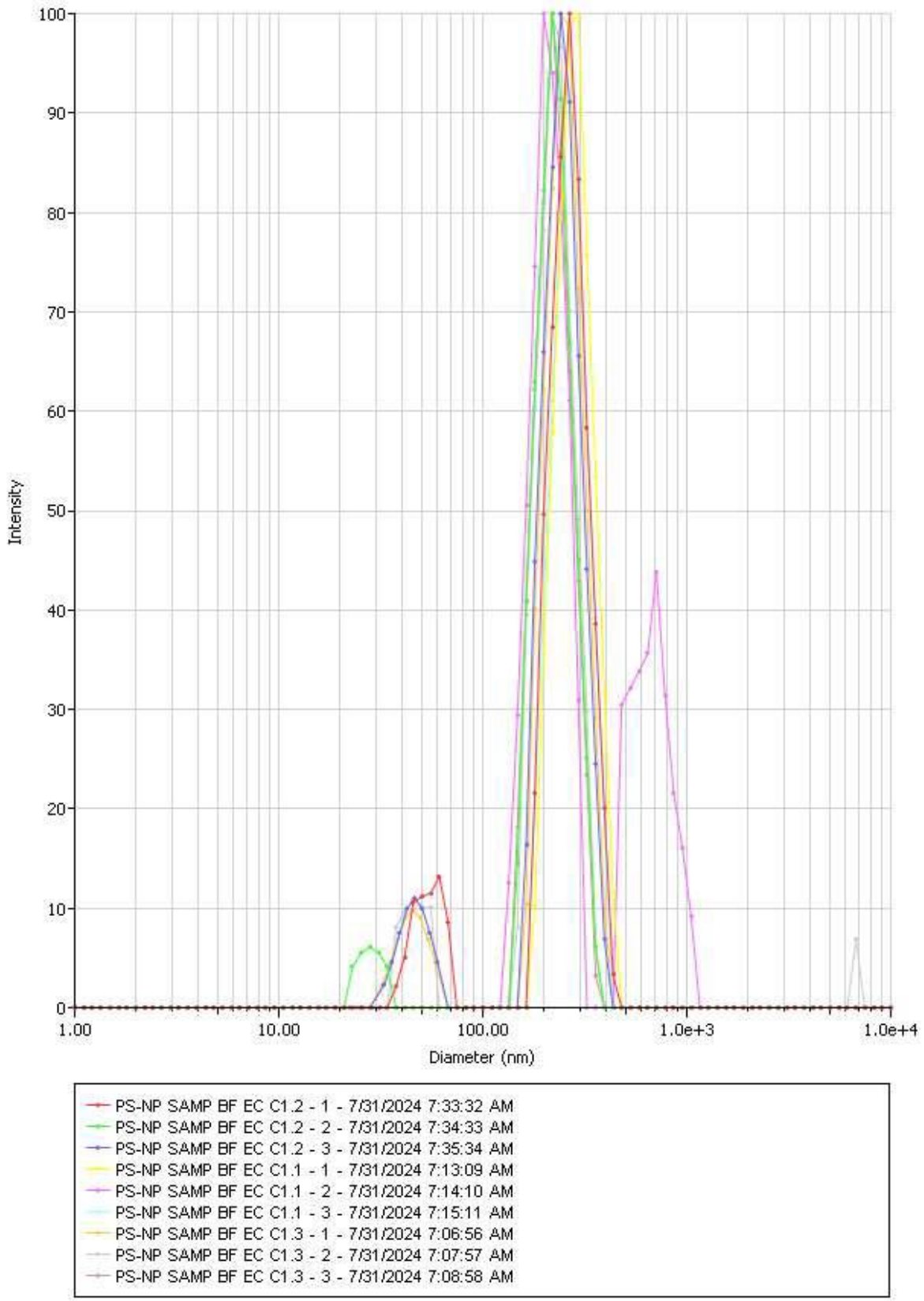

Figure 39 Particle size graph for first set of triplicates at 50 mA, 5V before EC

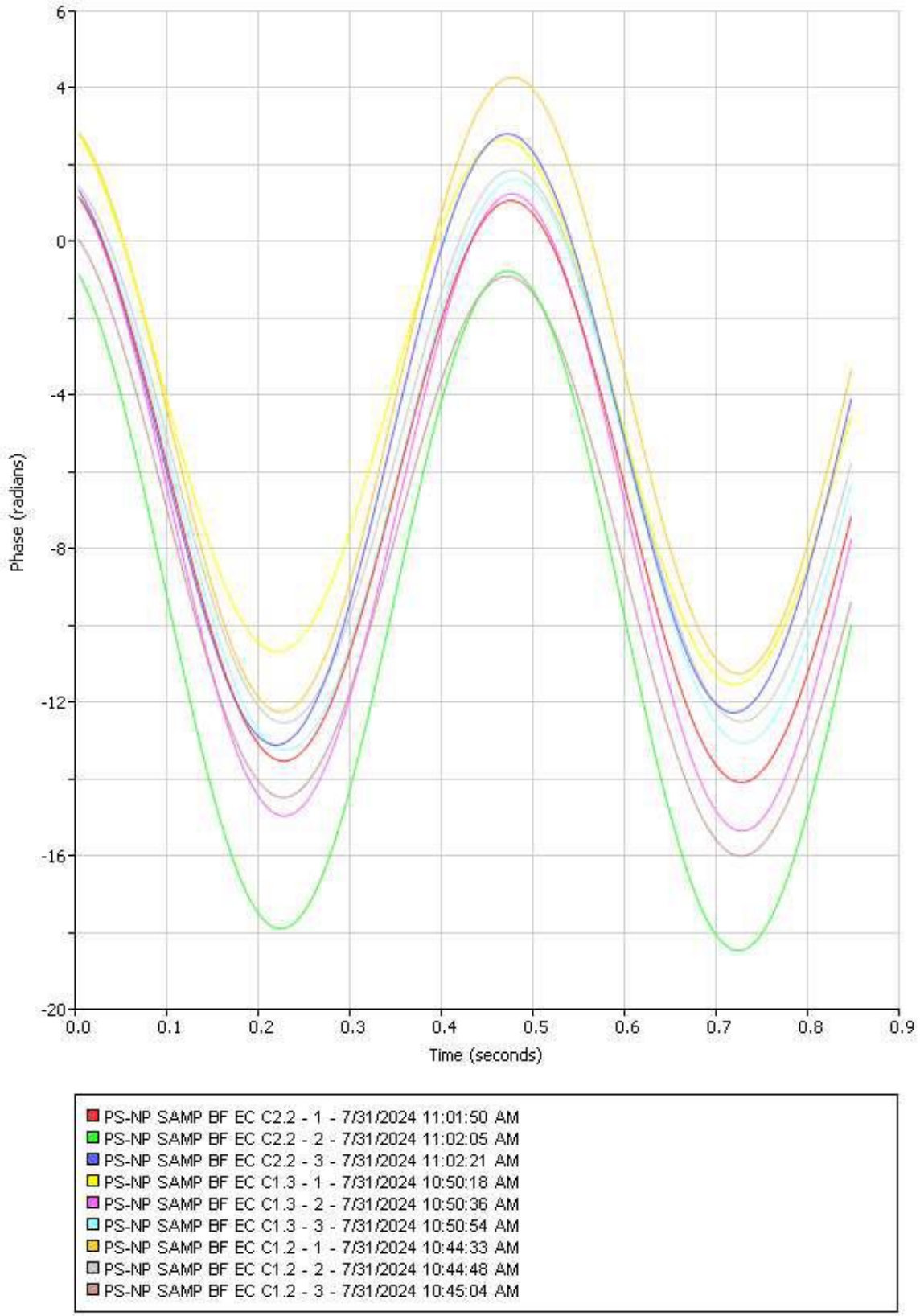

Figure 40 Zeta potential graph for first set of triplicates at 50 mA, 5V before EC

Table 32 Particle size measurement for second set of triplicates at 50 mA, 5V before EC

Sample ID	Eff. Diam. (nm)	Polydispersity	Baseline Index	Count Rate (kcps)	Data Retained (%)	Diffusion Coeff. (cm^2/s)	pH
PS-NP SAMP BF EC C2.1 - 1	194.8	0.242	2.3	534.4	95.29	2.52E-08	5.54
PS-NP SAMP BF EC C2.1 - 2	200.06	0.239	0	546.6	100	2.45E-08	5.54
PS-NP SAMP BF EC C2.1 - 3	190.43	0.216	6.7	531.6	98.43	2.58E-08	5.54
PS-NP SAMP BF EC C2.3 - 1	198.8	0.216	0	516.6	100	2.47E-08	5.43
PS-NP SAMP BF EC C2.3 - 2	196.21	0.225	1	504.5	95.29	2.50E-08	5.43
PS-NP SAMP BF EC C2.3 - 3	191.77	0.222	0	502.2	95.2	2.56E-08	5.43
PS-NP SAMP BF EC C3.2 - 1	632.53	0.664	6.4	8.3	100	7.76E-09	5.38
PS-NP SAMP BF EC C3.2 - 2	578.69	0.543	6.6	8	100	8.48E-09	5.38
PS-NP SAMP BF EC C3.2 - 3	518.96	0.622	0	7.7	100	9.46E-09	5.38
Mean:	322.47	0.354	2.6	351.1	98.25	1.96E-08	5.45
Std Err:	64.27	0.065	1	85.9	0.76	2.77E-09	0.02

Table 33 Zeta potential measurement for second set of triplicates at 50 mA, 5V before EC

Sample ID	Zeta Potential (mV)	Mobility (µ/s)/(V/cm)	Conductance (µS)	Sample Count Rate (kcps)	Ref. Count Rate (kcps)	RMS Residual	pH
PS-NP SAMP BF EC C2.1 - 1	-41.97	-3.28	1,522	160	1,314	6.9797E-02	5.54
PS-NP SAMP BF EC C2.1 - 2	-49.93	-3.90	1,528	160	1,314	3.6575E-02	5.54
PS-NP SAMP BF EC C2.1 - 3	-44.98	-3.51	1,535	160	1,314	4.5945E-02	5.54
PS-NP SAMP BF EC C2.2 - 1	-45.09	-3.52	1,527	472	1,195	4.9858E-02	5.43
PS-NP SAMP BF EC C2.2 - 2	-41.40	-3.24	1,528	472	1,195	5.3329E-02	5.43
PS-NP SAMP BF EC C2.2 - 3	-53.79	-4.20	1,533	472	1,195	4.3002E-02	5.43
PS-NP SAMP BF EC C2.3 - 1	-45.66	-3.57	1,538	366	1,295	4.7764E-02	5.38
PS-NP SAMP BF EC C2.3 - 2	-53.21	-4.16	1,541	366	1,295	6.6804E-02	5.38
PS-NP SAMP BF EC C2.3 - 3	-47.27	-3.69	1,542	366	1,295	4.4854E-02	5.38
Mean:	-47.03	-3.67	1,533	333	1,268	5.0881E-02	5.45
Std Err:	1.49	0.12	2	46	18	3.6431E-03	0.02

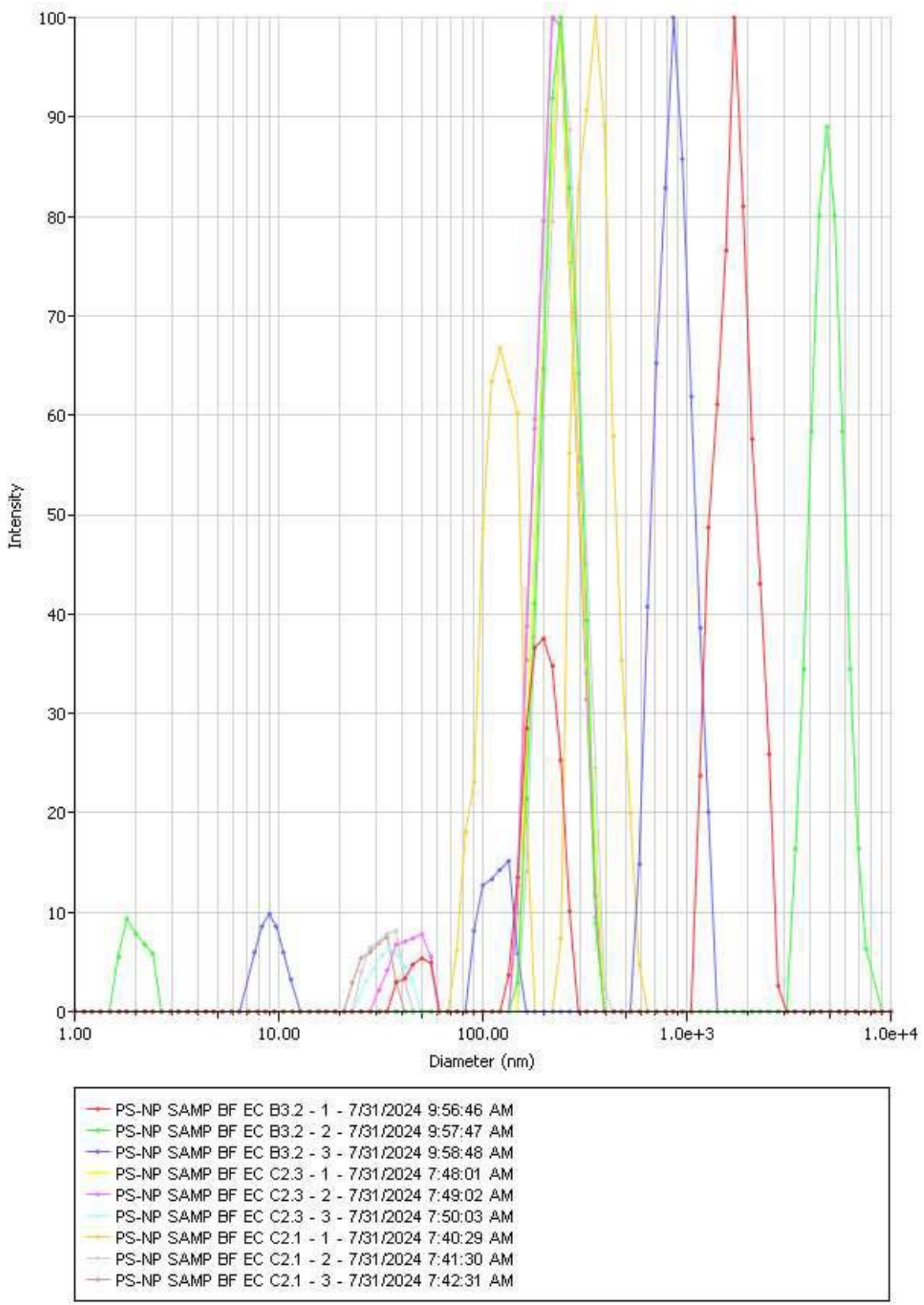

Figure 41 Particle size graph for second set of triplicates at 50 mA, 5V before EC

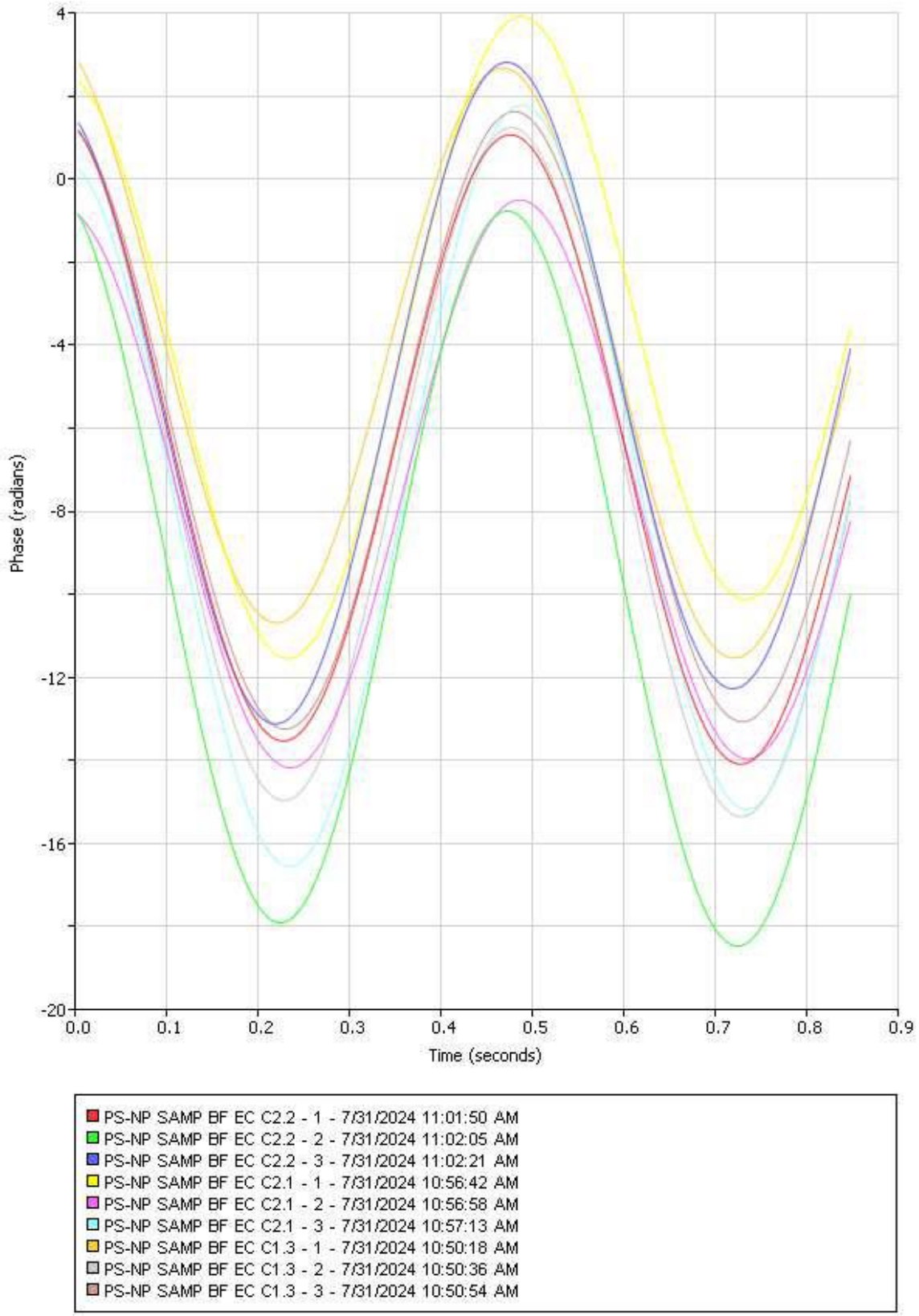

Figure 42 Zeta potential graph for second set of triplicates at 50 mA, 5V before EC

Table 34 Particle size measurement for third set of triplicates at 50 mA, 5V before EC

Sample ID	Eff. Diam. (nm)	Polydispersity	Baseline Index	Count Rate (kcps)	Data Retained (%)	Diffusion Coeff. (cm^2/s)	pH
PS-NP SAMP BF EC C3.1 - 1	237.23	0.155	2.2	549.5	100	2.07E-08	5.42
PS-NP SAMP BF EC C3.1 - 2	242.2	0.003	7.8	564.8	100	2.03E-08	5.42
PS-NP SAMP BF EC C3.1 - 3	233.62	0.048	4.5	563.7	98.43	2.10E-08	5.42
PS-NP SAMP BF EC C3.2 - 1	235.49	0.088	8.5	517	98.43	2.08E-08	5.12
PS-NP SAMP BF EC C3.2 - 2	227.33	0.166	8.4	511.7	96.86	2.16E-08	5.12
PS-NP SAMP BF EC C3.2 - 3	232.26	0.061	9.8	506.4	98.43	2.11E-08	5.12
PS-NP SAMP BF EC C3.3 - 1	234.94	0.143	9	566.6	100	2.09E-08	5.36
PS-NP SAMP BF EC C3.3 - 2	239.34	0.097	8.8	574.2	95.29	2.05E-08	5.36
PS-NP SAMP BF EC C3.3 - 3	234.49	0.035	4.6	567	100	2.09E-08	5.36
Mean:	235.21	0.088	7.1	546.8	98.61	2.09E-08	5.3
Std Err:	1.41	0.019	0.9	9.1	0.55	1.26E-10	0.05

Table 35 Zeta potential measurement for third set of triplicates at 50 mA, 5V before EC

Sample ID	Zeta Potential (mV)	Mobility (µ/s)/(V/cm)	Conductance (µS)	Sample Count Rate (kcps)	Ref. Count Rate (kcps)	RMS Residual	pH
PS-NP SAMP BF EC C3.1 - 1	-61.43	-4.8	1,062	1,052	1,141	1.48E-01	5.42
PS-NP SAMP BF EC C3.1 - 2	-53.54	-4.18	1,080	1,052	1,141	8.02E-02	5.42
PS-NP SAMP BF EC C3.1 - 3	-55.27	-4.32	1,083	1,052	1,141	6.51E-02	5.42
PS-NP SAMP BF EC C3.2 - 1	-49.85	-3.9	1,093	386	1,123	6.23E-02	5.12
PS-NP SAMP BF EC C3.2 - 2	-48.07	-3.76	1,105	386	1,123	7.45E-02	5.12
PS-NP SAMP BF EC C3.2 - 3	-47.15	-3.68	1,104	386	1,123	5.22E-02	5.12
PS-NP SAMP BF EC C3.3 - 1	-52.1	-4.07	1,088	128	1,205	9.63E-02	5.36
PS-NP SAMP BF EC C3.3 - 2	-61.64	-4.82	1,098	128	1,205	1.16E-01	5.36
PS-NP SAMP BF EC C3.3 - 3	-43.95	-3.43	1,096	128	1,205	7.70E-02	5.36
Mean:	-52.56	-4.11	1,090	522	1,156	8.57E-02	5.3
Std Err:	2.04	0.16	5	138	12	9.98E-03	0.05

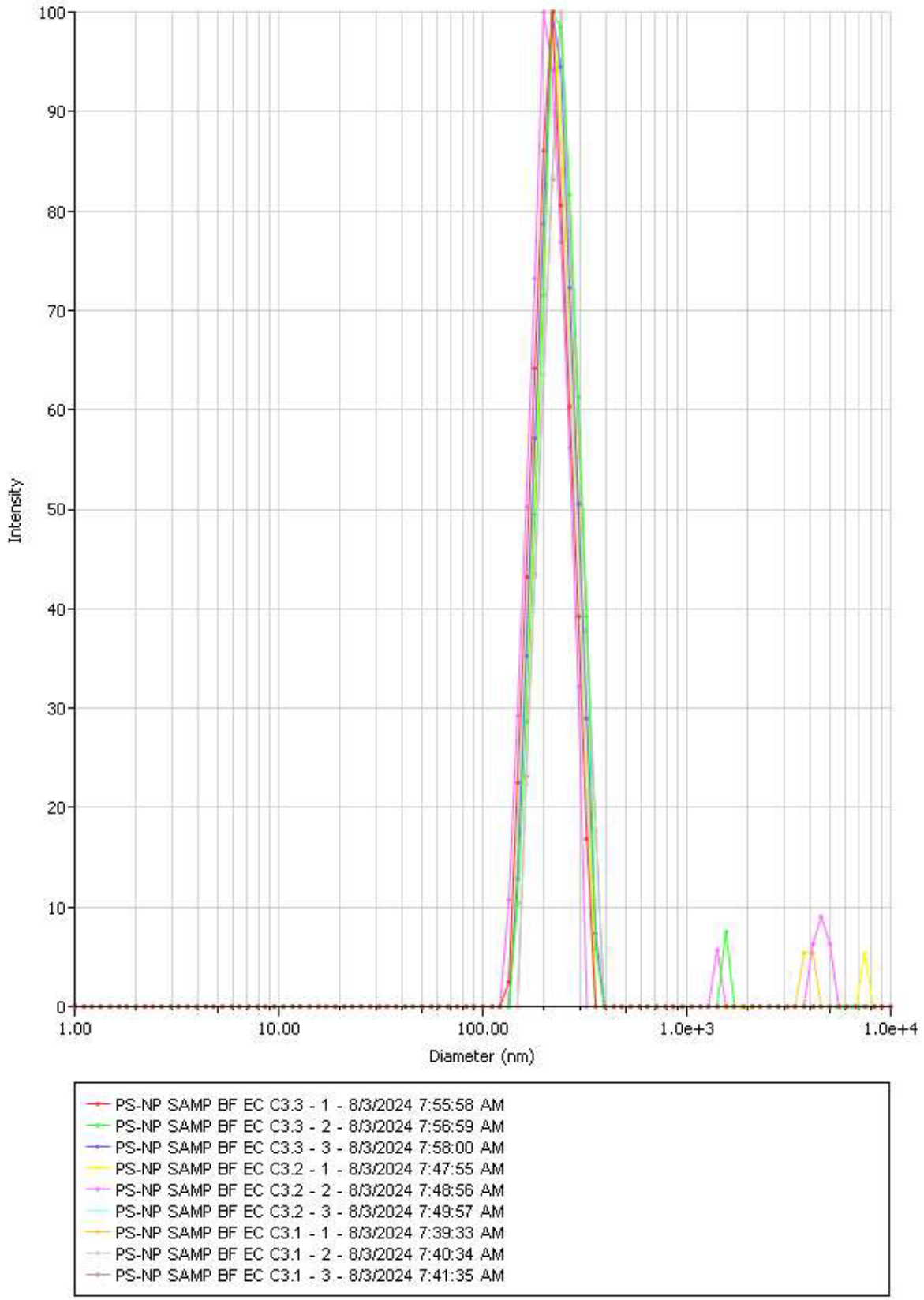

Figure 43 Particle size graph for third set of triplicates at 50 mA, 5V before EC

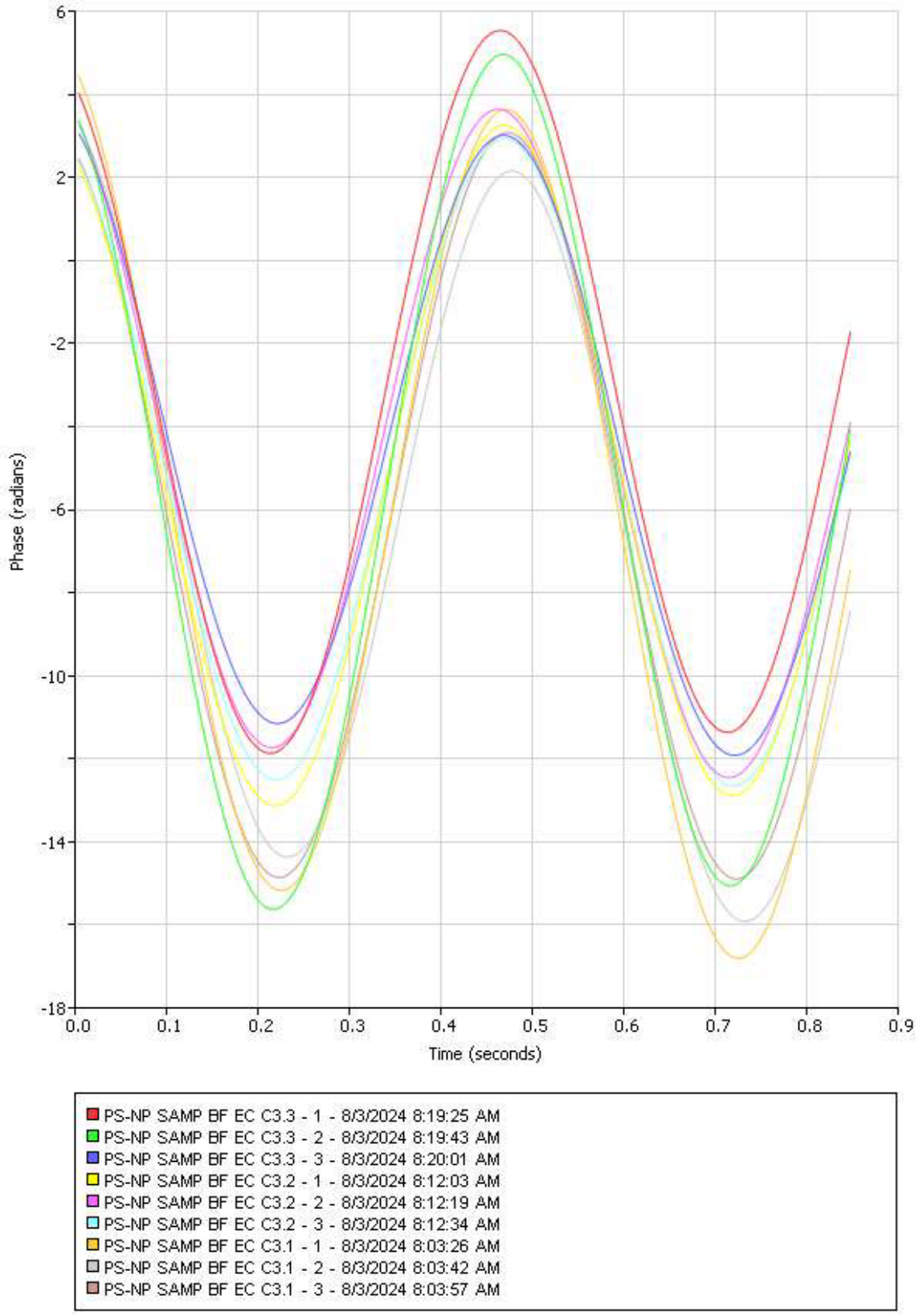

Figure 44 Zeta potential graph for third set of triplicates at 50 mA, 5V before EC

12.3 Appendix C

Table 36 Particle size measurement for first set of triplicates at 10 mA, 5V after EC

Sample ID	Eff. Diam. (nm)	Polydispersity	Baseline Index	Count Rate (kcps)	Data Retained (%)	Diffusion Coeff. (cm^2/s)	pH
PS-NP SAMP AF EC A1.1 - 1	21,674.51	0.43	0	62.1	100	2.26E-10	8.04
PS-NP SAMP AF EC A1.1 - 2	30,852.95	0.49	0	92	98.4	1.59E-10	8.04
PS-NP SAMP AF EC A1.1 - 3	2,575.25	0.421	0	68.5	100	1.91E-09	8.04
PS-NP SAMP AF EC A1.2 - 1	0	0	0	115.3	93.52	0.00E+00	8.09
PS-NP SAMP AF EC A1.2 - 2	43,811.67	0.619	0	139.2	87.63	1.12E-10	8.09
PS-NP SAMP AF EC A1.2 - 3	78,594.16	0.625	0	143.1	93.9	6.24E-11	8.09
PS-NP SAMP AF EC A1.3 - 1	23,148.04	0.123	0	8.7	83.23	2.12E-10	8.12
PS-NP SAMP AF EC A1.3 - 2	47,115.39	1.789	0	11	95.39	1.04E-10	8.12
PS-NP SAMP AF EC A1.3 - 3	133,617.30	0.596	0	44.7	90.31	3.67E-11	8.12
Mean:	42,376.59	0.566	0	76.1	93.6	3.13E-10	8.08
Std Err:	13,930.44	0.169	0	16.8	1.91	2.01E-10	0.01

Table 37 Zeta potential measurement for first set of triplicates at 10 mA, 5V after EC

Sample ID	Zeta Potential (mV)	Mobility (µ/s)/(V/cm)	Conductance (µS)	Sample Count Rate (kcps)	Ref. Count Rate (kcps)	RMS Residual	pH
PS-NP SAMP AF EC A1.1 - 1	24.05	1.88	1,384	26	1,215	2.50E-02	8.04
PS-NP SAMP AF EC A1.1 - 2	33.1	2.59	1,400	26	1,215	2.51E-02	8.04
PS-NP SAMP AF EC A1.1 - 3	19.47	1.52	1,403	26	1,215	4.32E-02	8.04
PS-NP SAMP AF EC A1.2 - 1	34.1	2.66	1,392	3	1,030	4.21E-02	8.09
PS-NP SAMP AF EC A1.2 - 2	17.75	1.39	1,405	3	1,030	2.88E-02	8.09
PS-NP SAMP AF EC A1.2 - 3	14.98	1.17	1,409	3	1,030	4.04E-02	8.09
PS-NP SAMP AF EC A1.3 - 1	18.45	1.44	1,428	3	1,149	6.14E-02	8.12
PS-NP SAMP AF EC A1.3 - 2	4.78	0.37	1,440	3	1,149	2.25E-02	8.12
PS-NP SAMP AF EC A1.3 - 3	13.38	1.05	1,440	3	1,149	3.52E-02	8.12
Mean:	20.01	1.56	1,411	11	1,131	3.60E-02	8.08
Std Err:	3.11	0.24	7	4	27	4.14E-03	0.01

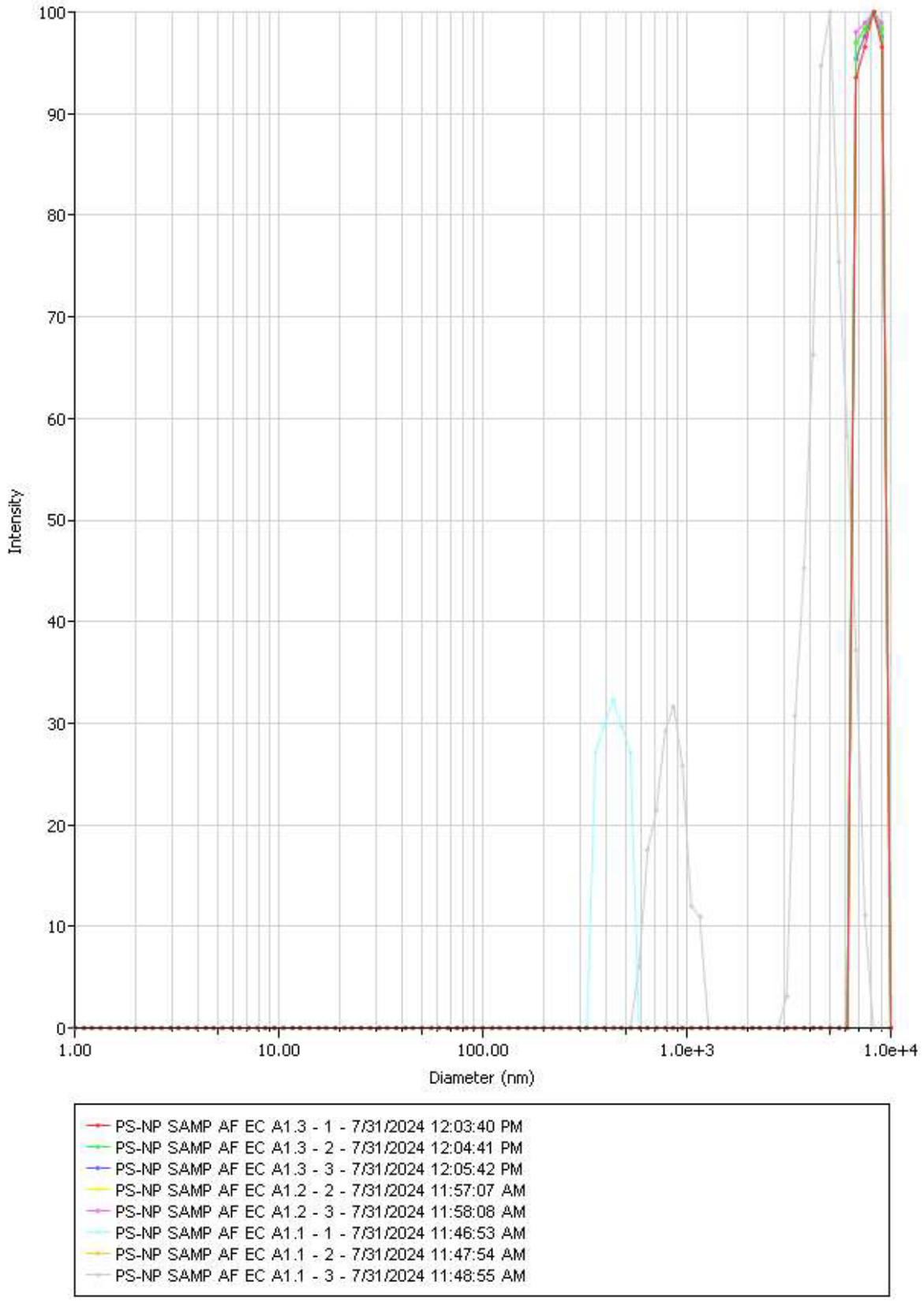

Figure 45 Particle size graph for first set of triplicates at 10 mA, 5V after EC

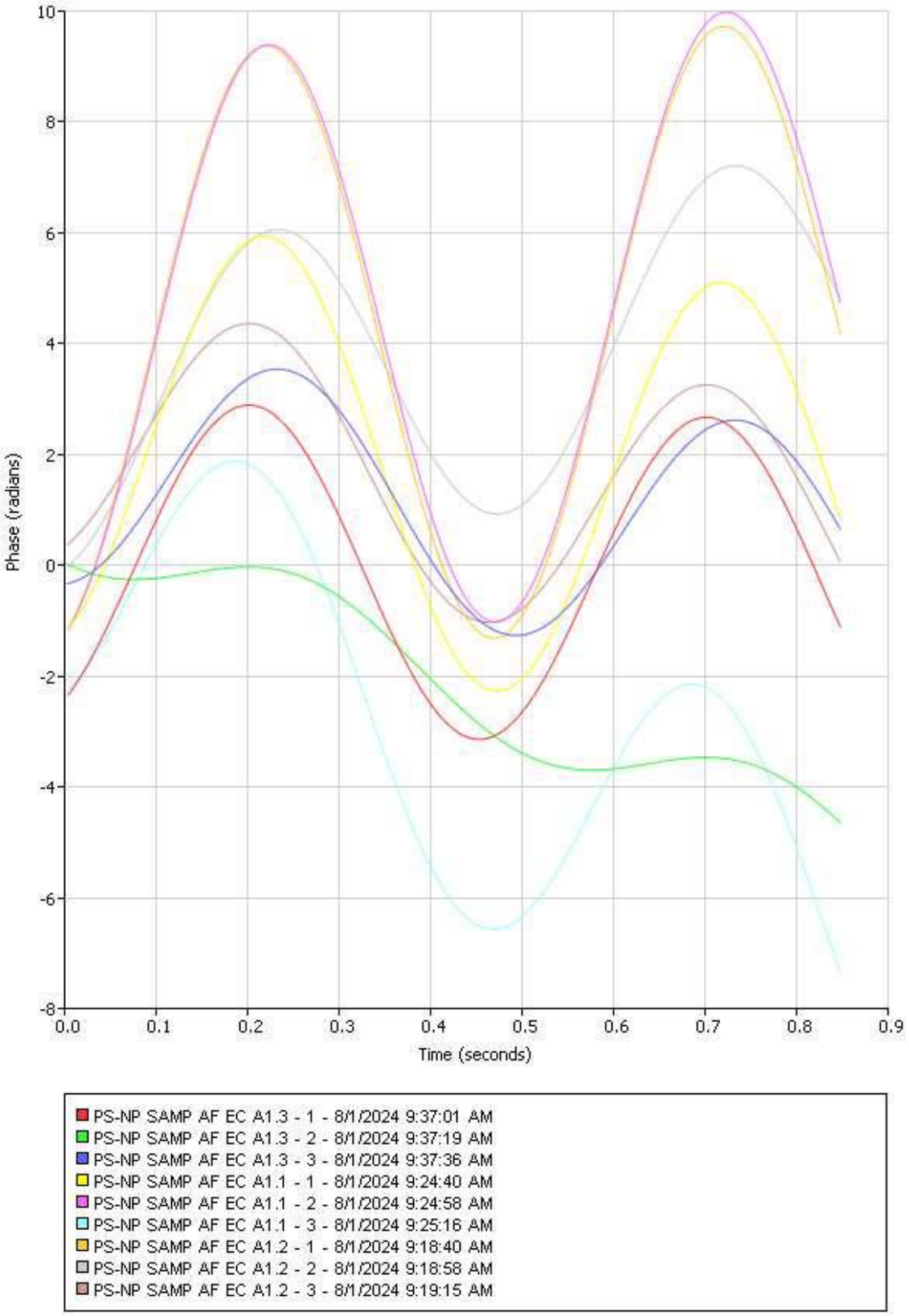

Figure 46 Zeta potential graph for first set of triplicates at 10 mA, 5V after EC

Table 38 Particle size measurement for second set of triplicates at 10 mA, 5V after EC

Sample ID	Zeta Potential (mV)	Mobility (µ/s)/(V/cm)	Conductance (µS)	Sample Count Rate (kcps)	Ref. Count Rate (kcps)	RMS Residual	pH
PS-NP SAMP AF EC A2.1 - 1	41.24	3.22	1,631	2,246	1,208	1.91E-02	7.99
PS-NP SAMP AF EC A2.1 - 2	34.64	2.71	1,636	2,246	1,208	4.12E-02	7.99
PS-NP SAMP AF EC A2.1 - 3	42.95	3.36	1,634	2,246	1,208	4.31E-02	7.99
PS-NP SAMP AF EC A2.2 - 1	4.24	0.33	1,408	797	559	2.78E-02	8.08
PS-NP SAMP AF EC A2.2 - 2	2.34	0.18	1,418	797	559	1.64E-02	8.08
PS-NP SAMP AF EC A2.2 - 3	4.27	0.33	1,421	797	559	1.83E-02	8.08
PS-NP SAMP AF EC A2.3 - 1	3.64	0.28	1,464	515	1,216	2.82E-02	8.13
PS-NP SAMP AF EC A2.3 - 2	26.01	2.03	1,471	515	1,216	2.72E-02	8.13
PS-NP SAMP AF EC A2.3 - 3	17.58	1.37	1,475	515	1,216	3.18E-02	8.13
Mean:	19.66	1.54	1,506	1,186	994	2.81E-02	8.07
Std Err:	5.66	0.44	33	268	109	3.17E-03	0.02

Table 39 Zeta potential measurement for second set of triplicates at 10 mA, 5V after EC

Sample ID	Eff. Diam. (nm)	Polydispersity	Baseline Index	Count Rate (kcps)	Data Retained (%)	Diffusion Coeff. (cm^2/s)	pH
PS-NP SAMP AF EC A2.1 - 1	32,969.62	0.711	0.1	3.4	94.79	1.49E-10	7.99
PS-NP SAMP AF EC A2.1 - 2	18,858.54	0.59	0	3.2	86.16	2.60E-10	7.99
PS-NP SAMP AF EC A2.1 - 3	3,221.35	0.79	0	3.3	89.62	1.52E-09	7.99
PS-NP SAMP AF EC A2.2 - 1	97,025.67	16.077	0	134.2	93.62	5.06E-11	8.08
PS-NP SAMP AF EC A2.2 - 2	46,133.07	0.135	0	135.5	89.3	1.06E-10	8.08
PS-NP SAMP AF EC A2.2 - 3	59,069.89	1.083	0	133.9	91.22	8.31E-11	8.08
PS-NP SAMP AF EC A2.3 - 1	0	0	0	19	86.67	0.00E+00	8.13
PS-NP SAMP AF EC A2.3 - 2	84,030.98	1.963	0	25.9	94.84	5.84E-11	8.13
PS-NP SAMP AF EC A2.3 - 3	44,817.49	0.585	0	12.9	85.71	1.10E-10	8.13
Mean:	42,902.96	2.437	0	52.4	90.21	2.60E-10	8.07
Std Err:	11,173.10	1.715	0	20.7	1.21	1.60E-10	0.02

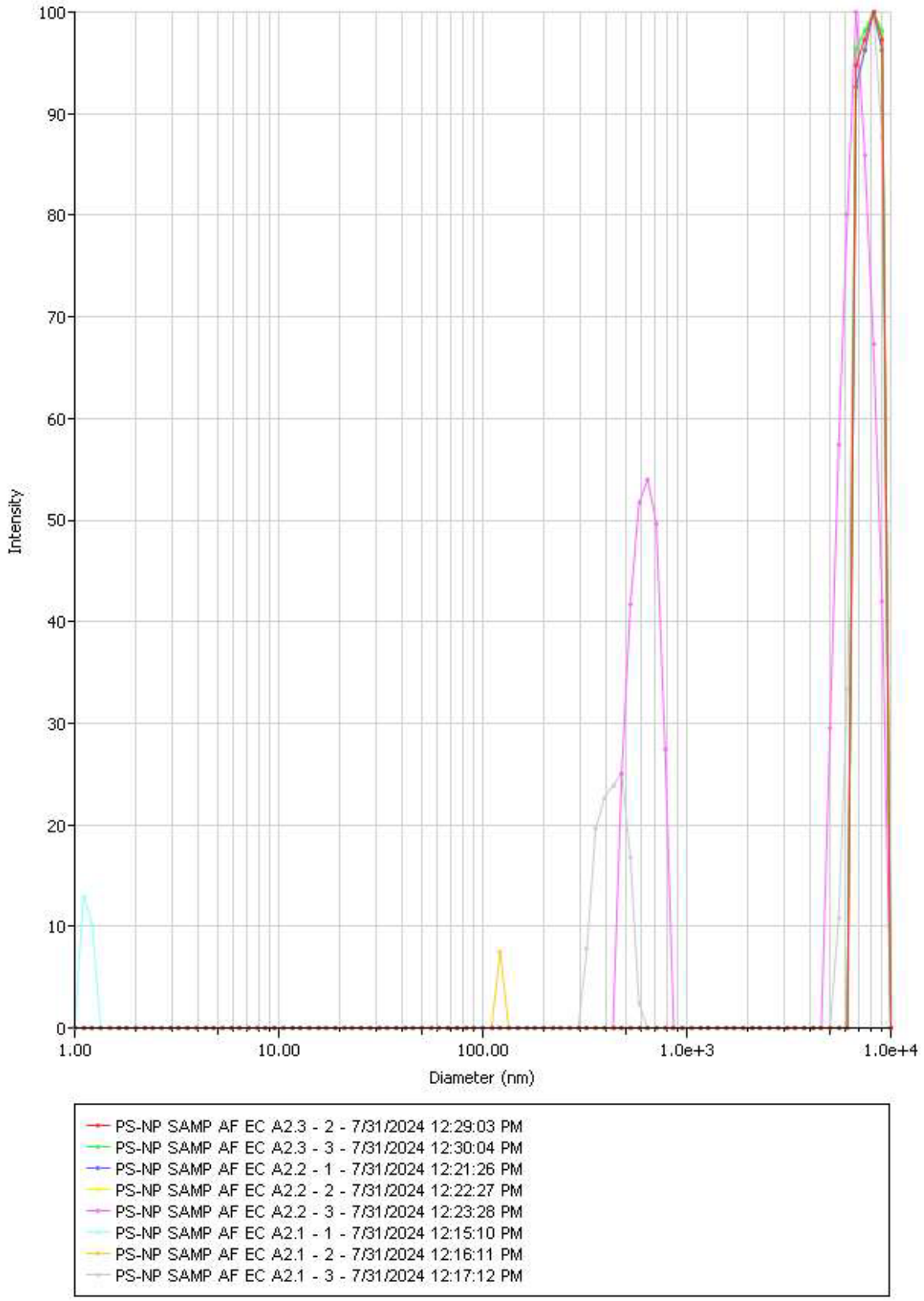

Figure 47 Particle size graph for second set of triplicates at 10 mA, 5V after EC

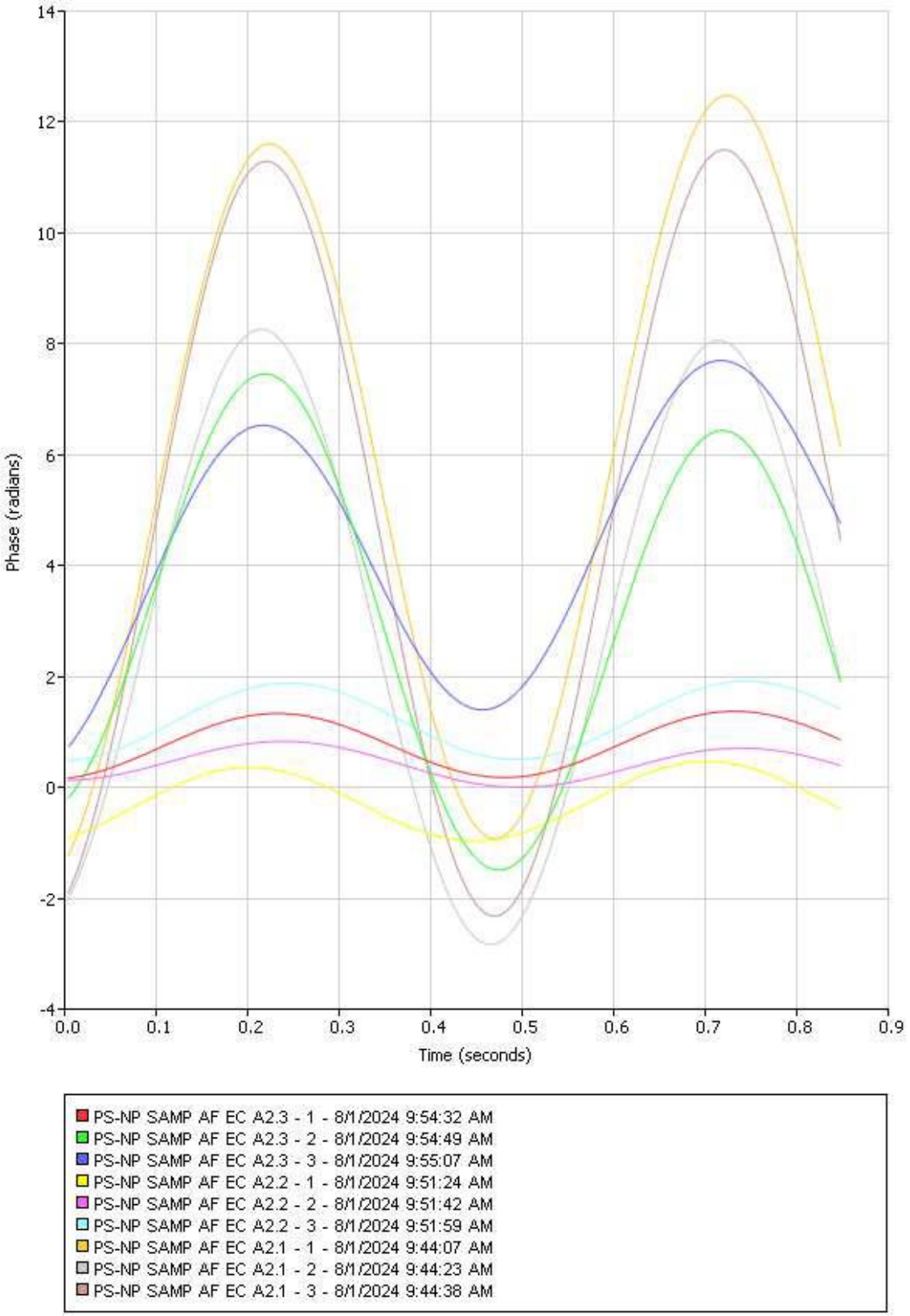

Figure 48 Zeta potential graph for second set of triplicates at 10 mA, 5V after EC

Table 40 Particle size measurement for third set of triplicates at 10 mA, 5V after EC

Sample ID	Eff. Diam. (nm)	Polydispersity	Baseline Index	Count Rate (kcps)	Data Retained (%)	Diffusion Coeff. (cm^2/s)	pH
PS-NP SAMP AF EC A3.1 - 1	1,359.49	1.105	0	0.7	95.17	3.61E-09	8.09
PS-NP SAMP AF EC A3.1 - 2	1,759.77	0.779	0	0.7	98.21	2.79E-09	8.09
PS-NP SAMP AF EC A3.1 - 3	1,889.20	0.798	1.4	0.8	92.81	2.60E-09	8.09
PS-NP SAMP AF EC A3.2 - 1	42,422.20	0.698	0	121.6	98.69	1.16E-10	7.89
PS-NP SAMP AF EC A3.2 - 2	392,816.80	25.31	0	140.4	92.78	1.25E-11	7.89
PS-NP SAMP AF EC A3.2 - 3	100,676.40	0.643	0	158.9	93.45	4.88E-11	7.89
PS-NP SAMP AF EC A3.3 - 1	18,513.36	0.375	0	400	97.97	2.65E-10	7.94
PS-NP SAMP AF EC A3.3 - 2	2,246.23	0.312	0	410.6	92.68	2.19E-09	7.94
PS-NP SAMP AF EC A3.3 - 3	1,746.02	0.4	0	417.1	89.8	2.81E-09	7.94
Mean:	62,603.27	3.38	0.2	183.4	94.62	1.60E-09	7.97
Std Err:	42,708.18	2.743	0.2	60	1.03	4.88E-10	0.03

Table 41 Zeta potential measurement for third set of triplicates at 10 mA, 5V after EC

Sample ID	Zeta Potential (mV)	Mobility (µ/s)/(V/cm)	Conductance (µS)	Sample Count Rate (kcps)	Ref. Count Rate (kcps)	RMS Residual	pH
PS-NP SAMP AF EC A3.1 - 1	38.61	3.02	1,466	3,585	1,164	5.78E-02	8.09
PS-NP SAMP AF EC A3.1 - 2	37.49	2.93	1,469	3,585	1,164	3.47E-02	8.09
PS-NP SAMP AF EC A3.1 - 3	38.28	2.99	1,469	3,585	1,164	3.93E-02	8.09
PS-NP SAMP AF EC A3.2 - 1	2.55	0.2	1,479	938	1,197	9.12E-03	7.89
PS-NP SAMP AF EC A3.2 - 2	4.97	0.39	1,488	938	1,197	2.79E-02	7.89
PS-NP SAMP AF EC A3.2 - 3	8.8	0.69	1,490	938	1,197	1.40E-02	7.89
PS-NP SAMP AF EC A3.3 - 1	32.31	2.52	1,472	3,389	792	4.37E-02	7.94
PS-NP SAMP AF EC A3.3 - 2	34.14	2.67	1,474	3,389	792	6.44E-02	7.94
PS-NP SAMP AF EC A3.3 - 3	31.82	2.49	1,473	3,389	792	4.52E-02	7.94
Mean:	25.44	1.99	1,476	2,637	1,051	3.73E-02	7.97
Std Err:	5.09	0.4	3	426	65	6.12E-03	0.03

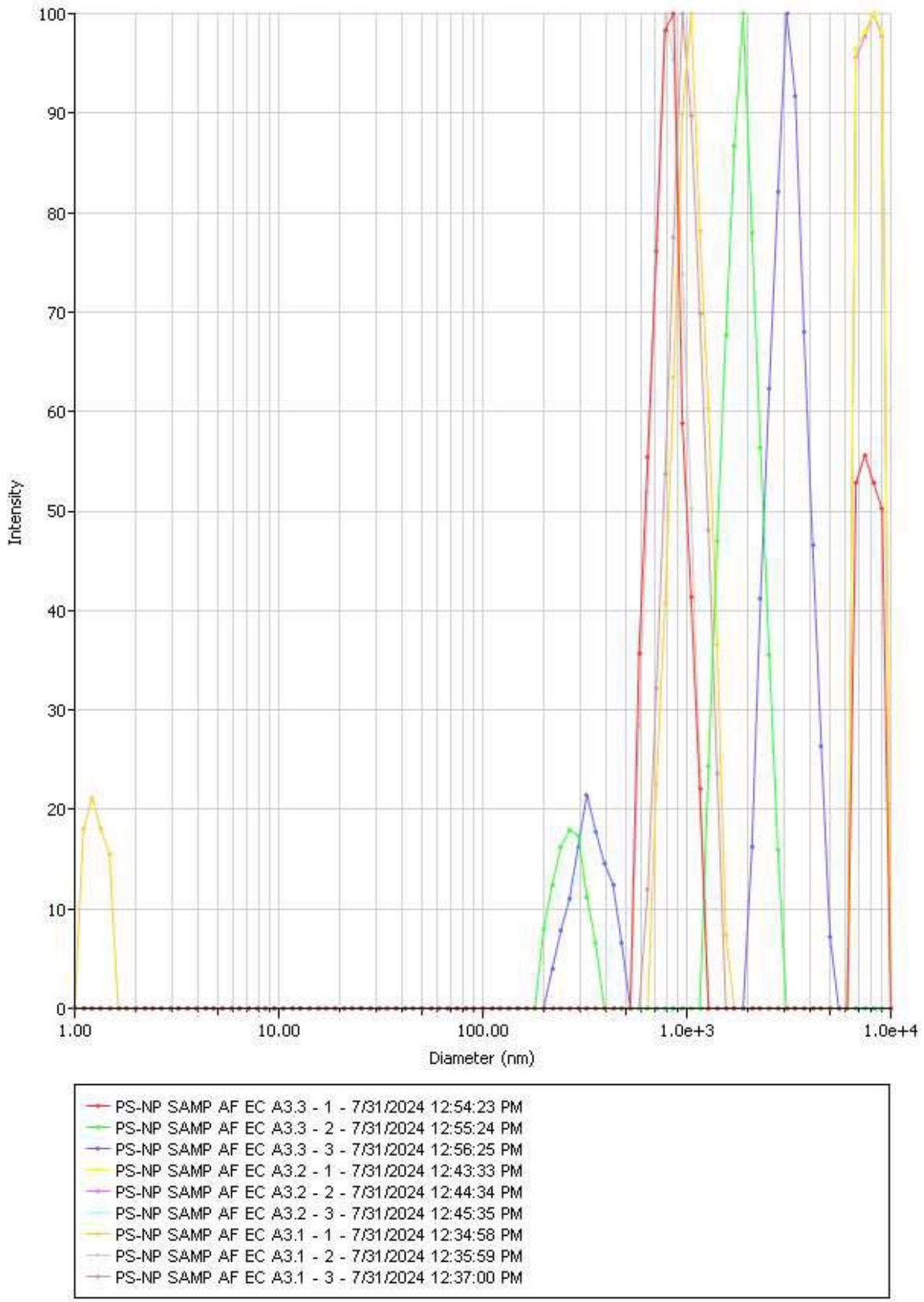

Figure 49 Particle size graph for third set of triplicates at 10 mA, 5V after EC

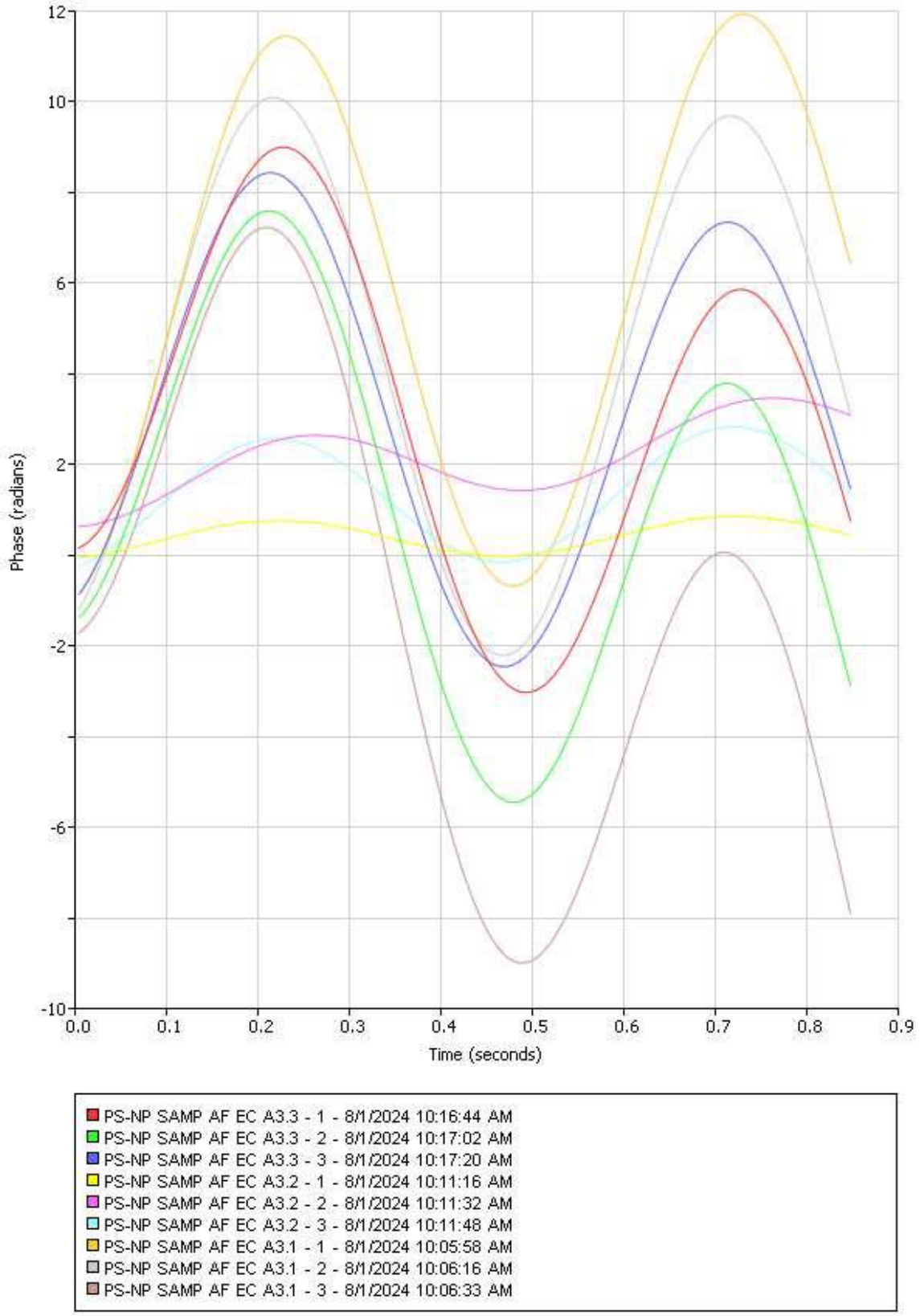

Figure 50 Zeta potential graph for third set of triplicates at 10 mA, 5V after EC

Table 42 Particle size measurement for first set of triplicates at 25 mA, 5V after EC

Sample ID	Eff. Diam. (nm)	Polydispersity	Baseline Index	Count Rate (kcps)	Data Retained (%)	Diffusion Coeff. (cm^2/s)	pH
PS-NP SAMP AF EC B1.1 - 1	0	0	0	13.9	96.85	0.00E+00	8.23
PS-NP SAMP AF EC B1.1 - 2	18,609.85	0.779	0	13.2	88.24	2.64E-10	8.23
PS-NP SAMP AF EC B1.1 - 3	31,647.46	1.077	0	12.5	83.65	1.55E-10	8.23
PS-NP SAMP AF EC B1.2 - 1	14,700.62	0.625	0	5.2	87.11	3.34E-10	8.31
PS-NP SAMP AF EC B1.2 - 2	20,116.44	0.489	0	4.1	98.08	2.44E-10	8.31
PS-NP SAMP AF EC B1.2 - 3	23,352.32	0.568	0	4.8	94.95	2.10E-10	8.31
PS-NP SAMP AF EC B1.3 - 1	41,775.24	0.468	0	1	96.53	1.18E-10	8.27
PS-NP SAMP AF EC B1.3 - 2	16,551.67	0.765	0	1	90.21	2.97E-10	8.27
PS-NP SAMP AF EC B1.3 - 3	30,636.18	0.204	0	0.8	85.71	1.60E-10	8.27
Mean:	21,932.20	0.553	0	6.3	91.26	1.98E-10	8.27
Std Err:	3,983.49	0.106	0	1.8	1.81	3.41E-11	0.01

Table 43 Zeta potential measurement for first set of triplicates at 25 mA, 5V after EC

Sample ID	Zeta Potential (mV)	Mobility (µ/s)/(V/cm)	Conductance (µS)	Sample Count Rate (kcps)	Ref. Count Rate (kcps)	RMS Residual	pH
PS-NP SAMP AF EC B1.1 - 1	27.1	2.12	1,620	936	992	2.15E-02	8.23
PS-NP SAMP AF EC B1.1 - 2	27.76	2.17	1,634	936	992	1.76E-02	8.23
PS-NP SAMP AF EC B1.1 - 3	29.52	2.31	1,636	936	992	4.14E-02	8.23
PS-NP SAMP AF EC B1.2 - 1	19.66	1.54	1,532	1,416	571	3.68E-02	8.31
PS-NP SAMP AF EC B1.2 - 2	21.02	1.64	1,544	1,416	571	2.60E-02	8.31
PS-NP SAMP AF EC B1.2 - 3	25.48	1.99	1,547	1,416	571	2.71E-02	8.31
PS-NP SAMP AF EC B1.3 - 1	23.4	1.83	1,663	15	1,190	1.57E-02	8.27
PS-NP SAMP AF EC B1.3 - 2	10.96	0.86	1,669	15	1,190	8.33E-02	8.27
PS-NP SAMP AF EC B1.3 - 3	32.57	2.54	1,671	15	1,190	2.92E-02	8.27
Mean:	24.16	1.89	1,613	789	918	3.32E-02	8.27
Std Err:	2.13	0.17	19	206	91	6.85E-03	0.01

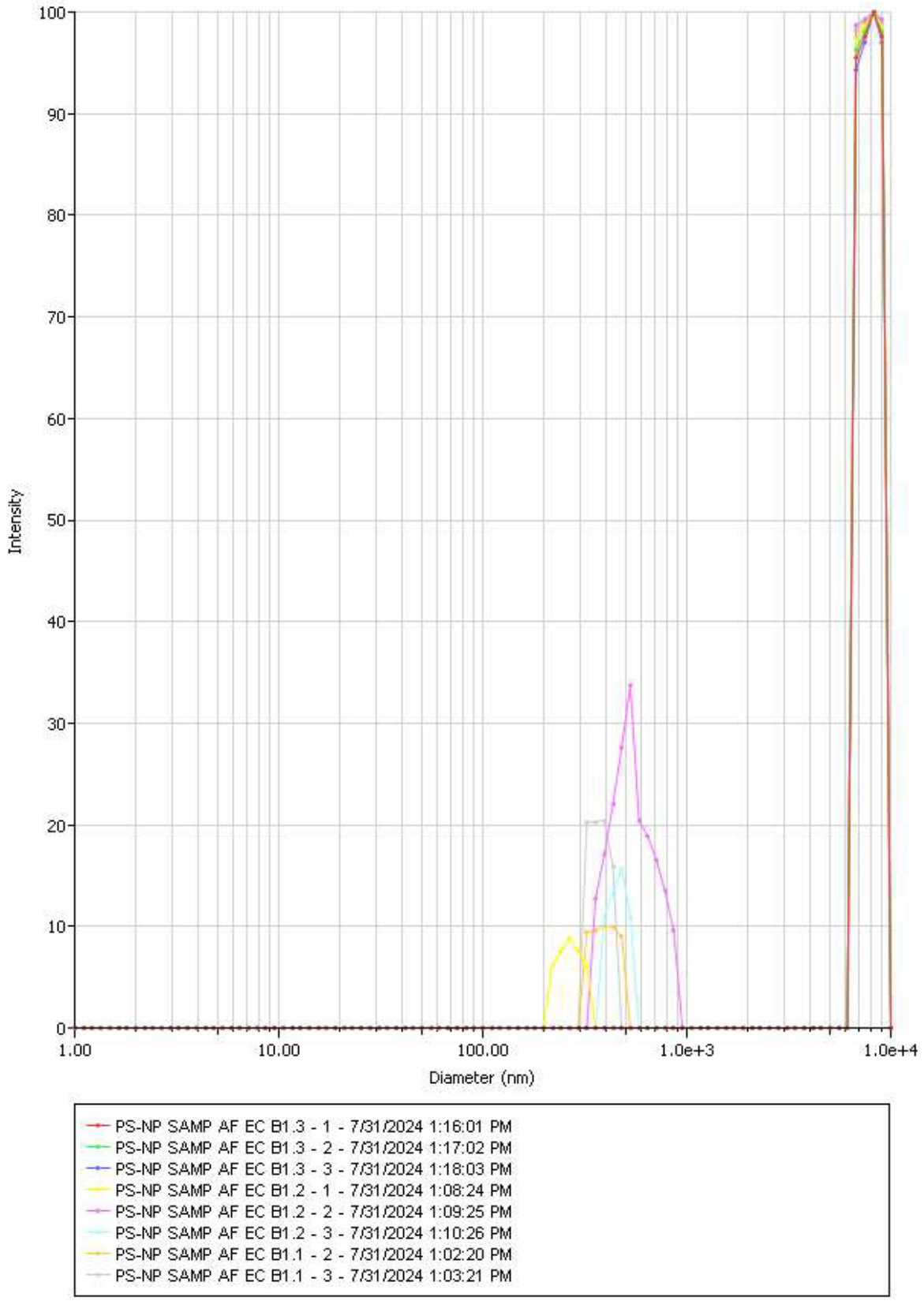

Figure 51 Particle size graph for first set of triplicates at 25 mA, 5V after EC

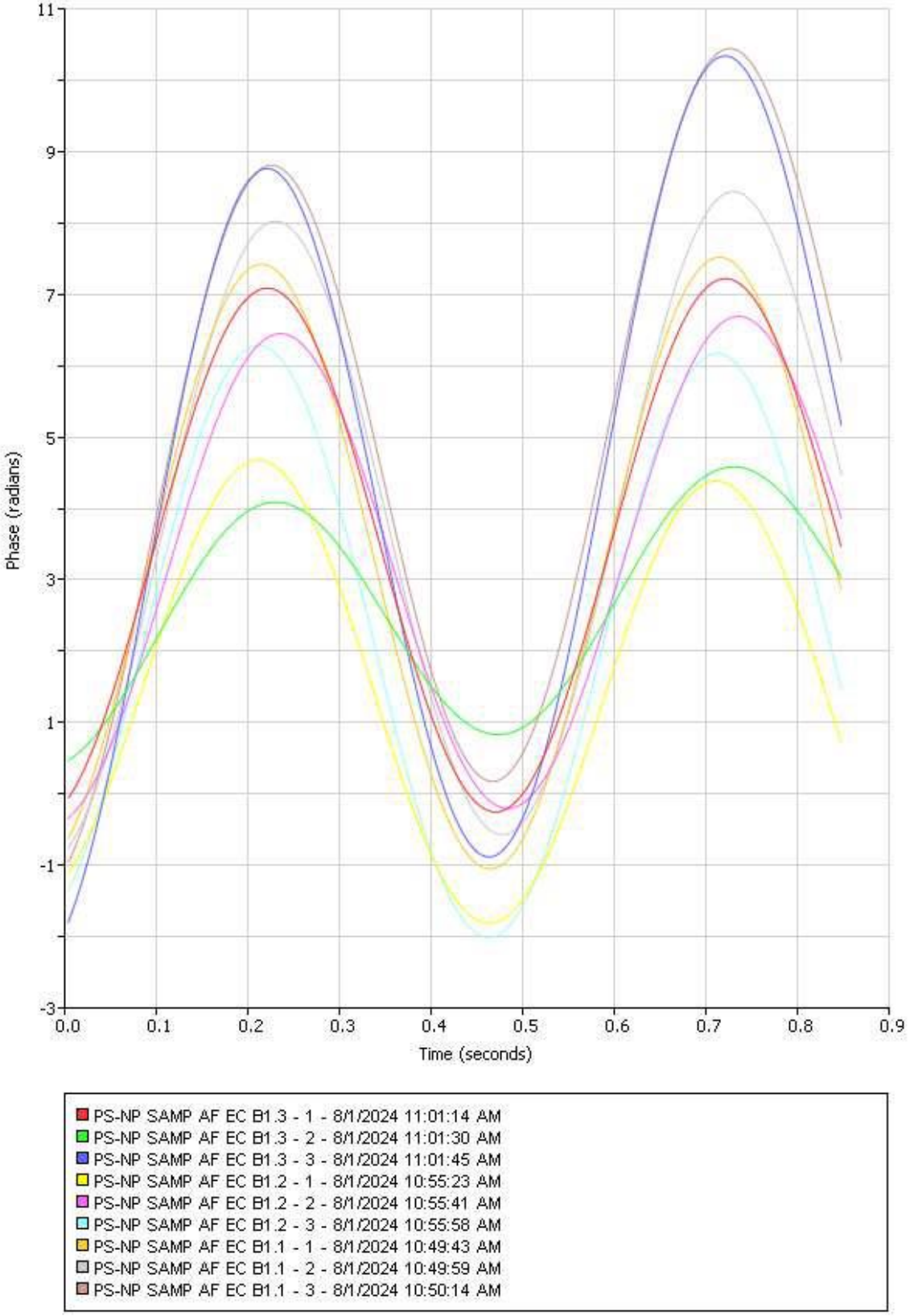

Figure 52 Zeta potential graph for first set of triplicates at 25 mA, 5V after EC

Table 44 Particle size measurement for second set of triplicates at 25 mA, 5V after EC

Sample ID	Eff. Diam. (nm)	Polydispersity	Baseline Index	Count Rate (kcps)	Data Retained (%)	Diffusion Coeff. (cm^2/s)	pH
PS-NP SAMP AF EC B2.1 - 1	51,996.81	0.829	0	4.6	91.82	9.44E-11	8.38
PS-NP SAMP AF EC B2.1 - 2	44,426.82	1.485	0	2.6	93.65	1.11E-10	8.38
PS-NP SAMP AF EC B2.1 - 3	0	0	0	2.4	87.7	0.00E+00	8.38
PS-NP SAMP AF EC B2.2 - 1	50,095.80	0.104	0	255.2	91.81	9.80E-11	8.35
PS-NP SAMP AF EC B2.2 - 2	56,187.78	0.173	0.3	248.9	93.29	8.73E-11	8.35
PS-NP SAMP AF EC B2.2 - 3	112,304.50	3.176	0	212.9	93.66	4.37E-11	8.35
PS-NP SAMP AF EC B2.3 - 1	59,298.16	0.629	0	146.3	93.64	8.28E-11	8.29
PS-NP SAMP AF EC B2.3 - 2	77,501.16	0.021	0	133.2	99.3	6.33E-11	8.29
PS-NP SAMP AF EC B2.3 - 3	34,123.95	0.427	0	108.6	90.38	1.44E-10	8.29
Mean:	53,992.78	0.76	0	123.8	92.81	8.04E-11	8.34
Std Err:	10,142.41	0.341	0	34.4	1.04	1.37E-11	0.01

Table 45 Zeta potential measurement for second set of triplicates at 25 mA, 5V after EC

Sample ID	Zeta Potential (mV)	Mobility (µ/s)/(V/cm)	Conductance (µS)	Sample Count Rate (kcps)	Ref. Count Rate (kcps)	RMS Residual	pH
PS-NP SAMP AF EC B2.2 - 1	27.16	2.12	1,513	42	1,134	2.77E-02	8.38
PS-NP SAMP AF EC B2.2 - 2	34.78	2.72	1,518	42	1,134	2.38E-02	8.38
PS-NP SAMP AF EC B2.2 - 3	21.93	1.71	1,519	42	1,134	2.53E-02	8.38
PS-NP SAMP AF EC B2.1 - 1	38.54	3.01	1,629	1,740	1,300	3.32E-02	8.35
PS-NP SAMP AF EC B2.1 - 2	40.82	3.19	1,651	1,740	1,300	3.54E-02	8.35
PS-NP SAMP AF EC B2.1 - 3	35.22	2.75	1,650	1,740	1,300	4.04E-02	8.35
PS-NP SAMP AF EC B2.3 - 1	33.64	2.63	1,521	592	1,160	2.82E-02	8.29
PS-NP SAMP AF EC B2.3 - 2	33.6	2.63	1,524	592	1,160	3.23E-02	8.29
PS-NP SAMP AF EC B2.3 - 3	33.69	2.63	1,525	592	1,160	4.32E-02	8.29
Mean:	33.27	2.6	1,561	791	1,198	3.22E-02	8.34
Std Err:	1.89	0.15	21	250	26	2.22E-03	0.01

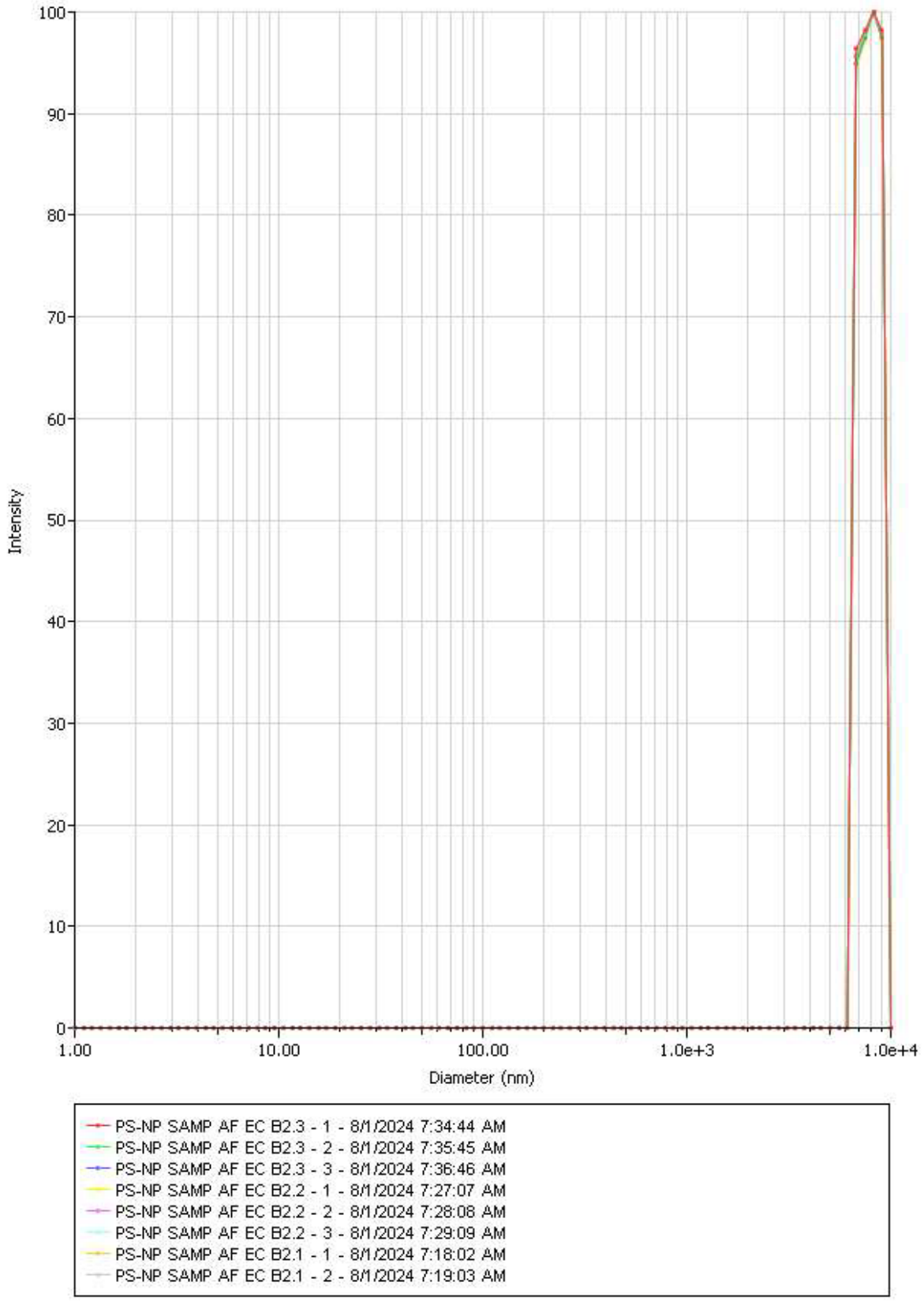

Figure 53 Particle size graph for second set of triplicates at 25 mA, 5V after EC

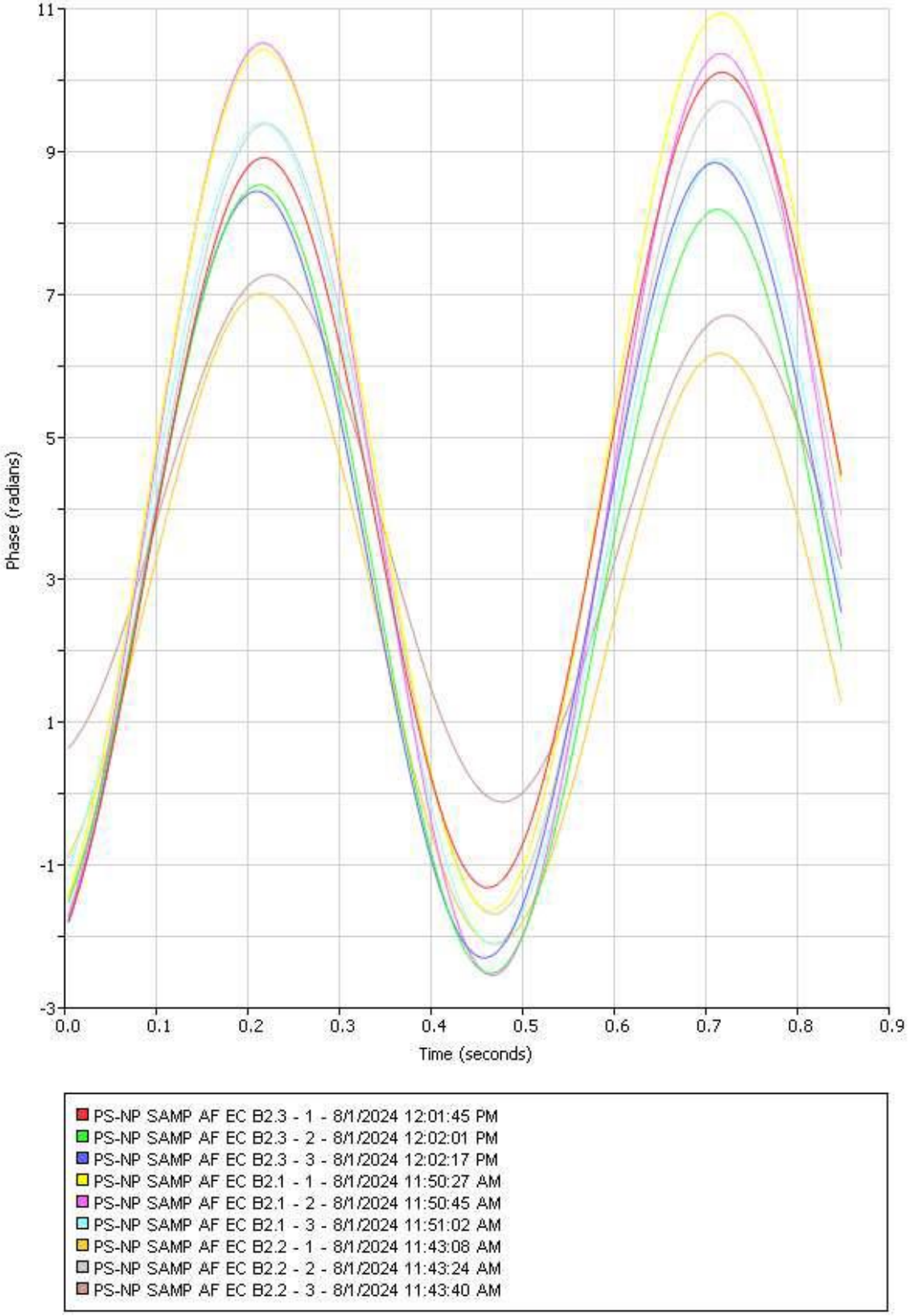

Figure 54 Zeta potential graph for second set of triplicates at 25 mA, 5V after EC

Table 46 Particle size measurement for third set of triplicates at 25 mA, 5V after EC

Sample ID	Eff. Diam. (nm)	Polydispersity	Baseline Index	Count Rate (kcps)	Data Retained (%)	Diffusion Coeff. (cm^2/s)	pH
PS-NP SAMP AF EC B3.1 - 1	26,998.59	0.438	0	616.7	85.44	1.82E-10	8.23
PS-NP SAMP AF EC B3.1 - 2	50,682.06	0.658	0	780.3	92.55	9.68E-11	8.23
PS-NP SAMP AF EC B3.1 - 3	18,825.49	0.519	0	370.5	89.84	2.61E-10	8.23
PS-NP SAMP AF EC B3.2 - 1	77,985.70	0.349	0	839.6	92.91	6.29E-11	8.26
PS-NP SAMP AF EC B3.2 - 2	96,203.48	0.589	0	942.5	98.02	5.10E-11	8.26
PS-NP SAMP AF EC B3.2 - 3	115,581.60	0.606	0	979	95.58	4.25E-11	8.26
PS-NP SAMP AF EC B3.3 - 1	53,283.69	0.11	0	505.8	85.24	9.21E-11	8.31
PS-NP SAMP AF EC B3.3 - 2	46,201.53	1.303	0	420.6	91.91	1.06E-10	8.31
PS-NP SAMP AF EC B3.3 - 3	98,501.51	0.033	0	546.1	87.69	4.98E-11	8.31
Mean:	64,918.18	0.512	0	666.8	91.02	1.05E-10	8.27
Std Err:	11,239.14	0.123	0	75.2	1.46	2.42E-11	0.01

Table 47 Zeta potential measurement for third set of triplicates at 25 mA, 5V after EC

Sample ID	Zeta Potential (mV)	Mobility (µ/s)/(V/cm)	Conductance (µS)	Sample Count Rate (kcps)	Ref. Count Rate (kcps)	RMS Residual	pH
PS-NP SAMP AF EC B3.1 - 1	33.08	2.58	1,426	7,450	1,014	1.90E-02	8.23
PS-NP SAMP AF EC B3.1 - 2	30.15	2.36	1,430	7,450	1,014	2.47E-02	8.23
PS-NP SAMP AF EC B3.1 - 3	28.3	2.21	1,429	7,450	1,014	2.12E-02	8.23
PS-NP SAMP AF EC B3.2 - 1	35.3	2.76	1,422	760	1,269	2.78E-02	8.26
PS-NP SAMP AF EC B3.2 - 2	32.43	2.53	1,428	760	1,269	2.44E-02	8.26
PS-NP SAMP AF EC B3.2 - 3	30.57	2.39	1,431	760	1,269	4.66E-02	8.26
PS-NP SAMP AF EC B3.3 - 1	26.97	2.11	1,429	674	667	2.57E-02	8.31
PS-NP SAMP AF EC B3.3 - 2	25.89	2.02	1,431	674	667	3.05E-02	8.31
PS-NP SAMP AF EC B3.3 - 3	27.13	2.12	1,434	674	667	3.22E-02	8.31
Mean:	29.98	2.34	1,429	2,961	983	2.80E-02	8.27
Std Err:	1.06	0.08	1	1,122	87	2.71E-03	0.01

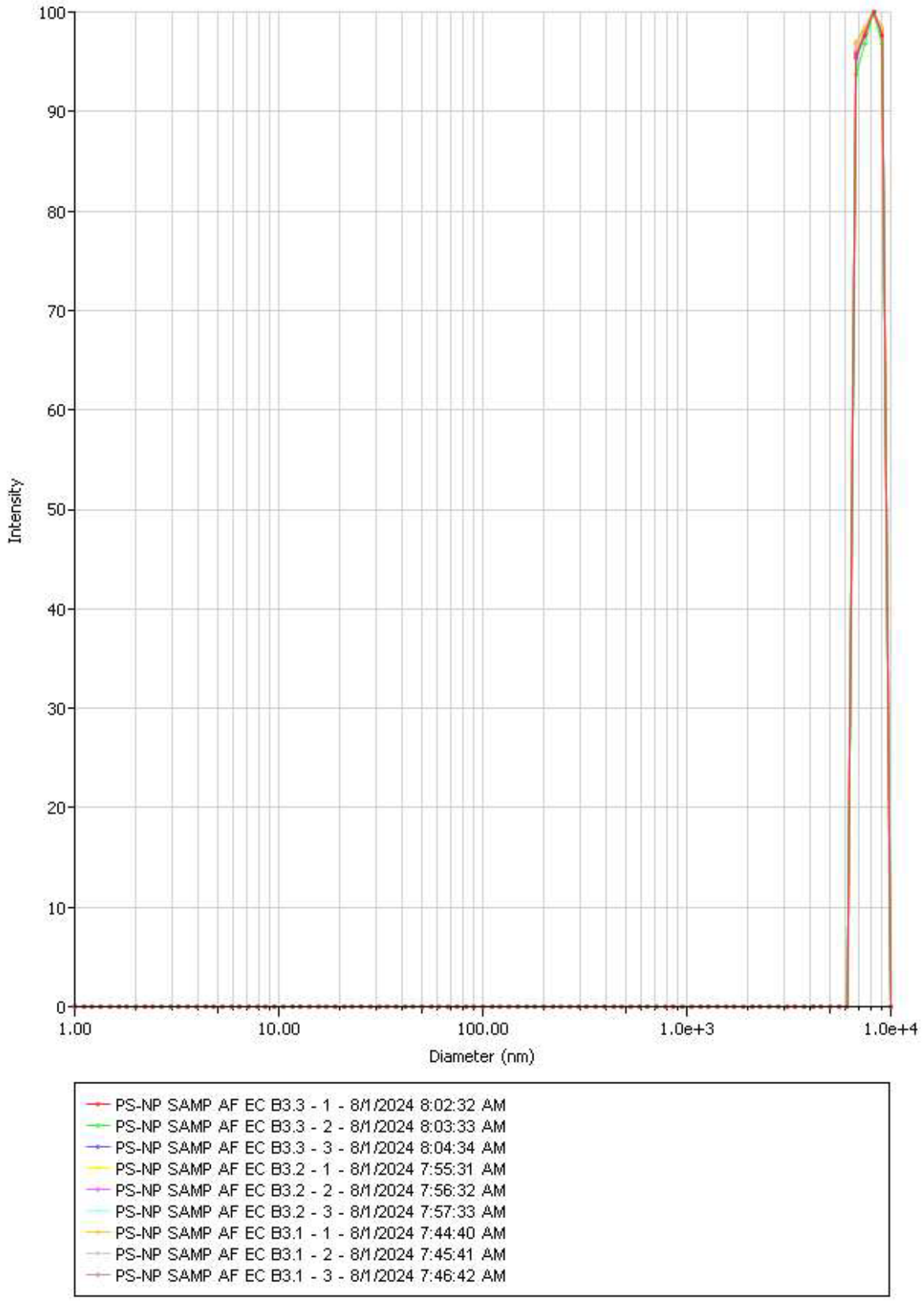

Figure 55 Particle size graph for third set of triplicates at 25 mA, 5V after EC

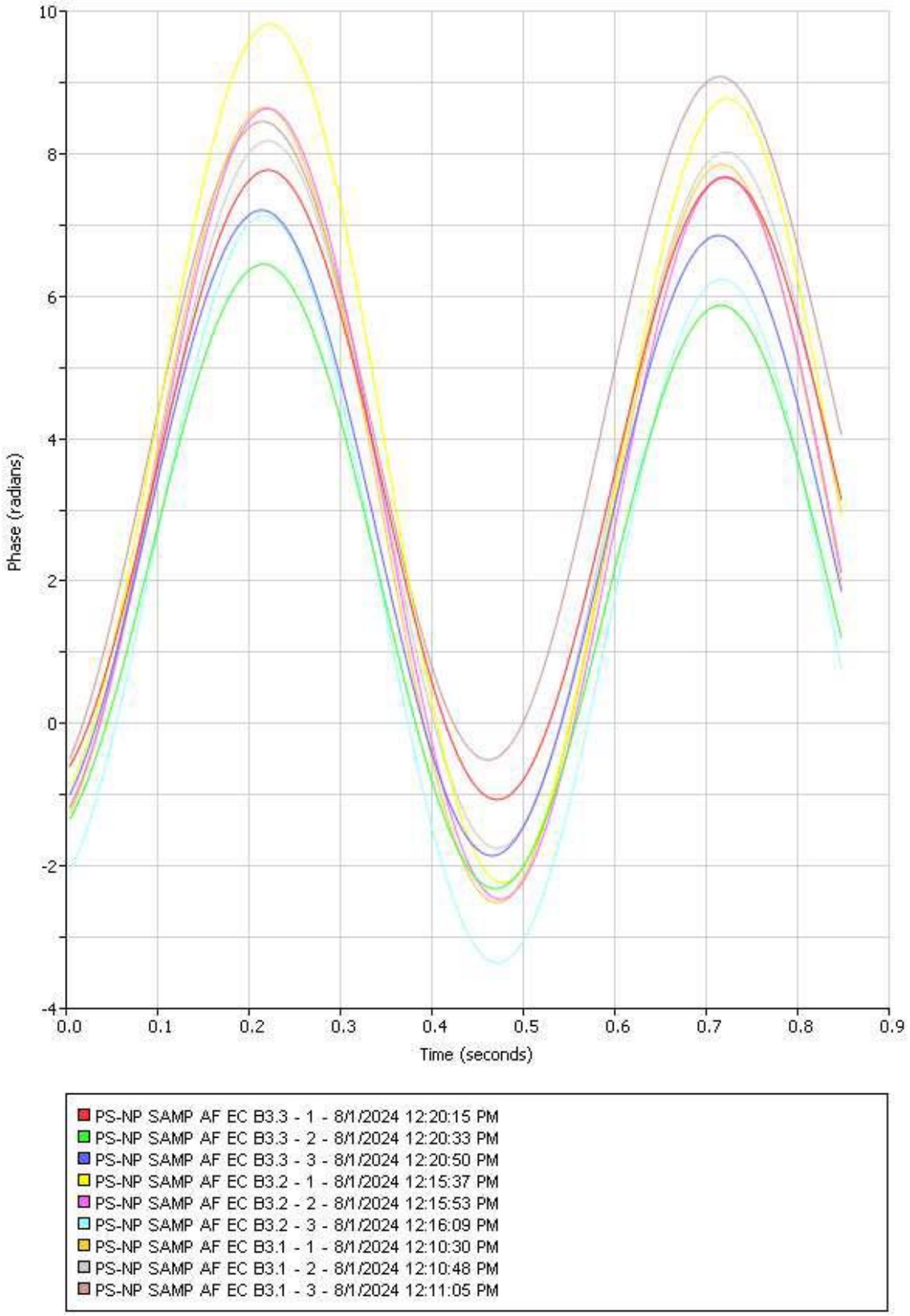

Figure 56 Zeta potential graph for third set of triplicates at 25 mA, 5V after EC

Table 48 Particle size measurement for first set of triplicates at 50 mA, 5V after EC

Sample ID	Eff. Diam. (nm)	Polydispersity	Baseline Index	Count Rate (kcps)	Data Retained (%)	Diffusion Coeff. (cm^2/s)	pH
PS-NP SAMP AF EC C1.1 - 1	951.39	0.296	0.0	455.9	94.42	5.16E-09	8.72
PS-NP SAMP AF EC C1.1 - 2	580.82	0.334	0.0	473.8	96.73	8.45E-09	8.72
PS-NP SAMP AF EC C1.1 - 3	1008.09	0.292	0.0	469.3	96.34	4.87E-09	8.72
PS-NP SAMP AF EC C1.2 - 1	20621.87	0.451	0.0	3509.9	100.00	2.38E-10	8.65
PS-NP SAMP AF EC C1.2 - 2	17763.07	0.410	0.0	2980.1	96.41	2.76E-10	8.65
PS-NP SAMP AF EC C1.2 - 3	29590.34	0.512	0.0	3261.2	96.36	1.66E-10	8.65
PS-NP SAMP AF EC C1.3 - 1	58011.30	0.787	0.0	543.4	89.58	8.46E-11	8.24
PS-NP SAMP AF EC C1.3 - 2	20347.59	0.418	0.0	547.5	90.70	2.41E-10	8.24
PS-NP SAMP AF EC C1.3 - 3	34624.21	0.588	0.0	658.4	94.78	1.42E-10	8.24
Mean:	20388.74	0.454	0.0	1433.3	95.04	2.18E-09	8.54
Std Err:	6297.60	0.053	0.0	456.9	1.07	1.05E-09	0.07

Table 49 Zeta potential measurement for first set of triplicates at 50 mA, 5V after EC

Sample ID	Zeta Potential (mV)	Mobility (µ/s)/(V/cm)	Conductance (µS)	Sample Count Rate (kcps)	Ref. Count Rate (kcps)	RMS Residual	pH
PS-NP SAMP AF EC C1.1 - 1	17.38	1.36	2,452	495	905	3.19E-02	8.72
PS-NP SAMP AF EC C1.1 - 2	19.95	1.56	2,529	495	905	1.64E-02	8.72
PS-NP SAMP AF EC C1.1 - 3	23.15	1.81	2,541	495	905	2.87E-02	8.72
PS-NP SAMP AF EC C1.2 - 1	25.97	2.03	2,457	456	977	2.54E-02	8.65
PS-NP SAMP AF EC C1.2 - 2	26.52	2.07	2,501	456	977	2.81E-02	8.65
PS-NP SAMP AF EC C1.2 - 3	25.41	1.99	2,512	456	977	3.11E-02	8.65
PS-NP SAMP AF EC C1.3 - 1	30.59	2.39	2,484	738	1,087	4.05E-02	8.24
PS-NP SAMP AF EC C1.3 - 2	32.44	2.53	2,502	738	1,087	6.20E-02	8.24
PS-NP SAMP AF EC C1.3 - 3	32	2.5	2,514	738	1,087	2.90E-02	8.24
Mean:	25.93	2.03	2,499	563	990	3.26E-02	8.54
Std Err:	1.74	0.14	10	44	26	4.24E-03	0.07

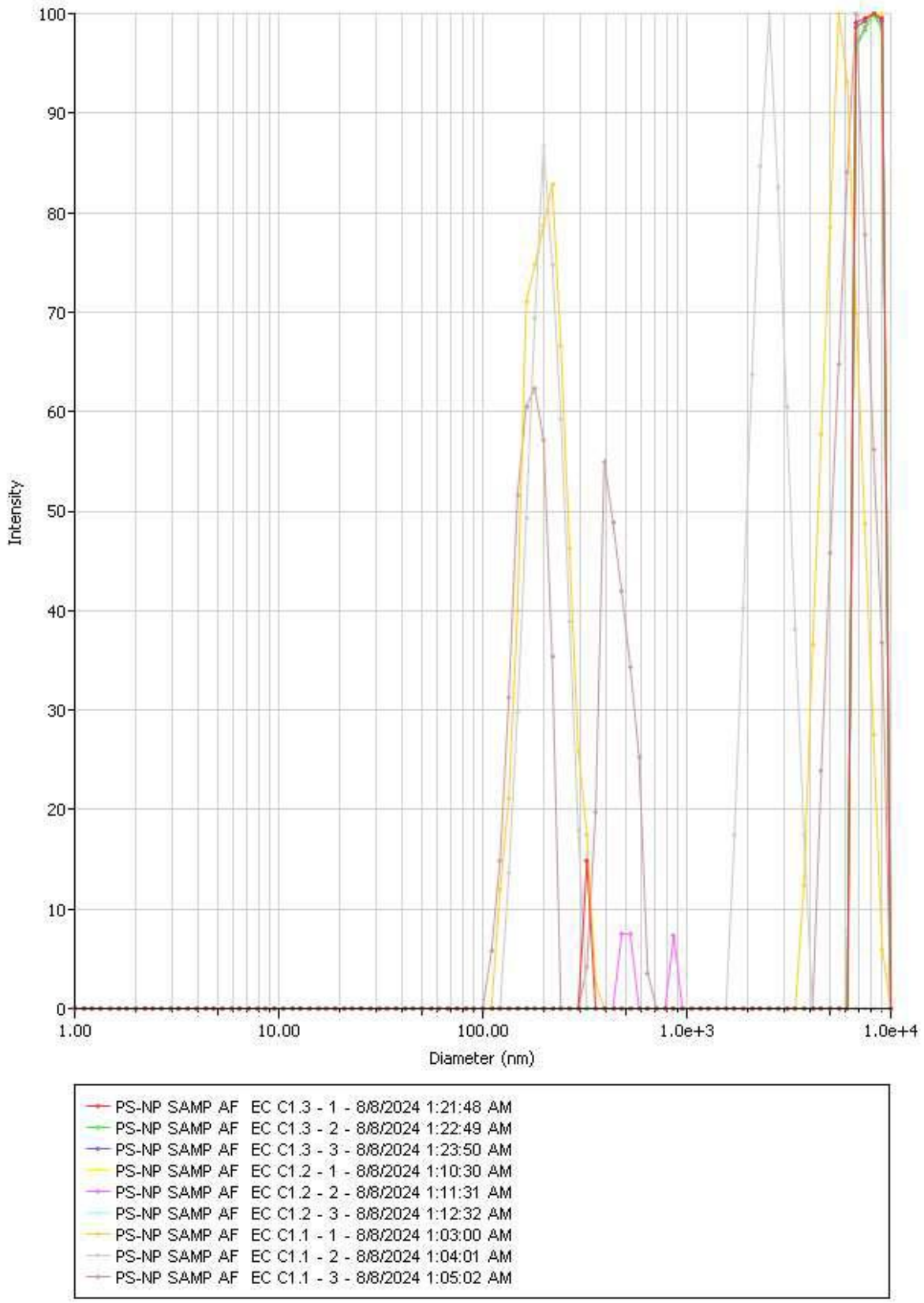

Figure 57 Particle size graph for first set of triplicates at 50 mA, 5V after EC

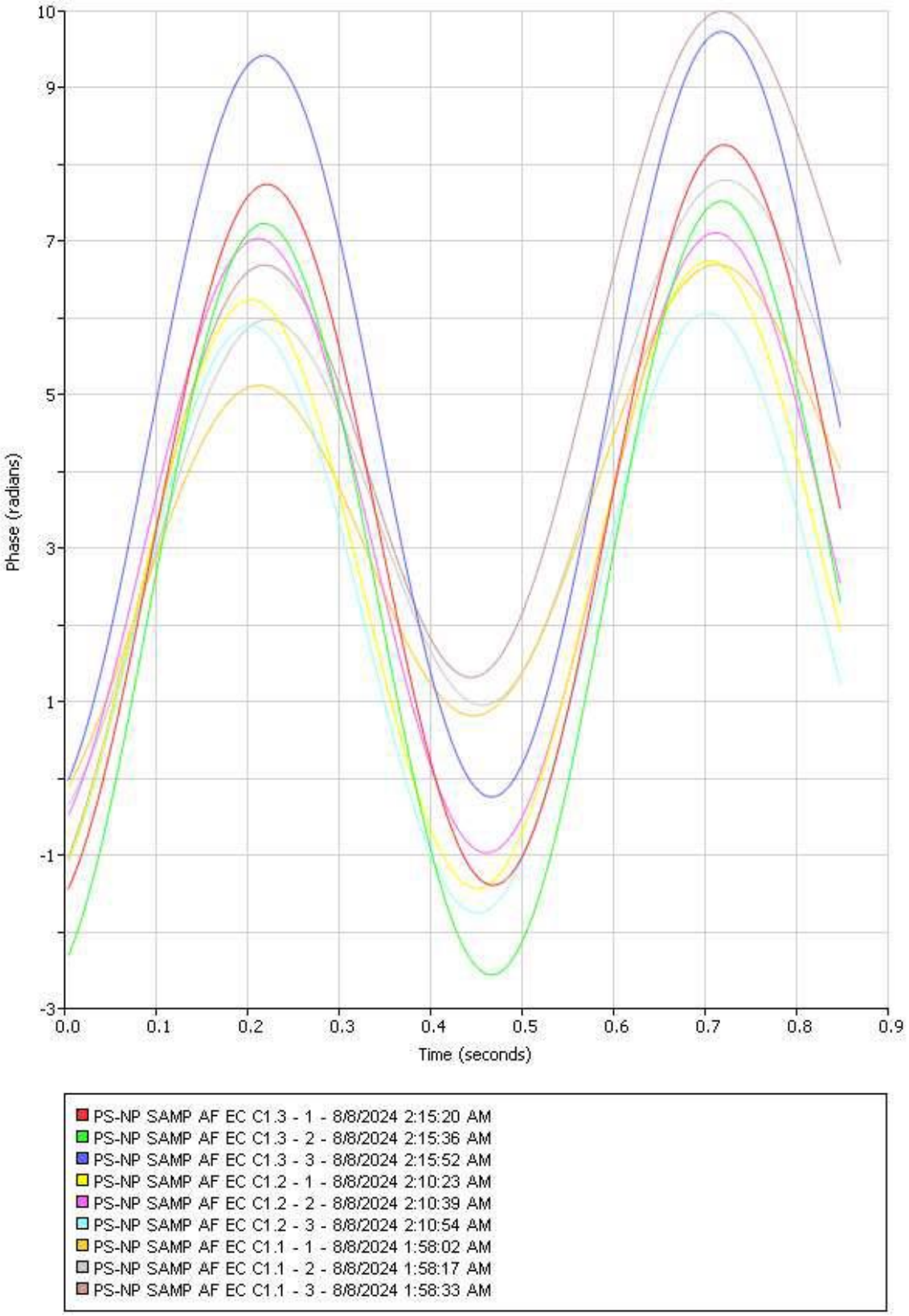

Figure 58 Zeta potential graph for first set of triplicates at 50 mA, 5V after EC

Table 50 Particle size measurement for second set of triplicates at 50 mA, 5V after EC

Sample ID	Eff. Diam. (nm)	Polydispersity	Baseline Index	Count Rate (kcps)	Data Retained (%)	Diffusion Coeff. (cm^2/s)	pH
PS-NP SAMP AF EC C2.2 - 1	18856.53	0.397	7.0	845.9	98.44	2.60E-10	8.65
PS-NP SAMP AF EC C2.2 - 2	22569.8	0.455	0.0	1013.4	98.44	2.17E-10	8.65
PS-NP SAMP AF EC C2.2 - 3	6388.678	0.444	0.0	762.4	93.75	7.68E-10	8.65
PS-NP SAMP AF EC C2.1 - 1	4626.959	0.609	0.0	457.2	93.49	1.06E-09	8.49
PS-NP SAMP AF EC C2.1 - 2	39284.91	0.611	0.0	435.9	96.63	1.25E-10	8.49
PS-NP SAMP AF EC C2.1 - 3	21929.54	0.410	0.0	493.3	100.00	2.24E-10	8.49
PS-NP SAMP AF EC C2.3 - 1	41455.66	0.616	0.0	453.3	93.02	1.18E-10	8.41
PS-NP SAMP AF EC C2.3 - 2	33868.2	0.587	0.0	580.0	98.47	1.45E-10	8.41
PS-NP SAMP AF EC C2.3 - 3	42762.1	0.474	0.0	597.3	98.44	1.15E-10	8.41
Mean:	25749.15	0.511	0.8	626.5	96.74	3.37E-10	8.52
Std Err:	4828.232	0.031	0.8	67.9	0.88	1.13E-10	0.04

Table 51 Zeta potential measurement for second set of triplicates at 50 mA, 5V after EC

Sample ID	Zeta Potential (mV)	Mobility (µ/s)/(V/cm)	Conductance (µS)	Sample Count Rate (kcps)	Ref. Count Rate (kcps)	RMS Residual	pH
PS-NP SAMP AF EC C2.1 - 1	24.82	1.94	2,538	566	607	2.24E-02	8.65
PS-NP SAMP AF EC C2.1 - 2	21.18	1.66	2,548	566	607	2.80E-02	8.65
PS-NP SAMP AF EC C2.1 - 3	26.61	2.08	2,559	566	607	3.81E-02	8.65
PS-NP SAMP AF EC C2.2 - 1	18.47	1.44	2,576	236	1,264	2.55E-02	8.49
PS-NP SAMP AF EC C2.2 - 2	21.47	1.68	2,604	236	1,264	2.23E-02	8.49
PS-NP SAMP AF EC C2.2 - 3	15.88	1.24	2,612	236	1,264	2.00E-02	8.49
PS-NP SAMP AF EC C2.3 - 1	2.11	0.16	0	236	1,310	4.43E-02	8.41
PS-NP SAMP AF EC C2.3 - 2	0.54	0.04	1	236	1,310	2.48E-02	8.41
PS-NP SAMP AF EC C2.3 - 3	1.33	0.1	1	236	1,310	1.58E-02	8.41
Mean:	14.71	1.15	1,715	346	1,060	2.68E-02	8.52
Std Err:	3.51	0.27	429	55	114	3.00E-03	0.04

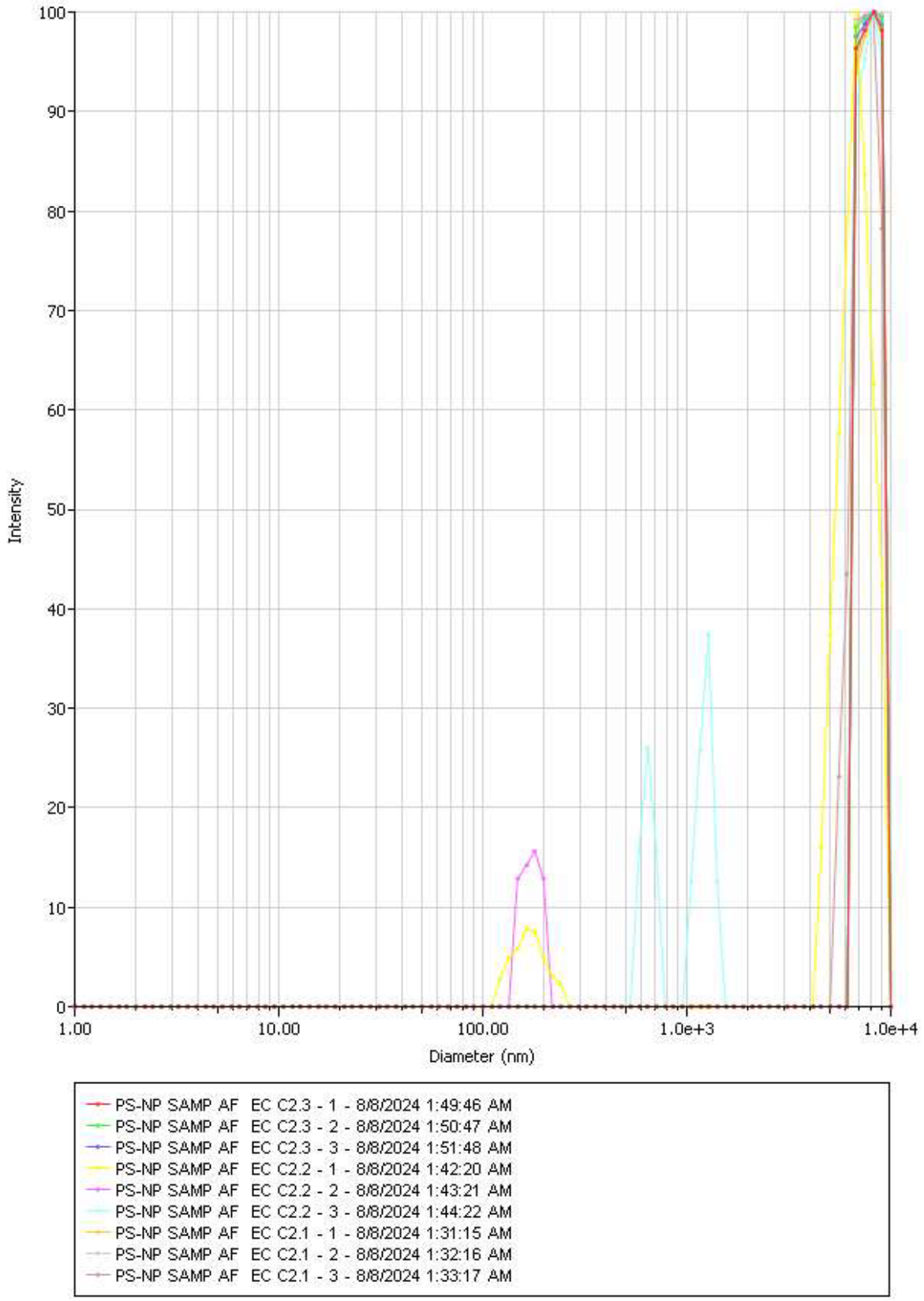

Figure 59 Particle size graph for second set of triplicates at 50 mA, 5V after EC

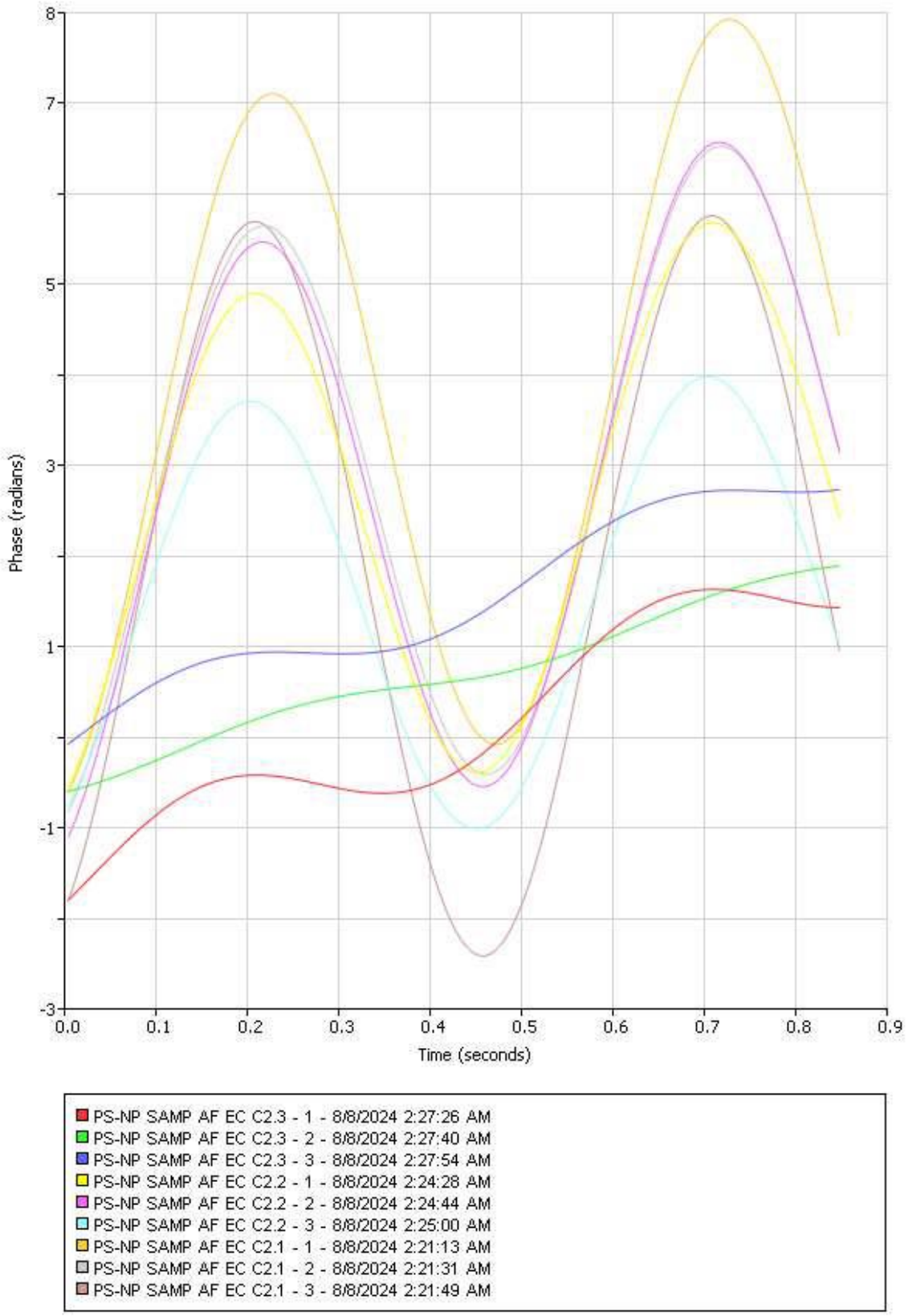

Figure 60 Zeta potential graph for second set of triplicates at 50 mA, 5V after EC

Table 52 Particle size measurement for third set of triplicates at 50 mA, 5V after EC

Sample ID	Eff. Diam. (nm)	Polydispersity	Baseline Index	Count Rate (kcps)	Data Retained (%)	Diffusion Coeff. (cm^2/s)	pH
PS-NP SAMP AF EC C3.1 - 1	25,599.17	0.137	0	6.3	98.37	1.92E-10	8.44
PS-NP SAMP AF EC C3.1 - 2	23,381.52	0.252	0	6	89.46	2.10E-10	8.44
PS-NP SAMP AF EC C3.1 - 3	18,998.12	0.503	0	5.7	94.57	2.58E-10	8.44
PS-NP SAMP AF EC C3.2 - 1	42,693.55	0.531	0	2.1	90.32	1.15E-10	8.31
PS-NP SAMP AF EC C3.2 - 2	45,451.62	0.375	0	1.4	85.8	1.08E-10	8.31
PS-NP SAMP AF EC C3.2 - 3	49,022.01	0.029	0	1.7	78.41	1.00E-10	8.31
PS-NP SAMP AF EC C3.3 - 1	22,905.90	0.392	0	4.2	100	2.14E-10	8.37
PS-NP SAMP AF EC C3.3 - 2	12,628.19	0.534	0	3.3	91.19	3.89E-10	8.37
PS-NP SAMP AF EC C3.3 - 3	38,928.60	0.433	8.2	4.3	95.21	1.26E-10	8.37
Mean:	31,067.63	0.354	0.9	3.9	91.48	1.90E-10	8.37
Std Err:	4,358.10	0.06	0.9	0.6	2.21	3.11E-11	0.02

Table 53 Zeta potential measurement for third set of triplicates at 50 mA, 5V after EC

Sample ID	Zeta Potential (mV)	Mobility (µ/s)/(V/cm)	Conductance (µS)	Sample Count Rate (kcps)	Ref. Count Rate (kcps)	RMS Residual	pH
PS-NP SAMP AF EC C3.1 - 1	31.65	2.47	1,302	10,138	1,105	6.57E-02	8.44
PS-NP SAMP AF EC C3.1 - 2	27.96	2.18	1,313	10,138	1,105	2.29E-02	8.44
PS-NP SAMP AF EC C3.1 - 3	33.33	2.6	1,314	10,138	1,105	2.48E-02	8.44
PS-NP SAMP AF EC C3.2 - 1	25.66	2.01	1,294	786	1,141	5.93E-02	8.31
PS-NP SAMP AF EC C3.2 - 2	26.89	2.1	1,300	786	1,141	5.49E-02	8.31
PS-NP SAMP AF EC C3.2 - 3	26.84	2.1	1,303	786	1,141	6.72E-02	8.31
PS-NP SAMP AF EC C3.3 - 1	30.97	2.42	1,298	1,049	1,198	5.28E-02	8.37
PS-NP SAMP AF EC C3.3 - 2	34.86	2.72	1,308	1,049	1,198	3.73E-02	8.37
PS-NP SAMP AF EC C3.3 - 3	28.07	2.19	1,312	1,049	1,198	2.51E-02	8.37
Mean:	29.58	2.31	1,305	3,991	1,148	4.56E-02	8.37
Std Err:	1.07	0.08	2	1,537	14	6.05E-03	0.02

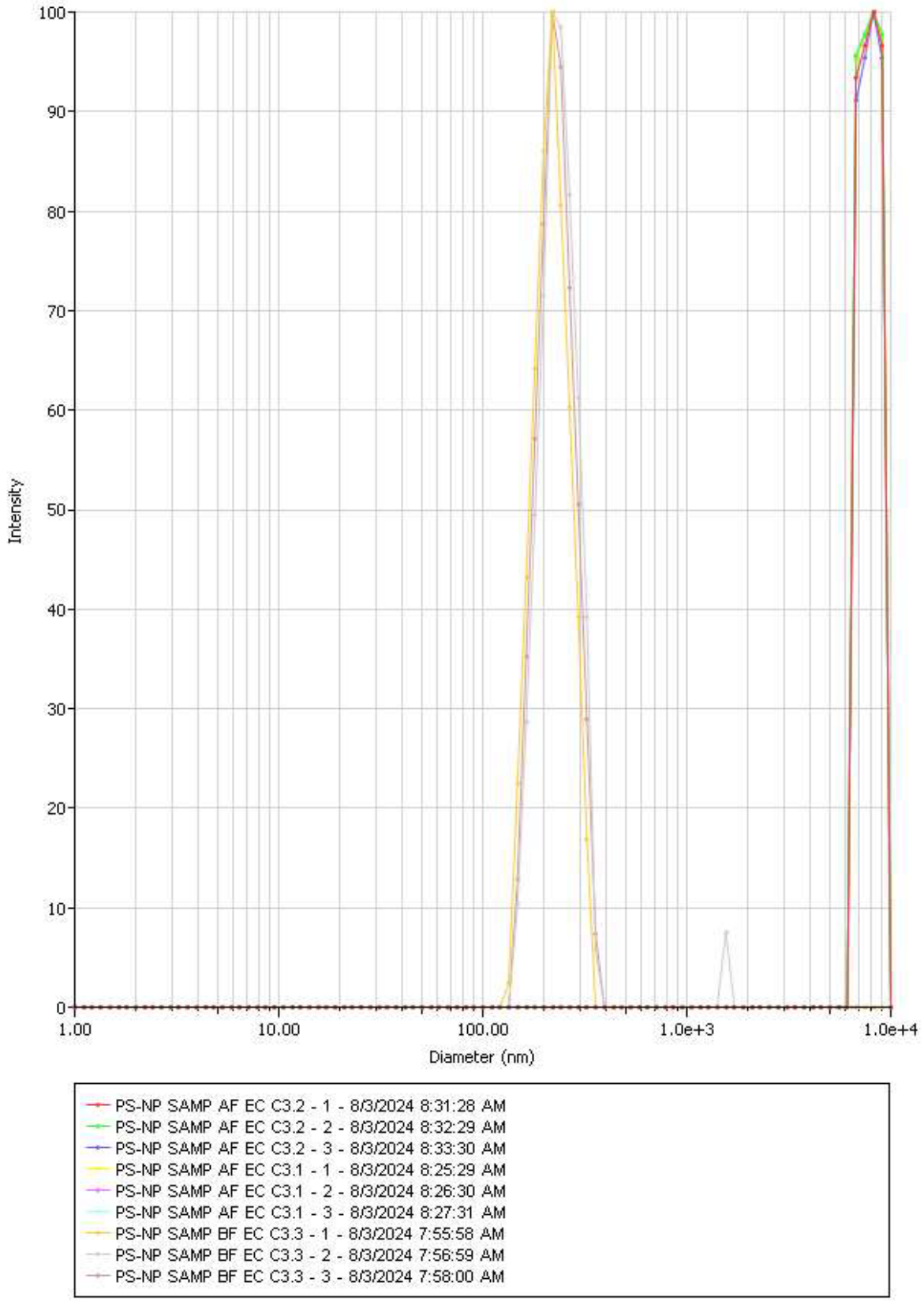

Figure 61 Particle size graph for third set of triplicates at 50 mA, 5V after EC

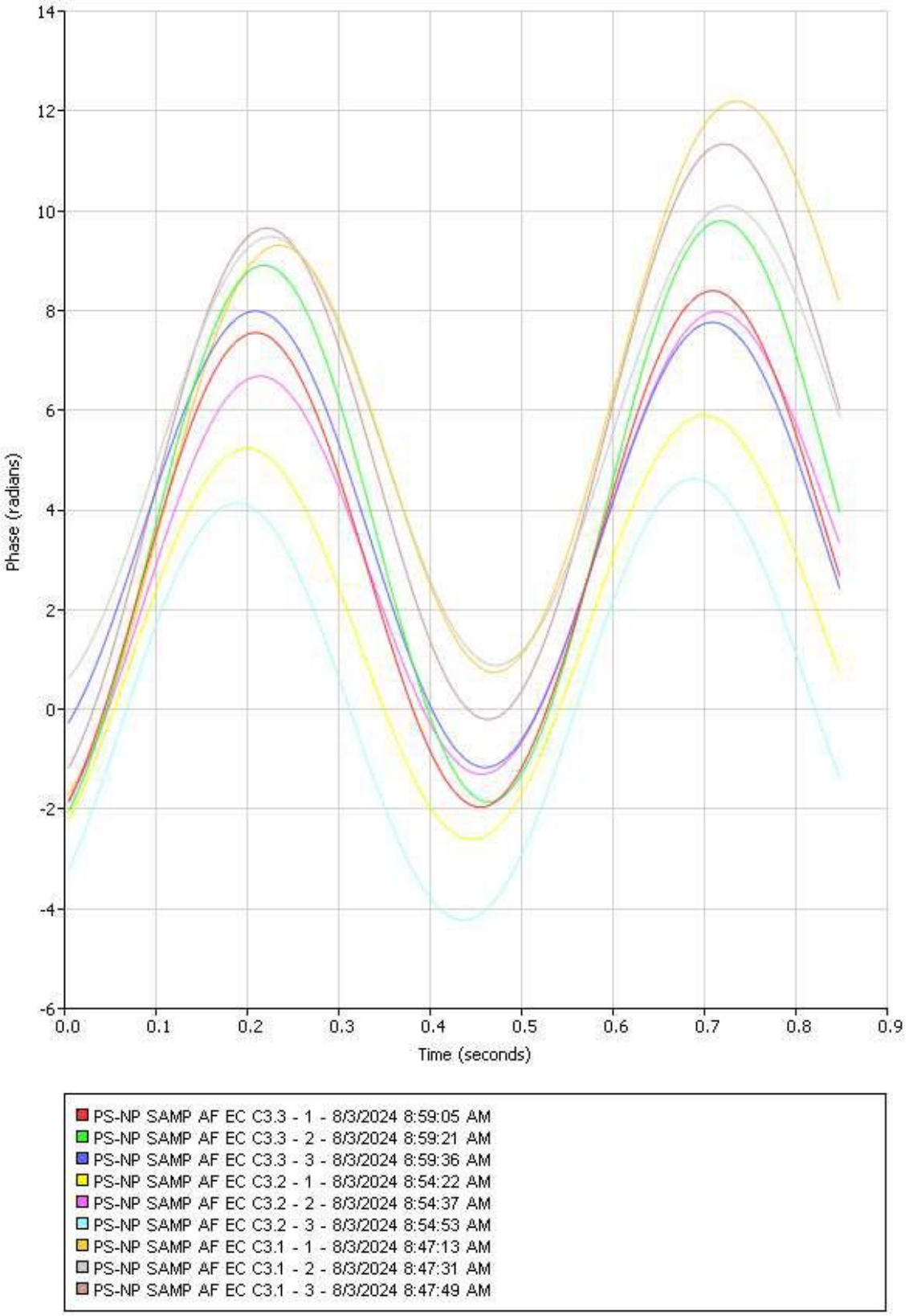

Figure 62 Zeta potential graph for third set of triplicates at 50 mA, 5V after EC